Gamma Factory Proof-of-Principle experiment

M. W. Krasny, A. Martens, Y. Dutheil

September 25, 2019

Gamma Factory

Proof-of-Principle Experiment

LETTER OF INTENT

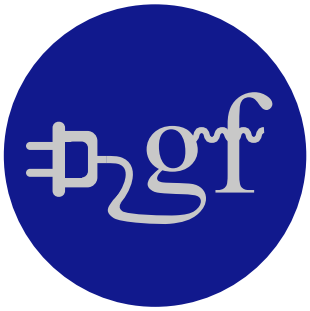

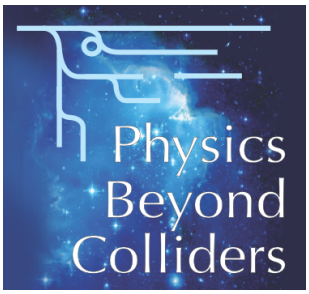

CERN-SPSC-2019-031 / SPSC-I-253
25/09/2019

Gamma Factory Study Group

Contact persons:

M. W. Krasny, krasny@lpnhe.in2p3.fr, krasny@mail.cern.ch – **Gamma Factory team leader**

A. Martens, martens@lal.in2p3.fr – **Gamma Factory PoP experiment spokesperson**

Y. Dutheil, yann.dutheil@cern.ch – **Gamma Factory PoP study – CERN coordinator**

Glossary

Some of the acronyms used in this letter are presented in the table below.

Abbreviation	Meaning
AMO	Atomic, Molecular and Optical physics
AWAKE	Advanced WAKEfield Experiment
BPM	Beam Position Monitor
BSM	Beyond Standard Model
CCD	Charge-Coupled Device
CKM	Cabibbo–Kobayashi–Maskawa (matrix)
CM	Centre-of-Mass (frame)
FEL	Free-Electron Laser
FP	Fabry–Perot (interferometer)
FPC	Fabry–Perot Cavity
GDR	Giant Dipole Resonance
GF	Gamma Factory
HEP	High Energy Physics
HiRadMat	High Radiation to Materials
HL-LHC	High-Luminosity LHC
IP	Interaction Point
IR	Interaction Region
LHC	Large Hadron Collider at CERN
LoI	Letter of Intent
LS2, LS3	Long Shutdown no. 2, 3
LSS	Long Straight Section
MD	Machine Development
NA	North Area fix-target experiments at CERN: NA61/SHINE, NA62 and NA64
PBC	Physics Beyond Colliders
PIE	Parasitic Ion/proton–Electron collider
PoP	Proof-of-Principle (experiment)
PS	Proton Synchrotron at CERN
PSI	Partially Stripped Ions
R&D	Research and Development
RF	Fadio Frequency
RMS	Root Mean Square
SPS	Super Proton Synchrotron at CERN
SPSC	SPS and PS Experiments Committee at CERN
QED	Quantum Electrodynamics
TDR	Technical Design Report
θ_W	Weinberg angle (mixing angle of electroweak interactions)
YETS	Year End Technical Stop

Contents

1 Executive summary

We propose an experiment to study collisions of a laser beam with ultra-relativistic atomic beam of Partially Stripped Ions (PSI), circulating in the SPS ring. It would be the first *collider experiment* of photons from a laser beam with ultra-relativistic, $\gamma \gg 1$, atomic beams ever made.

Over the years 2017 and 2018 the Gamma Factory (GF) study group, in the framework of the Physics Beyond Colliders (PBC) studies, demonstrated the capacity of the CERN accelerator complex to produce and store highly-charged atomic beams in its high-energy accelerator rings. The experiment proposed in this Letter of Intent (LoI) is the next natural step of the ongoing feasibility studies of the GF initiative for CERN [1–4]. It is a Proof-of-Principle (PoP) experiment designed to study the GF production scheme of X-rays at the SPS. The outcome of this experiment would enable us to evaluate the capacity of the GF scheme to produce unprecedented-intensity γ-ray beams by a colliding laser beam with atomic beams stored in the LHC.

The GF scheme is based on resonant excitation of the atoms with the laser beam tuned to the atomic transitions frequencies, followed by the process of spontaneous emission of photons. The resonant excitation of atomic levels of highly ionised atoms (ions) is possible due to the large energies of the ions generating a Doppler frequency boost of the counter-propagating laser beam photons by a factor of up to 2γ. Spontaneously emitted photons produced in the direction of the ion beam, when seen in the laboratory frame, have their energy boosted by a further factor of 2γ. As a consequence the process of absorption and emission results in a frequency boost of the incoming photon of up to $4\gamma^2$. In the GF scheme, the SPS (LHC) atomic beams play the role of passive photon frequency converters of eV-photons into keV (MeV) X-rays (γ-rays).

For the concrete implementation of the GF scheme at the SPS we propose to collide a lithium-like lead, $^{208}\mathrm{Pb}^{79+}$, beam with 1034 nm photon beam generated by a pulsed laser, based on Yb-doped optical materials. The beam energy will be tuned to resonantly excite the $2s \rightarrow 2p_{1/2}$ atomic transition[1] of the $^{208}\mathrm{Pb}^{79+}$ atoms. Such a specific choice of beam particles and a laser is purely technical. It minimises both the necessary work and the cost of the experiment while remaining, as far as the tuning of the laser wavelength to the resonant atomic transition is concerned, more challenging than the ultimate implementation of the GF γ-ray production scheme at the LHC.

Laser systems together with Fabry–Pérot (FP) optical cavities, allowing to boost the power of laser pulses, have already been implemented at DESY and KEK electron beam storage rings [5, 6] by teams including members of the GF group, with a high level of synergy for many of the technical issues, like the bunch-synchronisation scheme. A specificity of hadron storage rings is the much higher beam rigidity in conjunction with the larger bunch lengths.

On the basis of the 2018 beam tests we have already developed a scheme of producing and storing the lithium-like lead beam in the SPS. Construction of a new Hz-frequency insertable stripper in the PS to SPS transfer line – planned already as a consolidation step of the CERN ion collision programme independently of the present proposal – would allow us to operate this beam concurrently with the proton or fully stripped lead beams by using a dedicated cycle, within the canonical SPS supercycle.

The goals of the proposed experiment are:

- Demonstrate integration and operation of a laser and a Fabry–Pérot cavity (FPC) in a hadron storage ring.
- Benchmark simulations of atomic excitation rates.
- Develop a collision scheme and implement the required operational tools that demonstrate agreement of spatial and temporal properties of the ion and laser bunches; match laser spectrum to the

[1] The atomic levels are described, throughout this document, by specifying the orbital configuration of the outermost electron and the total angular momentum of the atom, J. For the nl_J level the outermost electron occupies the energy level specified by the principal quantum number n and has the orbital momentum l. For $l = s$, J-value representing the electron spin is omitted.

atomic excitation width to demonstrate resonant excitation of an adequate fraction of the ion bunch population; demonstrate reproducibility over many accelerator cycles.
- Demonstrate laser and atomic bunches timing synchronisation.
- Measure and characterise the photon flux from the spontaneous emission and unfold the spectrum of emitted X-rays.
- Develop atomic and photon beams diagnostic methods.
- Demonstrate laser cooling of relativistic beams and investigate different approaches.
- Investigate feasibility of atomic physics measurements in the ultra-relativistic regime.

In addition to measurements related to the GF photon beam production scheme there are two particularly exciting perspectives, which may even influence the ongoing and future CERN canonical research programme. Firstly, the resonant photon absorption and random emission naturally opens the path to a new technique of beam cooling. Methods of cooling of stationary atoms – exploiting internal degrees of freedom and the Doppler effect – have been mastered over the last three decades by the atomic physics community, and the elements of these cooling techniques could be implemented to the atomic beams stored in the SPS storage ring. A successful demonstration of the Doppler beam-cooling of atomic beams at the SPS could open the possibility of injecting low-emittance beams of fully stripped isoscalar ions into the LHC. Such beams will be very important in the “precision measurement phase" of the LHC experimental programme. Secondly, the production of high-intensity photon beams may open a path to a muon collider based on electromagnetic production of low-emittance muon beams.

It is estimated that three years will be needed for: the procurement and the “surface” tests of the vacuum chamber, the laser system, FPC and remote controls; the procurement of the photon-detector components; the construction of the new ion stripper and its installation in the PS–SPS beam transfer line; and for the installation of the vacuum chamber, the laser system, FPC and the photon-detection system in the Interaction Region (IR).

The installations are foreseen to take a place during the 2021/22 and 2022/23 winter Year End Technical Stops (YETS). From the year 2022 onward, after the installation of the new stripper, the majority of the beam tests in SPS can take place inside a supercycle with other beams. Over the year 2022 it is planned to commission the photon detector and to finalise the SPS beam characterisation. In 2023 and 2024, after the installation of the laser and FPC, the plan is to have a series of PoP runs totalling about 5 weeks per year, which would be split between the experiment commissioning with the beam and the measurements, and the machine development (MD) periods for further experiment development. The optimisation of particular aspects, like the photon-beam production efficiency, or special measurements, like beam lifetime or beam blowup, might require a few dedicated runs with coastable beams.

Beyond 2024, there will be an option for the laser system and photon detector upgrade over the long shutdown (LS3) period. The decision will be taken on the basis of the results of the 2023 and 2024 runs. The goal of such a phase 2 extension would be to use the GF PoP experiment for the atomic physics research programme. If this option is realised, the experiment will remain in the SPS for the LHC Run 4 period scheduled from 2026 to 2029. The SPS PoP programme may therefore cover about a decade. The operational experience with the experiment, its results and their extrapolation to the LHC running conditions will be essential to assess the feasibility of an LHC-based photon beam production scheme.

The existing PBC Gamma Factory study group can be considered as a proto-collaboration. It is already significant in size and includes – in most of the PoP experiment domains – a requisite expertise.

2 Introduction

The experimental studies of elementary particle collisions at the high energy frontier of the accelerator technologies have established, over the last century, the basic laws that govern our Universe at small distances. Each new generation of particle accelerators and particle colliders have delivered important discoveries. It is thus natural to continue the high-energy frontier path as the leading one in the High Energy Physics (HEP) research at CERN. The basic question which triggered the GF initiative is not whether this research path needs to be pursued – it certainly does – but if it is the most optimal one *in the present phase of the HEP research* in which:

- a large number of theoretical model scenarios for Beyond the Standard Model (BSM) phenomena exist without pointing to the optimal energy and beam particles for the future particle collider to observe these phenomena,
- the quantum field theory framework providing the link between the results of precise measurements of the quantum loop virtual phenomena and their (future) direct observation no longer provides any solid landmarks for *predicted discoveries* that are accessible for the present accelerator technologies or their incremental upgrades,
- we do not have a mature, affordable technology to make a significant leap into high energy "terra incognita".

The Gamma Factory (GF) initiative and its associated Proof-of-Principle (PoP) experiment, presented in this Letter of Intent (LoI), target a new and complementary research path which can be pursued concurrently with the ongoing CERN research programme and in parallel to preparing a novel technology for a cost-efficient return to the high-energy frontier research. Its primary goal is to extend the research scope of the existing world-unique CERN accelerator infrastructure. It is proposed at a crucial moment for CERN. The approval, financing and construction of CERN's next high-energy frontier project will very likely be a lengthy process. It is also possible that the on-going LHC-based research program will reach earlier its discovery potential saturation. This generates an opportunity for novel research programmes in basic and applied science which could re-use CERN's existing facilities in ways and at levels that were not conceived when the machines were designed.

The aim of the GF initiative is to create new research tools, allowing to open new, cross-disciplinary research domains. This initiative was presented in [1] and subsequently endorsed by the CERN management through the creation of the CERN GF study group, embedded within the Physics Beyond Colliders (PBC) studies framework. It proposes to produce, accelerate and store, for the first time at high energy, atomic beams in the *existing* CERN accelerator complex. Excitation of their atomic degrees of freedom by photons from a laser beam is proposed to be used to produce high intensity primary beams of gamma rays and, in turn, secondary beams of polarised charged leptons, neutrinos, vector mesons, neutrons and radioactive ions. The GF goal is to establish a new, highly efficient scheme of converting the accelerator RF power, selectively, to these primary and secondary beams, making use of the large Lorentz relativistic factor γ of the atomic beams which can be stored in the CERN storage rings. It has a potential to achieve a leap, by several orders of magnitude, in their intensity and/or brightness with respect to existing facilities. The GF tools potentially available through the different primary and secondary beams will be applicable to a wide range of physics communities and research programmes.

The GF initiative enters a new research territory where new conceptual and technological challenges have to be addressed to prove its technical feasibility. Its path from the initiative stage to the research project stage involves six key R&D steps:

1. Demonstration of efficient production, acceleration and storage of atomic beams in the CERN accelerator complex.

2. Development of the requisite GF research programme simulation tools.

3. Successful execution of the GF PoP experiment in the SPS.

4. Building up the physics cases for the LHC-based GF research programme and attracting wide scientific communities to use the GF tools in their respective research.

5. Extrapolation of the SPS PoP experiment results to the LHC case and realistic assessment of the performance figures of the LHC-based GF programme.

6. Elaboration of the Technical Design Report (TDR) for the LHC-based GF research programme.

The proposed six-step path to arrive at the feasibility proof of the GF concepts minimises both the infrastructure and hardware investments and interference with the ongoing CERN research programme. A large majority of the atomic-beam tests are planned to be executed and benchmarked at the SPS and subsequently extrapolated to the LHC running conditions.

The GF R&D programme started in 2017 by creating the GF study group within the PBC framework. The GF study group, involving now 65 physicists and engineers representing 24 institutions in 10 countries, has already achieved the first two of its milestones [7]. The next R&D step is the preparation and execution of the the GF PoP experiment at the CERN SPS to test the GF photon beam production scheme in collisions of relativistic atomic beams circulating in the SPS ring with laser pulses. This LoI is our initial step towards achieving the third of the GF initiative milestones. Contrary to the first two milestones, which were achieved within the PBC activities framework, by using the SPS and LHC Machine Development periods for the requisite beam tests, reaching this milestone requires dedicated SPS running time and the incorporation of the laser system together with its associated FPC into the SPS accelerator ring. It thus requires a consideration and an approval process by the SPSC.

The SPS PoP experiment plans to use the atomic beam of lithium-like lead, $^{208}\mathrm{Pb}^{79+}$, circulating in the SPS. The fully stripped lead beams are routinely accelerated in the CERN accelerators – it is only the electron stripping scheme in the PS-SPS transfer line which needs to be modified. The optimal stripping scheme, to maximise the beam intensity of the $^{208}\mathrm{Pb}^{79+}$ beam, has already been developed and tested by the GF group together with the SPS operation team. The proposal is to place the laser system in an available location in the SPS tunnel in the LSS6 sector. We plan to use the $2s \rightarrow 2p_{1/2}$ atomic transition, with the energy difference of $230.81\,(5)$ eV, see section 6.1.1 and Table 1 for details. This transition can be excited with a 1034 nm pulsed laser by tuning the Lorentz γ-factor of the stored SPS $^{208}\mathrm{Pb}^{79+}$ beam to the value of $\gamma \approx 96$. The choices of the ion beam type and the atomic transition are tightly constrained by the present quality of the SPS vacuum system. The expected lifetime of such a beam in the SPS of about 100 seconds is comfortably larger than our estimated cooling time of such a beam of approximately 20 seconds. The $2s \rightarrow 2p_{1/2}$ level$l$- transition width for the Li-like lead atoms, corresponding to the lifetime of the atomic excited state of 76.6 ps, is four orders of magnitude smaller than those for the n-level atomic transitions which are planned to be used to generate the GF photon beams at the LHC. As a consequence, the SPS PoP experiment will test the gamma-beam production scheme in a more challenging configuration than in the LHC case, providing an ideal testing ground for the LHC-based GF research programme.

The SPS PoP experiment proposed in this LoI represents one of the six GF R&D steps which must be accomplished before the GF initiative becomes a CERN project. Its role, proposed set-up and goals for physics and accelerator technology can be best understood in the context of the overall scope of the GF initiative. Therefore, the discussion of the PoP experiment is preceded by presentations of the physics motivation driving the GF initiative, its R&D challenges and recent accomplishments. The concept and practical aspects of the PoP experiment (its integration into the SPS machine, the optical system, the secondary photon detection system, simulations of the collisions, the beam cooling and the detector response) are discussed in the implementation section of this document, with preliminary resources requirements and a tentative schedule.

3 Key principles

The GF initiative proposes to use highly relativistic charged atomic beams and their resonant interactions with laser light.

Atomic beams, the primary GF beams, are composed of ions from which all but a few electrons have been stripped on the way between an ion source and a ring in which they are stored, which at CERN is the SPS or the LHC. In these synchrotrons, the beams can be stored at very high energies over a large range of the Lorentz factor: $30 < \gamma < 3000$, at high bunch intensities: $10^8 < N < 10^9$ and at high bunch repetition rate of up to 20 MHz. Laser beam wavelengths matched to the atomic transition frequencies can be used to manipulate the primary beams directly, or for the production of secondary beams via the emitted photons.

3.1 Absorption and emission of photons by ultra-relativistic ions

The resonant excitation of atomic levels is possible due to the large energies of the ions providing a Doppler frequency boost of the counter-propagating laser beam photons. The frequency of the absorbed photon, if analysed in the ion at rest reference system, is a factor of up to 2γ larger than in the laboratory frame. The resonant absorption cross section is in the gigabarn range, and the high γ factors available in the SPS and the LHC open the possibility to excite atomic transitions even of high-Z ions with fairly conventional laser systems.

In addition, spontaneously emitted photons produced in the direction of the ion beam, when seen in the laboratory frame, have their energy boosted by a further factor of up to 2γ, depending on the photon emission angle, which has a typical spread of $\sim 1/\gamma$. Therefore, the process of absorption and emission results in a frequency boost of the incoming photon of up to $4\gamma^2$. For LHC, this opens the possibility of producing γ-rays with energies above the muon-pair production threshold.

In order to maximise the excitation rate, the relative frequency spread of the laser pulse needs to be comparable to the relative ion beam energy spread (typically $\sim 10^{-4}$), and the laser pulse energy needs to be large enough. The typical transverse kick obtained by the ion due to the photon emission is very small compared to the typical angular spread of the ion beam. Therefore, the main effect of the photon emission on the ion motion is a small loss of the ion total momentum. A detailed discussion of the kinematics of the interaction of the incoming photons with the partially stripped ions is covered in Appendix 2, where the required laser pulse energy and saturation effects are considered.

3.2 Laser cooling of partially stripped ion bunches

The selective photon absorption and random emission naturally opens the path to new techniques of beam cooling [8–10]. Contrary to proton bunches, the charged atomic beams can be efficiently cooled, allowing to compress their bunch sizes and energy spread. Analogous methods of cooling of stationary atoms – exploiting internal degrees of freedom and the Doppler effect – have been mastered over the last three decades by the atomic physics community, and these cooling techniques could be applied to the atomic beams stored in the SPS and LHC storage rings which would open a new path to very high–luminosity collisions of isoscalar-ion beams.

The ions in a bunched beam experience synchrotron oscillations which are affected by the radiative energy loss. In general, the reduction of ion energy spread (i.e. the longitudinal cooling) happens because the energy radiated by the ion grows with the ion momentum. This occurs naturally because the emitted photon energy is proportional to the square of the ion energy, but the cooling process can be artificially enhanced [11] by using a specific shape of the laser frequency distribution which increases the dependence of the energy loss on the ion energy as shown in Fig. 1.

The randomness in the energy of emitted photon defined by the random angle of photon emission leads to stochastic heating of the longitudinal phase space. In some configurations this process can lead to the loss of the ion from the RF-bucket.

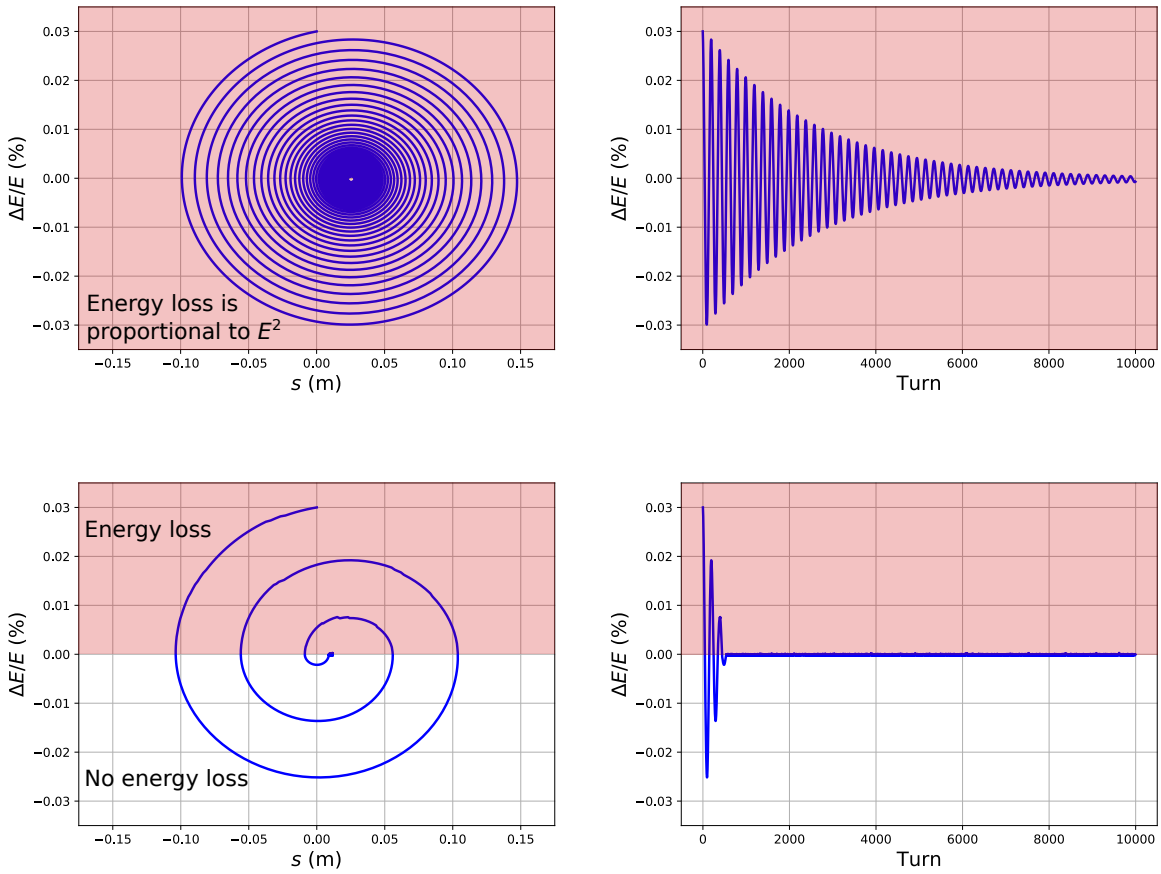

Fig. 1: Longitudinal trajectory (energy deviation vs. longitudinal position within a bunch) of the ion in a storage ring for two regimes of laser cooling. Top plots show the broad-band laser cooling [8] when the ion is always loosing the energy. The bottom plots show the regime of fast cooling [11] when the laser frequency spectrum has a sharp cut-off and the ion is interacting with the laser only if the ion energy is above the central energy.

Transverse cooling happens naturally because all components of the ion momentum are lost due to the emission of radiation but only the longitudinal component is restored in the RF-resonator of the storage ring. Therefore, the typical time required for the transverse cooling is the time it takes to radiate the full ion energy.

The equilibrium ion bunch parameters are determined by the balance between the laser cooling and different sources of beam heating (stochastic heating due to the randomness of emitted photon energy, heating due to the intra-beam scattering and collective instabilities).

In the case of broad-band laser cooling [8] (with the uniform frequency spectrum of the laser light), if the photon emission happens in dispersion-free region, and neglecting collective effects, the equilibrium energy spread can be found as

$$\frac{\sigma_E}{E} = \sqrt{\frac{1.4(1+D)\hbar\omega_1^{\max}}{mc^2}}, \tag{1}$$

where D is the saturation parameter which is normally below one (see [8] for details), $\hbar\omega_1^{\max}$ the maximum energy of the emitted photon, and m the ion mass. The equilibrium emittance reads

$$\epsilon_{x,y} = \frac{3}{20}\frac{\hbar\omega_1^{\max}}{mc^2\gamma^2}\beta_{x,y}, \tag{2}$$

where $\beta_{x,y}$ is the beta-function in the interaction region.

In the case of non-zero dispersion function in the interaction region it is possible to use dispersive coupling between longitudinal and transverse motion in order to achieve faster transverse cooling [12]. The mechanism of the longitudinal–horizontal coupling through dispersion is illustrated in Fig. 2.

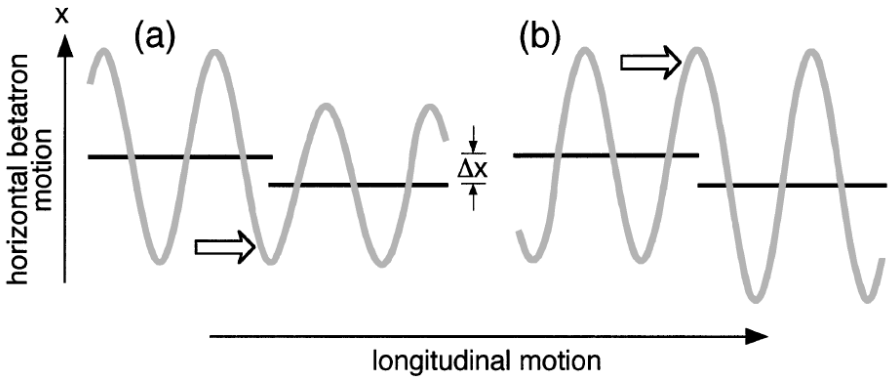

Fig. 2: Horizontal betatron oscillations of a stored ion around the central orbit in a region with positive dispersion. The moment of photon emission and the corresponding change of the central orbit is indicated by the arrow. A reduction (increase) of the amplitude of the oscillation which occurs when the ion radiates a photon in a negative $x < 0$ (positive $x > 0$) phase of the betatron oscillation is depicted on the left (a) (right (b)). The transverse cooling will occur in the case depicted on this figure if more photons are emitted at $x < 0$ rather than at $x > 0$. (Adapted from [12].)

4 Physics motivation

4.1 Introductory remarks

The physics motivation for the GF initiative is to open new research domains at CERN and to provide new type particle beams for the ongoing and future CERN research programme by using its existing accelerator infrastructure in unconventional but innovative way. The GF goal is to achieve a significant leap in their intensity, purity and energy range by using the high-energy atomic beams of partially stripped ions stored in the LHC rings. The GF is thus essentially the LHC-based research programme proposing a possible future exploitation scenario for this machine. It could be executed in parallel to the ongoing LHC research programme in a similar way as the already existing ion collision programme.

Implementation of the GF at the LHC requires extensive R&D studies. Such studies, if conducted at the LHC, would require allocating a non-negligible fraction of its running time for the beam tests – unlikely to happen in the coming years. Since the dominant fraction of these implementation studies can be done at the SPS and subsequenly extrapolated to the LHC running, we propose the GF PoP experiment to be done at the SPS. The physics motivation for the SPS-based experiment is thus essentially driven by the future LHC-based GF research programme.

The future LHC-based GF research programme will exploit the following three broad categories of the GF beams: *Atomic beams*, *Gamma-ray beams* and *Secondary beams*. The atomic beams are the beams of partially stripped ions accelerated and stored in the LHC. The gamma-ray beams can be produced in the collisions of the atomic beams with the laser beams. The secondary beams can be produced in collisions of the high-intensity gamma-ray beams with the external target(s). In Fig. 3 physics domains which could profit from the availability of the GF beams are listed together with examples of the GF research highlights. The GF beams and the research highlights are discussed in the next section.

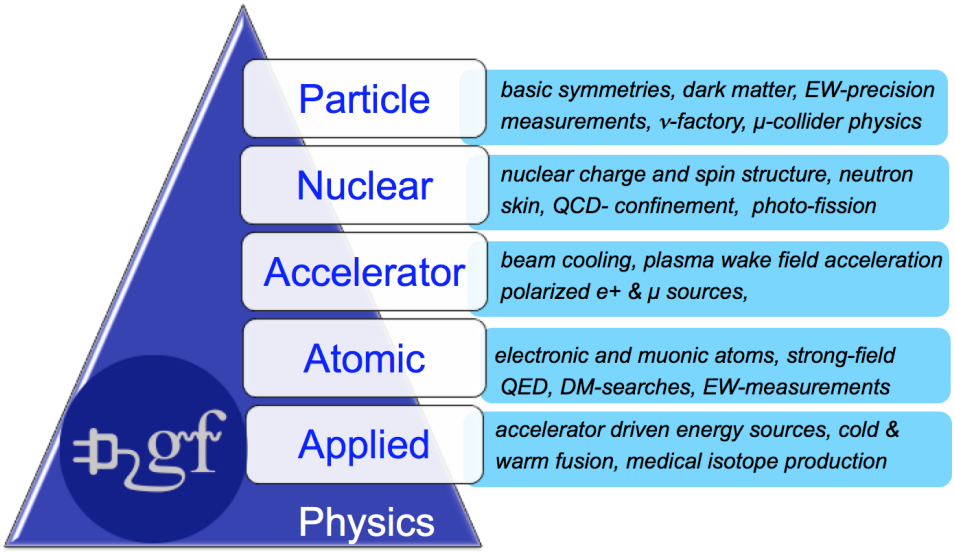

Fig. 3: Physics domains and potential specific research applications of the GF programme.

4.2 Atomic beams

Beams for atomic, molecular and optical physics research

High-energy beams of highly charged high-Z atoms, such as hydrogen-, helium-, or lithium-like lead, are of particular interest for the Atomic, Molecular and Optical (AMO) physics community but have, so far, never been technologically accessible as tools for AMO research [13]. Their principal merits are the following:

- strong electric field binding the remaining electrons to the nucleus – larger by up to five orders of magnitude with respect to hydrogen atoms – providing unprecedented sensitivity to QED-vacuum effects,
- strong amplification of the weak-interaction effects – larger by up to nine orders of magnitude with respect to hydrogen atoms – allowing to study atomic and nuclear weak interactions with unprecedented precision,
- straightforward interpretation of experiments with hydrogen-like or helium-like atoms – simplicity and high-precision calculations are inaccessible for multi-electron atoms,
- high-energy atomic transitions of highly charged ions, normally inaccessible with the existing lasers, can be excited owing to the Doppler effect – the large Lorentz γ-factor of the ion beam compensates the $\sim Z^2$ increase of the electron binding energies,
- residual (or injected) gas molecules in the storage ring could be used to excite the atoms, allowing for precise studies of their emission spectra.

The AMO research highlights include: (1) studies of the basic laws of physics, (2) precise measurement of $\sin^2\theta_W$ in the low-momentum-transfer regime, (3) measurements of the nuclear charge radius and neutron skin depths in high-Z nuclei and (4) searches for dark matter particles using the AMO detection techniques which are complementary to those used in particle physics. The AMO research programme can be addressed already by the PoP experiment at the SPS.

Isoscalar beams for precision electroweak physics at LHC

Isoscalar nuclei such as Ca or O, containing the same number of protons and neutrons, are optimal for the LHC electroweak (EW) precision measurement programme. Thanks to their weak and strong isospin

symmetry they allow to circumvent the dominant sources of uncertainties in the measurement of the EW parameters of the Standard Model [14–17]. The relationship between the W^+, W^- and Z bosons production spectra for isoscalar beams simplifies the use of the Z-boson as a precision 'standard candle' for the W-boson production processes [14]. As an example, with isoscalar beams one could measure the W-boson mass at the LHC with the precision better than 10 MeV [17]. However, their present production schemes result in luminosities which are much lower than can be achieved with protons, negating this advantage.

For these relatively light ions, unlike Pb–Pb collisions, the nucleon–nucleon luminosity is not limited by e^+e^--pair production and electron capture or by electromagnetic dissociation, but by the beam emittance and the ion bunch intensity. A reduction of the beam emittance through cooling could allow for an increase of the nucleon–nucleon collision luminosity.

The GF recipe to achieve this goal is to cool the partially-stripped atomic isoscalar beams in the SPS and, following the stripping of the remaining electrons in the transfer line between the SPS and the LHC, to collide the low emittance beams in the LHC. If the transverse beam emittance of the colliding LHC beams of Ca or O ions could be reduced by a factor of 10, then the effective nucleon–nucleon luminosity in the Ca–Ca and O–O collision modes would approach the nominal *pp*-collisions luminosity. For Ca–Ca collision mode, the average number of beam-particle collisions per bunch crossing ν, would always be smaller than 1 – even at the highest effective nucleon–nucleon luminosity. This represents another advantage of with respect to *pp*-collisions where it could reach the values of $\nu = 100$ at the highest *pp*-collision luminosity.

Electron beam for ep operation of LHC

The hydrogen-like or helium-like lead beams can be considered as the carriers of the effective electron beams circulating in the LHC rings. Collisions of such a beam with the counter propagating beam of protons can allow to observe both the proton–lead-nucleus and the electron–proton collisions in the LHC detectors. LHC could thus be operating as an effective parasitic electron–proton(ion) collider (PIE) [18]. The PIE *ep* collider could reach the centre-of-mass (CM) energy of 200 GeV and the luminosity of 10^{29} $\mathrm{cm}^{-2}\mathrm{s}^{-1}$, both inferior to the corresponding parameters of the HERA collider, but sufficiently large to provide a precise, in situ, detector-dependent diagnostics of the emittance of partonic beams at the LHC, in the low Bjorken-x region, and a precise, percent-level, calibration of the luminosity of the proton–nucleus collisions at the LHC.

Atomic beams for plasma wake-field acceleration

The GF atomic beams have been already used by the AWAKE experiment to calibrate its electron spectrometer with monochromatic electrons attached to lead ions over their acceleration cycle and stripped off at the entry to the spectrometer [19]. They have two other potential merits which can be evaluated and exploited in the future. The high-intensity atomic beams could be efficient drivers for hadron-beam-driven plasma wake-field acceleration [20]. Beam cooling can reduce their emittance allowing for the increased density of the driver beam in plasma, resulting in higher acceleration rate of the witness beam.

In addition, atomic beams carry "ready-to-accelerate" electrons. These electrons exploited initially in the cooling process of the driver beam can be subsequently used – following their stripping – to form a precisely synchronised witness bunch.

Our preliminary studies show that the reduction of the beam emittance by at least an order of magnitude and cooling time below tens of seconds are feasible both for the SPS and LHC atomic beams.

4.3 Gamma-ray beams

With the GF approach, the laser light excites a resonant atomic transition of a highly-charged relativistic ion resulting in a spontaneously emitted photon. The frequency boost is up to $4\gamma^2$, so that a photon beam

in a broad energy range reaching up to 400 MeV can be driven by the high-γ CERN atomic beams. The resonant photon absorption cross section is up to a factor 10^9 higher than for the inverse Compton photon scattering on point-like electrons and, as a consequence, an atomic-beam-driven light source intensity can be higher than that of electron-beam-driven ones by a large factor.

Gamma ray source

The presently operating high-intensity Free Electron Laser (FEL) light sources produce photon beams up to the energies of ≈ 25 keV. The GF photon beams could extend their energy range by four orders of magnitude with FEL-like beam intensities using the atomic beams stored in the LHC. While the FEL photon beams are optimal to study the atomic and molecular structure of matter, the GF beams would allow to resolve the structure of atomic nuclei. In addition, they have sufficient energies and intensities to produce secondary beams of matter particles.

Low-intensity light sources in the MeV energy range have already been constructed and are still in operation in several countries. The highest flux which has been achieved so far is 10^{10} photons per second. All the existing facilities rely on the process of the inverse Compton scattering of a laser beam on a highly relativistic electron beam. Since the cross section of the inverse Compton process is small, in the $\mathcal{O}(1$ barn) range, in order to achieve the flux of 10^{10} photons per second, both the laser and energy recovery linac technologies have to be pushed to their technological limits.

With short excited-state lifetimes, the GF photon-beam intensity is expected not to be limited by the laser-light intensity but by the available RF power of the accelerator ring in which atomic beams are stored. For example, a flux of up to 10^{17} photons emitted per second can, in principle, be reached for photon energies in the 10 MeV region already with the present 16 MV circumferential voltage of the LHC RF cavities. This photon flux would be a factor of 10^7 higher than that of the highest-intensity electron-beam-driven light source HIγS@Durham operating in the same energy regime.

Such an intense photon flux, corresponding to up to 10^{24} photons per year, would sizeably increase the sensitivity of searches for very weakly interacting dark matter particles in the "anthropologica" keV–MeV mass region, e.g. in a beam-dump, light-shining-through-the-wall type of experiment, using a broad-energy-band beam of the GF photons.

Photon collision schemes

A high-intensity and high-brilliance photon beam produced by the GF facility can be used to conceive the first realisation of two types of photon–photon colliders at CERN:

- *elastic photon scattering* collider (below the threshold of producing matter particles), covering the range of CM energies of up to 100 keV, achievable in collisions of the GF photon beam with the laser beam stacked in a FPC,
- *matter particle producing* collider covering the energy range of up to 800 MeV, achievable in collisions of the photon beam with its counter-propagating twin photon beam.

The first of the two colliders can explore the domain of fundamental QED measurements, such as the elastic large-angle light-by-light scattering observed with a rate of up to ≈ 1000 events per second. For comparison, only tens of events of this type are detected over one year of the present LHC operation.

The second scheme, having sufficient energy to produce both opposite charge and colourless pairs of fermions (electron or muon) and opposite charge colour-carrying pairs of fermions (quarks) could explore colour-confinement phenomena at the colour-production threshold.

Should any signal of e.g. an axion-like particle or a dark photon be observed in a shining-through-the-wall experiment, one of the above two colliders could become a Dark Matter Production Factory by maximising the resonant production rate of dark matter particles through a suitable narrow-band choice of photon energy.

Finally, the photon beam could also collide with the LHC proton or ion beams. The CM energy range of the corresponding photon–proton and photon–nucleus colliders would be in the range of $4 - 60$ GeV.

4.4 Secondary beams

The GF beam of gamma rays can be used to produce secondary beams in collisions with an external target. Such a scheme represents a change of paradigm for the secondary beams production: from *mining*, in which the dominant fraction of the energy of the primary beams is wasted, to *precision*, or production-by-demand.

The GF secondary beam production scheme is based on the peripheral, small-momentum-transfer electromagnetic collisions of its photon beam with atoms of the target material. As a consequence, a large fraction of the wall-plug power which needs to be delivered to the atomic beam storage ring for continuous production of the primary photon beam could be transmitted to a chosen type of the secondary beam. Such a scheme could reduce considerably the target heat load at a fixed intensity of the secondary beam, facilitating its design and circumventing the principal technological challenges which limit the intensities of the proton-beam-driven muon, neutrino and neutron beams.

Polarised electron, positron and muon beams

The high-intensity GF beam of gamma-rays could be converted into a high-intensity beam of positrons and electrons. If the photon beam energy is tuned above the muon-pair production threshold, such a beam also contains a small admixture of μ^+ and μ^-. Beams of different lepton flavours could easily be separated using the time of flight method, since the produced electrons and positrons move with almost the speed of light while the GF muons are non-relativistic.

For the resonant absorption and subsequent spontaneous emission of photons by atoms with spin-0 nuclei which do not change their electrons-spin state, the initial polarisation of the laser beam is transferred to the emitted photon beam. Circularly polarised photons, if converted to lepton-pairs in the electromagnetic field of atoms (or nuclei), produce longitudinally polarised leptons.

The target intensity of the GF source of polarised electrons/positrons is 10^{17} positrons per second, assuming the present CERN accelerator infrastructure and presently available laser technology. Such an intensity, if achieved, would be three orders of magnitude higher than that of the KEK positron source [21], and would largely satisfy the source requirements for the ILC and CLIC colliders, or for a future high-luminosity ep (eA) collider project based on an energy recovery linac.

The target intensity of the GF beam of polarised muons is 10^{12} muons per second. If achieved, it would be four orders of magnitude higher than that of the $\pi E4$ beam [22]. Two schemes can be envisaged to reach such an intensity target. In the first one, the energy of the photon beam is tuned to its maximal value and muon pairs are produced by photon conversions. For the LHC energies, this scheme requires a significant leap in the intensity and bandwidth of a dedicated FEL source of $\sim 100\,\text{nm}$ photons and an upgrade of the circumferential voltage of the LHC RF system. Alternatively, positron bunches produced by a low-energy photon beam would have to be accelerated a the dedicated positron ring to the energy exceeding the muon-pair production threshold in collisions with a stationary target, i.e. $E_e \sim (2m_\mu^2)/(m_e)$ [23, 24]. For this scheme no LHC upgrade is necessary and the conventional laser technology is sufficient. The intensity of the muon beam in the above two schemes will always be inferior to the proton-beam-driven muon sources. However, for both the above schemes the product of the muon source longitudinal and transverse emittances would be smaller by at least four orders of magnitude than that for the pion-decay-originated muons. The GF driven high-brilliance beams of polarised positrons and muons may therefore help to reactivate, in a new way, R&D programmes on: (1) the TeV-energy-scale muon collider, (2) the polarised lepton–hadron collider, (3) fixed-target Deep Inelastic Scattering (DIS) experiments and (4) the neutrino factory.

High-purity neutrino beams

The low-emittance muon beams could be used to produce high-purity neutrino beams. Thanks to the initial muon polarisation and the $(V-A)$-structure of the weak currents, muon-neutrino (muon-antineutrino) beams could be separated from the electron-antineutrino (electron-neutrino) admixture on the bases of their respective angular distributions. In addition, the neutrino and antineutrino bunches of each flavour could be separated with nearly 100% efficiency using their timing. The fluxes of the neutrino and antineutrino beams would be equal and they could be predicted to a per-mille accuracy.

The high-purity neutrino and antineutrino beams could be used e.g. for the precision measurements of the CP-violating phase in the neutrino CKM matrix.

Neutron and radioactive ion beams

The energy of the GF photons could be tuned to excite the Giant Dipole Resonance (GDR) or fission resonances of large-A nuclei, providing abundant sources of: (1) neutrons with the target intensity reaching 10^{15} neutrons per second (first-generation neutrons), (2) radioactive and neutron-rich ions with the target intensity reaching 10^{14} isotopes per second. The above fluxes would approach those of other European projects under construction, such as ESS, FAIR and the future EURISOL facilities. The advantage of the GF sources is their high efficiency – almost 10% of the LHC RF power can be converted into the power of the neutron and radioactive-ion beams.

4.5 Roadmap and strategy

The phases of the GF studies and its milestones are discussed in details in Section 7.1. The implementation of the LHC-based GF research programme is conditioned, on the one hand, by a successful execution of the SPS PoP experiment and extrapolation of its results to the LHC conditions and, on the other hand, by the schedule of the LHC operation. Our initial vision assumes a staged approach.

In the first stage, assuming a successful demonstration of the Doppler cooling capacity of the PSI beams by the PoP experiment, cooled ion beams would become available: for collisions at the LHC – decicated to precision EW measurements and for the AWAKE experiment as low-emittance plasma wake-field driver beams. The GF helium(hydrogen)-like lead beam could also be injected to the LHC, following the LS3 installation of the new beam collimators, for the operation of the LHC as an *electron–proton* collider. The second stage could start following the installation of the laser system in the LHC tunnel and would include production of the photon beams for dark matter searches, atomic physics programme and precision studies of non-linear QED. The production of the secondary beams could be realised in the third phase of the project. Realistically, it is unlikely that the second and the third stage of the GF research programme could start before the LS4 shutdown. This leaves a sufficient time for the execution of the SPS PoP experiment, extrapolation of its results to the LHC running, and for the preparations for the LHC-based GF programme, respecting both the technical constraints identified by the PoP experiment and the actual interests of the physics community.

5 Challenges and accomplishments

5.1 Challenges

The existing CERN accelerator infrastructure has already demonstrated its capacity to produce, accelerate and store the fully and partially stripped ions in its storage rings. So far the lead and xenon ions have been accelerated and stored at the LHC, but an extension of the LHC ion running programme to include the oxygen, calcium or argon ions is already under discussion. The step to include the corresponding atomic beams of partially stripped ions requires only a minor conceptual and hardware investment with development of a new stripping scheme, and production and installation of new strippers in the beam transfer line(s). Several factors may limit the lifetime of the atomic beams: the vacuum quality, molecu-

lar compositions of the residual gas, space-charge effects, intra-beam stripping and intra-beam scattering and the Stark effect.

Laser systems together with FP optical cavities have already been implemented at DESY and KEK electron beam storage rings [5, 6] by teams including members of the GF group, with a high level of similarity for many of the technical issues, like the bunch-synchronisation scheme. A specific feature of the hadron storage rings is the much higher beam rigidity in conjunction with the larger bunch lengths which complicates the design of the interaction region. The design needs to make the best compromise between matching the laser frequency bandwidth both to the width of the atomic excitation and to the momentum spread and angular dispersion of the ensemble of atomic particles.

For the extreme case of the largest photon-beam energy and intensity, the maximal power of the GF photon beam may reach 0.1–1 MW. The exploitation of such a powerful photon beam produced in a superconducting storage ring is anything but obvious, and its feasibility remains to be demonstrated.

The development of targets for the secondary beams will profit from the present development of the target designs and R&D on neutrino and neutron spallation sources. Using the photon instead of proton beams is, by far, more convenient – the targets will be thinner, with only a small fraction of energy wasted. An efficient separation scheme of the electron and positron beams from the muon beams will have to be developed.

Another challenge is to develop, very often *ab nihilo*, the GF simulation software required to: (1) optimise the stripping scheme of atoms, (2) describe the effect of the vacuum quality at various stages of the acceleration of the atomic beams, (3) simulate the beam dynamics of the atomic bunches (betatron oscillations, intrabeam scattering, beam impedance, etc.), (4) simulate the collisions of the laser pulses with the atomic bunches, (5) evaluate various beam-cooling scenarios and (6) study the properties of the primary and secondary beams.

5.2 Accomplishments to date

The GF R&D programme started in 2017 and has already achieved the first two of its six milestones, with the successful SPS and LHC beam tests and the development of software tools for the beam tests and SPS experiment design. The achievements and lessons drawn are presented in the following sections.

SPS and LHC beam tests in 2017 and 2018

In 2017 the $^{129}\mathrm{Xe}^{39+}$ atomic beam was accelerated, stored in the SPS and studied at different flat-top energies [25–27]. The lifetime was shown to be limited by electron stripping in collisions with residual gas. The analysis of the measured lifetime constrained the molecular composition of the residual gas and allowed the expected lifetimes of the hydrogen- and helium-like lead beams to be estimated to at least 100 seconds. With only 40 seconds needed to fill the SPS and to accelerate the bunches up to the LHC injection energy, this measurement-based prediction opened the possibility of injecting such beams to the LHC ring.

In 2018, after the installation of a new aluminium stripper foil in the PS to SPS transfer line, both $^{208}\mathrm{Pb}^{81+}$ and $^{208}\mathrm{Pb}^{80+}$ beams were successfully injected to the SPS and accelerated to 270 GeV proton equivalent energy. The observed lifetimes of the $^{208}\mathrm{Pb}^{80+}$ and $^{208}\mathrm{Pb}^{81+}$ beams of, respectively, 350 ± 50 and 600 ± 30 seconds agreed with our predictions based on the extrapolation from the 2017 $^{129}\mathrm{Xe}^{39+}$ runs. The achieved intensities of the $^{208}\mathrm{Pb}^{81+}$ and $^{208}\mathrm{Pb}^{80+}$ beams were also in a good agreement with our expectations based on the calculations of the stripping efficiency for the initial $^{208}\mathrm{Pb}^{54+}$ beam. Finally, and most importantly, the achieved bunch intensity of the $^{208}\mathrm{Pb}^{81+}$ beam, of 8×10^9 unit electric charges, was comfortably higher than the minimum required for monitoring such bunches in the SPS and the LHC.

The $^{208}\mathrm{Pb}^{81+}$ beam was, later in 2018, injected into the LHC and ramped to a proton equivalent

energy of $6.5\,\mathrm{TeV}$ [28]. The observed lifetime at top energy was $\sim$ 40 hours, and with 6 bunches circulating in the LHC the intensity was 7×10^9 unit charges per bunch.

The principal outcome of the 2017 and 2018 GF test runs was the proof that the atomic beams can be formed, accelerated and stored in the existing CERN SPS and LHC rings. The majority of the operation aspects for such beams have been successfully tested. An important specific achievement was to demonstrate that bunches of 10^8 hydrogen-like lead atoms per bunch can be efficiently produced and maintained at the LHC top energy with the lifetime and intensity fulfilling the GF requirements. One of the pivotal concepts of the GF initiative – that relativistic atomic beams can be produced, accelerated and stored – has therefore already been experimentally proven.

The tests also validated our initial software tools, which will be elaborated further to extrapolate the production efficiencies of $^{208}\mathrm{Pb}^{81+}$ and $^{208}\mathrm{Pb}^{80+}$ to arbitrary species (characterised both by the nucleus charge and the number of attached electrons) and to predict their lifetimes in both the SPS and the LHC.

Two outstanding issues were identified in the 2017 and 2018 beam tests. Firstly, the lifetimes measured in the SPS and the inferred vacuum pressure and compositions indicate that, presently, only the high-Z atoms carrying electrons only on the K and L atomic shells can be efficiently accelerated/stored in the SPS before being transferred to the LHC. Once injected into the LHC rings, where the residual gas pressure is a factor ≈ 1000 lower than in the SPS rings, the beam lifetimes, even for low-Z atoms, satisfy with a large safety factor the GF requirements. The present poor SPS vacuum quality constraints the design of the SPS PoP experiment – both by reducing the type of atomic beams which can be used and by the necessity to develop fast beam-cooling schemes, such that the cooling time is significantly smaller than the beam lifetime.

Secondly, the collimation efficiency for the $^{208}\mathrm{Pb}^{81+}$ beam in LHC was, as expected, inferior to that for the fully stripped $^{208}\mathrm{Pb}^{82+}$ beam. The present LHC beam collimation system was not designed for atomic beams and is far from being optimal, and mitigation strategies are needed to reduce the most critical losses. Initial simulations indicated that the likely reason for the poor collimation performance is the parastitic stripping action of the primary collimators. Simulations show that the TCLD collimator scheduled to be installed in LS2 can substantially reduce the losses, and preliminary calculations did not reveal any showstopper for reaching the nominal HL-LHC Pb intensity the $^{208}\mathrm{Pb}^{81+}$ ions. Alternative mitigation strategies, such as orbit bumps, will also be investigated.

Development of software tools

The GF programme to date has already required the development of new software tools to prepare the beam tests, to generalise their results to other beam species, to evaluate the intensity reach of the GF, to optimise the Interaction Point (IP) of the laser pulses and the atomic bunches, to study the internal dynamics of the atomic bunches exposed to collisions with the laser light, to optimise the Doppler beam-cooling methods and to study the extraction and diagnostics of the GF primary and secondary beams.

Existing software tools to study stripping of electrons in metallic foils and to study beam–gas collisions of highly charged ions [29] have been calibrated for their high-energy applications using striping efficiencies and beam lifetimes measured at the SPS and at the LHC.

Two parallel GF group projects are pursued to develop the requisite, new software tools for simulation studies of the atomic beam dynamics: (1) based on a semi-analytical approach and (2) based on Monte Carlo techniques to study dynamics of individual atoms. The goal of these two projects is to simulate the time evolution of the atomic-beam bunch parameters exposed to collisions with the laser beam – the bunch emittances, the energy spread and the bunch length – and to study various beam-cooling scenarios.

Several Monte Carlo generators are being developed independently within the GF group. They simulate the production of the photon beams in collisions of atomic bunches with the laser pulses. The

major challenge for these developments is to incorporate, for the first time, resonant atomic-physics processes into the frameworks developed by the particle physics community.

6 Implementation of PoP Experiment in SPS

6.1 Overview

The SPS PoP aims to demonstrate the feasibility of the most important aspects of the GF scheme. To provide a foundation for the main technological and accelerator concepts, an early choice was made to locate the experiment in the SPS tunnel on the circulating beam. The objectives of the experiment are:

- Demonstrate integration and operation of a laser and a FPC in a hadron storage ring.
- Benchmark simulations of atomic excitation rates.
- Develop a collision scheme and implement the required operational tools that demonstrate agreement of spatial and temporal properties of the ion and laser bunches; match laser spectrum to the atomic excitation width to demonstrate resonant excitation of an adequate fraction of the ion bunch population; demonstrate reproducibility over many accelerator cycles.
- Demonstrate laser pulse and PSI bunch timing synchronisation.
- Measure and characterise the photon flux from the spontaneous emission and unfold the spectrum of emitted X-rays.
- Develop atomic and photon beams diagnostic methods.
- Demonstrate laser cooling of relativistic beams and investigate different approaches.
- Investigate feasibility of relativistic atomic physics measurements.

The proposed setup is based on an optical resonator, with the FPC constructed around the IP, with an optical length harmonic of the spacing between bunches. The laser would pump this resonant cavity with a much higher frequency of $40\,\mathrm{MHz}$ and much lower pulse energy of the order of µJ, relying on a cavity Q-factor in the range of $10,000$ to provide the high photon flux needed at the interaction point.

6.1.1 Key experimental parameters

With the available SPS magnetic rigidity, vacuum pressure and ion species, an extensive study of the available atomic transitions concluded that the PSI species should be the Li-like Pb (i.e. with a charge state of 79^+), and that the transition to be excited by the photons should be the $2s \rightarrow 2p_{1/2}$ transition. The most recent results on the calculated $2s \rightarrow 2p$ transition energies for the Li-like Pb ion are collected in Table 1. The three latest calculations include the estimates of their uncertainty. The result of the measurement $2s \rightarrow 2p_{3/2}$ transition energy is presented in the last line of Table 1 as an indication of the precision level of the corresponding calculations. Comparisons of the theoretical predictions and the experimental results for both the $2s \rightarrow 2p_{1/2}$ and $2s \rightarrow 2p_{3/2}$ transitions are available only for the Li-like Xe. Four recent theoretical results are compared with experimental data (last two lines) in Table 2.

We assume the $2s \rightarrow 2p_{1/2}$ transition energy for the $^{208}\mathrm{Pb}^{79+}$ ion to be $230.81\,(5)\,\mathrm{eV}$ – the average value of the calculation results presented in Ref. [36] and Ref. [37] – and the lifetime of excited state $\tau(2p_{1/2})$ to be $76.6\,\mathrm{ps}$, from Ref. [36].

The full set of high-level parameters for the SPS PoP experiment used for simulations and the experiment design are summarised in Table 3.

6.1.2 Compatibility with SPS operation mode

The GF PoP experiment can make use of a cycle within the normal SPS supercyle provided that the ion stripper foil can be moved in and out on a cycle-by-cycle basis (see Section 6.2.1) and also that any movable devices in the PoP experiment itself, like the X-ray detector, can be positioned outside the

Table 1: Transition energies (eV) of the $2s \to 2p_{1/2}$ and $2s \to 2p_{3/2}$ lines in the Pb, Li-like ion. To date there is no measurement of the $2s \to 2p_{1/2}$ energy.

$2s \to 2p_{1/2}$	$2s \to 2p_{3/2}$	year	method	reference
231.374	2642.297	1990	MCDF VP SE	[30]
230.817	2641.980	1991	MCDF VP SE	[31]
230.698	2641.989	1995	RCI QED NucPol	[32]
231.16	2642.39	1996	3-rd order MBPT	[33]
230.68	—	2010	RCI QED NucPol	[34]
230.76(4)	2642.17(4)	2011	S-m. 2-l. NucPol	[35]
230.823(47)(4)	2642.220(46)(4)	2018	RCI QED NucPol	[36]
230.80(5)	2642.20(5)	2019	S-m. 2-l. NucPol	[37]
—	2642.26(10)	2008	EBIT (measured)	[38]

Table 2: Transition energies (eV) of the $2s \to 2p_{1/2}$ and $2s \to 2p_{3/2}$ lines in the Xe, Li-like ion.

$2s \to 2p_{1/2}$	$2s \to 2p_{3/2}$	year	method	reference
119.84	492.22	1993	RCI QED NucPol	[39]
119.82	492.21	1995	RCI QED NucPol	[32]
119.83	492.23	2010	RCI QED NucPol	[34]
119.82	492.21	2011	S-matrix 2-loop NucPol	[35]
—	492.34(62)	1992	Beam-foil (measured)	[40]
119.820(8)	—	2000	Beam-foil (measured)	[41]

aperture needed for all other beams (or left in safely for all beams). In addition, the prompt radiation environment produced by other beams must be acceptable for the laser and cavity electronics.

Under these conditions a *dedicated* GF cycle could be used for the experiment with a flat-top length which could be up to $\sim 10\,\mathrm{s}$. For very specific measurements that require long flat-top length a dedicated coasting beam cycle could be used (see Section 6.2.3).

6.1.3 Summary of subsystems

Laser

The seed laser for the FPC version is described in detail in Section 6.3.1. An Yb laser operating at the fifth sub-harmonic of the RF, approximately $40\,\mathrm{MHz}$, and at a wavelength of $1034\,\mathrm{nm}$ is proposed, consisting of a low phase noise oscillator and two amplifier stages delivering about $50\,\mathrm{W}$ average power. A pulse stretcher and compressor together with tunable bandwidth filters are implemented to match the required spectral and temporal characteristics of the PSI beam.

Resonant cavity

The resonant cavity is described in detail in Section 6.3.3. The key features are a vertical crossing, with total cavity round-trip length $L = 7.5\,\mathrm{m}$ (mirror spacing of $3.75\,\mathrm{m}$), corresponding to a frequency of $40\,\mathrm{MHz}$, with the length tunable to match the PSI revolution frequency. A two-mirror geometry is

Table 3: SPS PoP experiment parameters.

PSI beam	$^{208}\mathrm{Pb}^{79+}$
m – ion mass	193.687 GeV/c^2
E – mean energy	18.652 TeV
$\gamma = E/mc^2$– mean Lorentz relativistic factor	96.3
N – number ions per bunch	0.9×10^8
σ_E/E – RMS relative energy spread	2×10^{-4}
ϵ_n – normalised transverse emittance	$1.5\,\mathrm{mm\,mrad}$
σ_x – RMS transverse size	$1.047\,\mathrm{mm}$
σ_y – RMS transverse size	$0.83\,\mathrm{mm}$
σ_z – RMS bunch length	$6.3\,\mathrm{cm}$
Laser	Infrared
λ – wavelength ($\hbar\omega$ – photon energy)	1034 nm (1.2 eV)
σ_λ/λ – RMS relative band spread	2×10^{-4}
U – single pulse energy at IP	$5\,\mathrm{mJ}$
σ_L – RMS transverse intensity distribution at IP ($\sigma_L = w_L/2$)	$0.65\,\mathrm{mm}$
σ_t – RMS pulse duration	$2.8\,\mathrm{ps}$
θ_L – collision angle	2.6 deg
Atomic transition of $^{208}\mathrm{Pb}^{79+}$	$2s \rightarrow 2p_{1/2}$
$\hbar\omega_0'$ – resonance energy	230.81 eV
τ' – mean lifetime of spontaneous emission	76.6 ps
$\hbar\omega_1^{\max}$ – maximum emitted photon energy	44.473 keV

proposed, with one motorised mirror. The mirrors will be placed inside the SPS vacuum, in a dedicated vessel which will contain the input and output windows. A crucial aspect for the integration of the laser cavity into the SPS is to keep the impedance of the system low enough in order not to disturb the high-intensity proton beam runs. This will be accounted for at the design phase of the FPC and will be further validated with SPS experts and dedicated simulations to make sure that it complies with the SPS specifications. In the current design of the FPC, an impedance shield is foreseen inside the vacuum vessel with two slots for the laser beam and RF contacts at the extremities.

Photon detection

The detection of the X-ray photons downstream of the interaction point will be performed with a dedicated in-vacuum monitor. Since the excited-state lifetime has a decay length of $\sim 2\,\mathrm{m}$, the flux and energy spectrum of the corresponding X-ray beam would depend on the distance from the IP to the position of the detector. The number of X-ray photon produced is high and would allow different detector technologies to be considered, including scintillators coupled to photomultipliers or a CCD camera, or semiconductors, such as Silicon pixel detectors or diamond detectors. The instrument will need a rather large dynamic range, since the off-resonance X-ray flux will be up to several orders of magnitude lower than on resonance.

For the initial experiment, the baseline solution is to use a detection system composed of a scintillating screen and a camera, see Section 6.4.2. This would provide a robust and simple solution that can be integrated into the accelerator beam line and its control system using technologies already available on the SPS.

Synchronisation

The laser and ion bunches require accurate and precise synchronisation. A new master RF oscillator at high frequency (for instance $400\,\mathrm{MHz}$) can be used to lock both the laser and the SPS RF system. This system, similar to the one used for the AWAKE experiment, would provide stable and reproducible synchronisation between the laser pulse and the ion bunch. A variable fine delay will be required to allow the precise adjustment of the phasing between both beams.

6.1.4 Experimental stages and procedure

The experimental procedure can be divided into two basic stages of "Resonance Finding" and "Optimisation and Characterisation" to demonstrate the basic concept of resonant exciting highly relativistic atomic transitions and detecting the emitted photons, with two further stages of "Cooling" and "Atomic Physics" targeted at demonstrating the feasibility of specific applications.

Stage 1: Resonance finding

The natural resonance linewidth Γ is around $10^{-5}\,\mathrm{eV}$, which means that the rest-frame spread in resonant energies in the ensemble of ions in the bunch is dominated by the Doppler broadening arising from the momentum spread. This is of the order of $0.05\,\mathrm{eV}$ for a RMS momentum spread σ_p/p of 2×10^{-4}.

To maximise the fraction of the ions in resonance, a number of experimental parameters need to be tuned independently:

- the relative timing between the laser pulse and the PSI bunch, referred to as the synchronisation;
- the PSI beam energy to match the photon energy in the ion reference frame to the central transition energy;
- the spatial overlap between the ion and laser beams in the vertical and horizontal planes.

The laser beam transverse size at the IP is $\sigma_L = 0.65\,\mathrm{mm}$, comparable to the ion bunches of around $\sigma_x = 1.2\,\mathrm{mm}$ in the horizontal plane and $\sigma_y = 0.8\,\mathrm{mm}$ in the vertical one. The initial alignment of the PSI beam will make use of two BPMs located upstream and downstream of the laser cavity (see Secion 6.2.5). These BPMs will be fiducialised to the laser system to ensure a relative alignment between their electric centre and the design IP of $\Delta^{\mathrm{BPMs}}_{xy,\,\mathrm{fiducial}} < 0.1\,\mathrm{mm}$. With a typical performance in the measurement of a closed orbit these BPMs should measure the position of the PSI beam with an error $\Delta^{\mathrm{BPMs}}_{xy,\,\mathrm{beam}} < 0.1\,\mathrm{mm}$. Therefore a conservative estimate of the total transverse initial misalignment between the laser and beam axis in the horizontal plane is $\Delta x < 0.2\,\mathrm{mm}$.

In the vertical plane the same initial misalignment of $\Delta y < 0.2\,\mathrm{mm}$ is considered. However, the laser axis crosses the ion beam axis with the design crossing angle of $\theta_L = 2.6°$ in that plane which transforms a vertical misalignment into a longitudinal one of $\Delta y \to s < 4\,\mathrm{mm}$. Depending on the model used for the interaction between the ion bunch and the laser, either of those quantities may be used.

The control of the temporal overlap between the laser pulse and the ion bunch is critical and is further discussed in Section 6.3.7. This will be controlled by the SPS phasing or cogging system. The implementation could be very similar to the system already in use for the synchronisation of the extracted bunch and laser of the AWAKE experiment [42]. The proposed system is discussed Section 6.2.5 and would ensure an initial timing offset $\Delta t < 0.5\,\mathrm{ns}$.

For the spectral overlap, the nominal RMS relative laser bandwidth of 2×10^{-4} is identical to the RMS Doppler spread in the ion beam of 2×10^{-4}. The relative uncertainty in the calculated transition energy is around 2×10^{-4} or $46\,\mathrm{meV}$ in the ion reference frame. The central laser frequency will be measured with a much better precision and can thus be neglected. The absolute relative SPS momentum stability is about 1×10^{-4}, while the relative uncertainty on the absolute value is estimated at 3×10^{-4} [43,44]. It adds an absolute uncertainty on the energy of the photon in the ion reference frame of $69\,\mathrm{meV}$.

We also consider a misalignment of the laser cavity mirrors by $0.25\,\mathrm{mm}$ causing a relative uncertainty on the interaction angle of $0.5\,\%$ or $\Delta\theta = 0.227\,\mathrm{mrad}$ and a shift in the energy of the photon in the ion reference frame of $1.2\,\mathrm{meV}$. Overall, these combine to give a total maximum (i.e. linear sum) uncertainty in the relative energy of $116\,\mathrm{meV}$, or around $\pm 5 \times 10^{-4}$ relative. Therefore a systematic scan of the SPS PSI beam momentum in 5 steps of 2×10^{-4} is assumed to be needed to bring the system into resonance and we can consider a relative energy offset of $\Delta E/E = 2 \times 10^{-4}$.

Those expected initial offsets are summarised in Table 4. Overall, for this initial resonance finding, the spatial and time overlap between the PSI bunch and the laser pulse is ensured by the laser cavity instrumentation and its accurate fiducialisation. The matching of the PSI beam to the laser energy is accomplished by a small scan in beam momentum.

Table 4: Initial offsets between the ion bunch and the laser pulse.

Δx – Horizontal offset	$0.2\,\mathrm{mm}$
Δy – Vertical offset	$0.2\,\mathrm{mm}$
Δt – Timing offset	$0.5\,\mathrm{ns}$
$\Delta E/E$ – Relative energy offset	2×10^{-4}

In case excitation is not detected at this stage, for example because of a very large undetected systematic offset in the cavity BPM readings, two fallback scenarios could be implemented. The PSI beam could be diluted in every dimension in order to observe at least some photons. The SPS transverse damper and RF system can be configured to achieve the required blow-up in all 6 dimensions. Alternatively or in addition, systematic scans of the transverse beam position at the IP and energy of the PSI beam could be repeated until X-ray photons are detected.

Stage 2: Optimisation and Characterisation

Once an X-ray signal has been reliably detected, an optimisation routine can be deployed to maximise the signal, using the four parameters listed Table 4 and the X-ray detector signal as the observable. The advantages of a numerical approach are speed and resilience to any systematic drifts or hidden dependencies. For instance, the relative timing is correlated to the vertical position of the IP. This optimisation is somewhat complicated by the natural decay of the PSI intensity, an effect which will need to be factored into the algorithm.

An important part of the experiment will then consist in careful measurement of the dependencies of the observed signal on the parameters under control. For this PoP, the aim is to make measurements from which basic 'physics' parameters can be derived: reproducibility, stability, resonance width, resonant frequency, cross section and excited-state lifetime. The possible observables are the X-ray flux and the X-ray energy spectrum, and the parameters that can be varied are the laser power, the laser–PSI phase, the laser–PSI offset in position and angle, the PSI relativistic γ-factor (beam momentum), and the PSI bunch length and momentum spread. The response of the X-ray signal to the controlled variations in these parameters will be the basis for the determination of the physics parameters.

Some time will be dedicated to measuring the reproducibility of the signal, both for the cycle-to-cycle stability and also the stability of the signal decay through the fill. For this, the tools already in use in the SPS for the analysis of the harmonic content of the slow extraction can be deployed, again taking into account the natural signal decay [45]. This will also give information about the stability of the resonance through the SPS fill, which will be affected by variations in the contributing machine parameters, like the momentum. Methods of untangling these variations from the signal reduction obtained through the PSI lifetime and emittance growth need to be developed, in order be able to properly measure the PSI lifetime.

Calculations of the excitation cross section from the measurements will require absolute measurement of the flux, knowledge of the excited state lifetime, together with as precise as possible knowledge of the 6D PSI distribution, as well as the laser beam intensity distribution in space, time and energy at the IP.

The measurement of the resonance width will be dominated by the Doppler broadening, and only the width of the ensemble (basically the momentum spread) can be characterised. The accuracy of the measurement of the resonant frequency (transition energy) will be determined by the momentum spread and distribution in the beam, as well as the knowledge of the SPS momentum and of the laser spectral distribution.

Characterisation of the PSI beam size evolution through the fill in the different dimensions will be important. It may also be required to make systematic measurements of the bunch characteristics if the cycle-to-cycle variation is large, to factor out the dependence of the measured X-ray flux on those parameters.

Stage 3: Cooling demonstration

The feasibility of cooling will be investigated once the basic setup and optimisation is complete. For this, a precise relative alignment of the SPS momentum with the laser wavelength is needed to ensure that the optimum number of PSIs with positive momentum offset are excited, maximising the cooling rate (see Section 6.5).

Achieving this precise alignment is likely to be somewhat delicate, and will rely on the previous measurements of stability and drift. If the machine is reproducible enough, the initial adjustment of the particle momentum would be enough. Otherwise, a precise scan of the momentum might be needed to find the resonance, maximising the X-ray flux to fix the optimum particle momentum. If this needs to be done for every cycle (for instance if the reproducibility is a sizeable fraction of the laser bandwidth) then an automatic tool will be needed. With a relative laser bandwidth of $\sim 2 \times 10^{-4}$ and the expected momentum reproducibility around an order of magnitude smaller, this should not be considered as an issue (see Section 6.2.6).

Once optimised, the longitudinal cooling will be observed as a reduction in bunch length, which could be detected in the SPS by the existing wall current monitor. The effects of the transverse cooling are more difficult to observe as the reduction in emittance is expected to be slower. The transverse beam size monitor currently installed in the SPS, based on beam gas ionisation (BGI) [46], could be used for that purpose.

Stage 4: Atomic Physics demonstration

The phase 1 photon detector setup discussed in Section 6.4.2 will allow us to enter the domain of atomic physics measurements with ultra-relativistic atomic beams. A measurement of the $2s \rightarrow 2p_{1/2}$ transition energy will be the first measurement of the "Lamb-like-shift" in high-Z Lithium-like atoms by their direct excitation. Achieving an ultimate measurement precision of atomic transitions in high-Z atoms below the 10^{-4} level, in phase 2 of the PoP experiment operation, would allow us to study the relativistic, vacuum polarisation, electron–electron interaction and weak interaction effects with unprecedented precision.

Initially, the measurement of the absolute SPS beam energy, using the present dedicated calibration techniques [43, 44], is expected to be accurate to 0.04% and will limit the precision of the absolute measurement of transition energies to that level. Other factors limiting the measurement precision that will have to be studied and taken into account are the RMS momentum spread in the beam of 0.02% and the imperfect knowledge of the detailed longitudinal distribution. They may limit the precision on the spectroscopic measurement at around the same level. The impact of these factors are expected to be largely reduced by Doppler cooling of the PSI beams. Other effects, like the PSI intensity decay and emittance growth, will also need to be studied and accounted for.

The initial, phase 1, measurement of the excited-state lifetime with a single plane detector will be very crude. Its precise determination will require adding new detector planes at suitable spacing downstream and introducing the secondary photon collimation system allowing to separate early and late decays of excited atoms. This could be done in phase 2 of the PoP experiment following the LS3 shutdown. In this phase, new techniques of absolute calibration of the SPS energy, based on dedicated SPS runs with low-Z PSI beams and/or with non-zero spin ions could also be employed to improve the precision of the atomic transition energies measurement below the 10^{-4} level. In the first case, the SPS beam energy could be calibrated using calculated transition energies for low-Z atoms for which the relativistic, vacuum polarisation, electron–electron interaction and weak interaction effects can be neglected. In the second case, the measurement could be based on optical pumping of the nucleus polarisation followed by the measurement of the nucleus spin precession. Finally, complementary methods developed for the calibration of the electron beam energy by Compton back-scattered laser photons at the VEPP-2000 electron-positron collider [47] could also be used. They were demonstrated to provide a 5×10^{-5} precision of the absolute energy calibration.

Another exciting phase 2 option for the atomic physics research would be to search for exotic excited states of the lithium-like lead atoms, in particular long-lived states which could be excited by beam-gas collisions. The photon detector system would have to be upgraded to measure single photons with high spacial and energy resolution.

Finally, the phase 2 of the experiment may involve a precise relative measurement of the differences in the atomic energy levels for the four available lead isotopes. These measurements could provide a precise insight into the internal structure of the nuclei.

6.2 Partially stripped ion beams in SPS

The SPS presently operates at 450 GeV energy for the LHC proton injection and at 400 GeV for the Fixed-Target protons to the North Area (NA). In addition, ion species including fully- and partially-stripped ^{208}Pb have been accelerated and transferred to the NA and the LHC. For long fills (coasts) where the flat-top length is greater than about $10\,\mathrm{s}$, the proton energy is limited to 270 GeV (magnetic rigidity of $900\,\mathrm{T\,m}$) by the maximum RMS power the network can supply for the SPS dipoles and quadrupoles.

An important parameter for the Gamma Factory experiments is the average vacuum pressure, which determines the PSI lifetime – this is $1.2 \times 10^{-8}\,\mathrm{mbar}$, since the SPS vacuum system is not baked out. The main parameters of the SPS accelerator pertaining to the PoP experiment are shown in Table 5.

Table 5: SPS accelerator parameters.

Circumference	6911.566 m
f_{rev} ($^{208}\mathrm{Pb}^{79+}$ γ96)	43 373 Hz
f_{RF} ($^{208}\mathrm{Pb}^{79+}$ γ96)	200.384 MHz
Transition γ	22.7
Transverse horizontal tune	26.13
Transverse vertical tune	26.18
Maximum magnetic rigidity (cycled)	1498.2 Tm
Maximum magnetic rigidity (coast)	900 Tm
Average vacuum pressure	1.2×10^{-8} mBar
Annual total operational time	5150 h
Annual physics (FT) time	3200 h
Annual dedicated machine development time	370 h

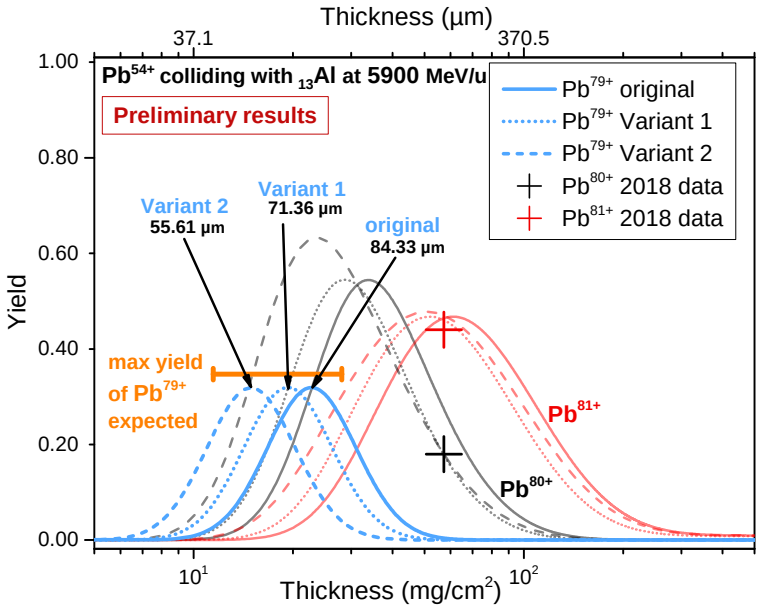

Fig. 4: Transmission efficiency simulations using BREIT for the production of $^{208}\mathrm{Pb}^{80+}$and $^{208}\mathrm{Pb}^{81+}$. A thinner foil of about 70 µm will be used for a 35% yield of $^{208}\mathrm{Pb}^{79+}$. The plot also shows the measured values during the SPS tests in 2018, black cross for $^{208}\mathrm{Pb}^{80+}$and red cross for $^{208}\mathrm{Pb}^{81+}$.

6.2.1 Ion Stripping in PS to SPS Transfer Line

The minimum solution to deliver the beam of the $^{208}\mathrm{Pb}^{79+}$ ions to the SPS is based on the existing stripper infrastructure and on the present scheme for the fully stripped ion beam. The existing stripper station in the PS–SPS transfer line will have to be equipped with a new foil which can be retracted every supercycle for the other beam types. The foil material and thickness should maximise the production rate of the $^{208}\mathrm{Pb}^{79+}$ ions by stripping 25 electrons of the initial $^{208}\mathrm{Pb}^{54+}$ ions delivered by the PS beam.

One of the multiple goals of the beam tests with $^{208}\mathrm{Pb}^{81+}$ and $^{208}\mathrm{Pb}^{80+}$, discussed in Section 5.2, was to calibrate the BREIT simulation code [48]. This code was then used to define the requisite stripper material and the stripper thickness. In Fig. 4 the measured stripping efficiencies for the $^{208}\mathrm{Pb}^{81+}$ and $^{208}\mathrm{Pb}^{80+}$ beams with the initial beam of $^{208}\mathrm{Pb}^{54+}$ are shown. Three versions of the BREIT code, adjusted to describe the measurements, were used to extrapolate these results to the case of the $^{208}\mathrm{Pb}^{79+}$ beam and to define the optimal thickness of the Aluminium foil and its uncertainty. The maximum stripping efficiency ($^{208}\mathrm{Pb}^{79+}$ production fraction) which can be achieved is 35%.

6.2.2 Ion beam performance and bunch characteristics

For the proposed stripping scenario the characteristics of the atomic beam of the $^{208}\mathrm{Pb}^{79+}$ ions can be unambiguously extrapolated from the typical beam conditions in the SPS during the canonical operation of the beam of the fully stripped lead ions.

Table 6 shows the relevant beam parameters expected for the PoP experiment. The longitudinal parameters are achieved with a total RF gap voltage of 7 MV. Lower voltages down to $\sim$ 2 MV are possible to achieve a lower momentum spread, at the expense of the larger bunch length. Concerning the bunch pattern, two scenarios are possible and both were used in 2018 for the fully stripped lead beam [49]:

– 4 bunches separated by 100 ns and up to 9 injections separated by 150 ns,

– 3 bunches separated by $75\,\mathrm{ns}$ and up to 12 injections separated by $150\,\mathrm{ns}$.

These two schemes see different spacing between bunches. A system running at least at $40\,\mathrm{MHz}$ would be capable of interacting with every bunch. The ions per bunch at injection is derived from the LIU target [50] (see Table 2.4 therein), scaled by the transmission efficiency of $^{208}\mathrm{Pb}^{79+}$.

Table 6: $^{208}\mathrm{Pb}^{79+}$ bunch parameters in the SPS. Ions per bunch at injection is calculated from the LIU target bunch intensity in SPS [50] for the fully stripped lead ions, scaled by the stripping efficiency of $^{208}\mathrm{Pb}^{79+}$calculated using BREIT and shown in Fig. 4.

Transverse normalised emittance	$1.5\,\mathrm{mm\,mrad}$
Bunch length	$213\,\mathrm{ps}$
Momentum spread	2×10^{-4}
Expected lifetime	$100\,\mathrm{s}$
Ions per bunch at injection	0.9×10^{8}
Maximum number of bunches in the ring	36

6.2.3 Operational scenarios

The SPS is a cycling machine serving different users from cycle to cycle according to a programmable sequence which is called the supercycle. The proposed experiment will require a short cycle within the SPS supercycle to do most of the beam commissioning and measurements. In case acceleration up to different energies is needed, each flat-top energy will correspond to a different cycle. This operational scenario has been already demonstrated during the 2017 and 2018 beam tests.

Only for specific measurements or in the case the resonant finding procedure that require to spend more than $10\,\mathrm{s}$ at flat-top, a dedicated coasting beam cycle could be used.

The maximum acceptable RMS resistive power dissipated in the main dipole magnets for the SPS is $37.9\,\mathrm{MW}$, while the total maximum power for the main dipoles and the main quadrupoles is $44\,\mathrm{MW}$. This constraint may, for large momentum beams, limit the possible supercycle combinations, and also the allowed maximum flat-top length. This is illustrated in Fig. 5. The beam can be coasted for indefinite periods only if the momentum of the beam particles satisfies the condition: $p \leq 270\,\mathrm{ZGeV/c}$, which corresponds to the maximal value of $\gamma = 110$ for $^{208}\mathrm{Pb}^{79+}$. For the $^{208}\mathrm{Pb}^{79+}$ beam having its momentum tuned to excite the $2s \rightarrow 2p_{1/2}$ atomic transition $\gamma = 96.3$. The flat-top length for such a beam is thus not constrained by the maximal value of the power dissipated in the SPS magnets.

6.2.4 Location for Interaction Region

The SPS has six Long Straight Sections (LSS), each with four dipole-free half cells with about $30\,\mathrm{m}$ drift space. At the extremities of each LSS a dispersion suppression cell has 2 missing dipoles at the end of the first arc cell with a drift space of around $13\,\mathrm{m}$. Much of the LSS space is taken up with the existing equipment (RF in LSS3, injection in LSS1, dump in LSS5, slow extraction in LSS2). The main criteria for the selection of suitable locations are:

– no major changes can be made to the SPS lattice (main magnets, key functional elements);
– the installed equipment must be compatible with aperture required for the Fixed-Target and LHC beams;
– the radiation environment should be as low as possible (prompt and residual);
– a location with strong bumper magnets is preferred for steering beam at high energy.

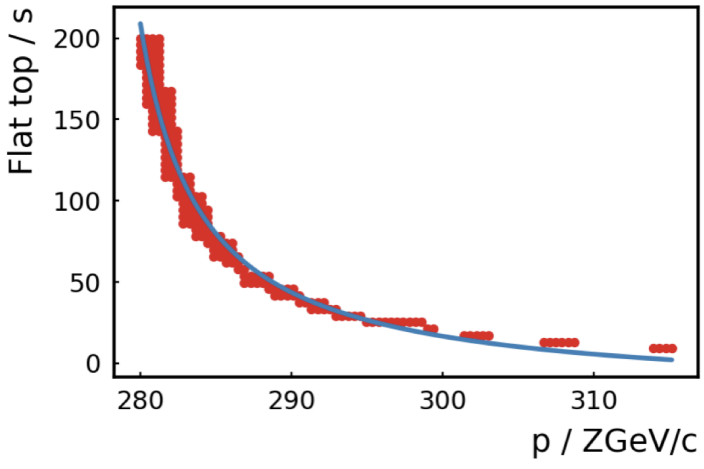

Fig. 5: The maximum possible SPS flat-top length as a function of beam momentum, respecting the power limits in the main magnets. For $^{208}\mathrm{Pb}^{79+}$ a momentum of $280\,\mathrm{ZGeV/c}$ corresponds to a γ of 114, for which a maximum flat-top length of around $200\,\mathrm{s}$ would be possible.

Locations on the LSS were investigated first, and the half-cell 621 has been selected in the drift left by the missing dipoles for the dispersion suppressor. The location is free of other devices and can make use of the strong dipole (extraction bumper) magnets used to establish the SPS extraction trajectory.

Fig. 6a shows a top view of the region with the SPS tunnel, the TT60 line for fast extraction of the SPS beam towards the LHC or HighRadMat and the TI18 side tunnel. This tunnel was used for transferring positrons from the SPS to the LEP, and is now empty. As it lies very close to the SPS ring it is proposed to be used to house the laser electronics in order to shield it from radiation coming from the SPS (see Section 6.3.8). In addition, the existing penetrations between the SPS and the side tunnel could be used to transport the primary laser beam to the laser cavity – they can be seen on the top left corner of Fig. 6b.

Optical lattice parameters at IP

The optics assumed for the GF PoP experiment is based on an integer tune of 26 (Q26) and is standard for the Pb ion beams for the LHC and the NA. The optics parameters at the IP are listed Table 7, together with the RMS beam sizes obtained with the beam parameters in Table 6. The beam size, divergence, dispersion and dispersion derivative are all important for the dynamics of the laser–PSI interaction.

Layout and aperture constraints

Figure 7 shows the evolution of the beam size and optical functions around the proposed PoP experiment location. To ensure that the PoP does not interfere with nominal SPS operation we consider the space around the reference beam axis that needs to be kept free of any element, the stay-clear region. In the horizontal plane this region is computed based on the maximum excursions of:

- injected proton fixed target beam at $14\,\mathrm{GeV}$ and the $12\,\mathrm{mm\,mrad}$ normalised emittance plus the alignment error and tolerances;
- slowly extracted separatrix with $400\,\mathrm{GeV}$ protons on the 1/3 resonance (asymmetric);
- the bumped or extracted beam, although not a concern in the dispersion suppressor region.

In the vertical plane only the injected proton fixed target at $14\,\mathrm{GeV}$ and the $8\,\mathrm{mm\,mrad}$ normalised

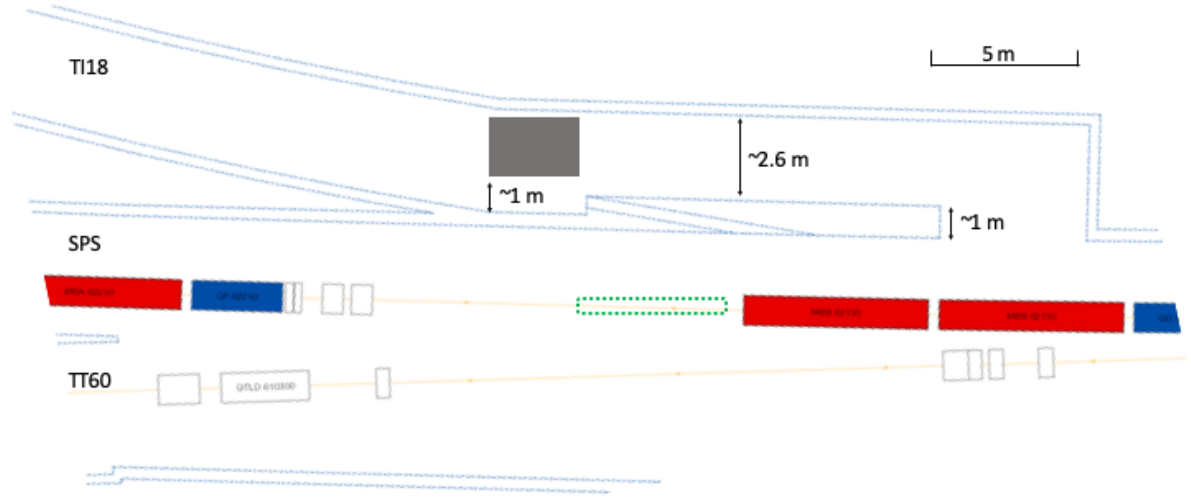

(a)

(b)

Fig. 6: (a) The schematic view around the SPS half-cell 621 with the proton beam going from right to left and (b) panoramic picture taken from downstream the cell. The green-dashed box represents the location considered for the laser cavity and the red-dashed box the projected location of the optical room located in TI18 on the SPS wall. The optical room is represented with a filled grey rectangle on the schematic view (a). Some approximate lengths are also given.

emittance is considered, with the alignment error and tolerances. The resulting stay-clear regions in each plane is shown as dotted lines in Fig. 7. The aperture of the SPS magnetic elements is sized to roughly follow the envelope of the largest beams accelerated and we can see that the stay-clear region is very close to the apertures of the elements on either sides of the dispersion suppressor. In details, the stay-clear region is $90\,\mathrm{mm} \times 45\,\mathrm{mm}$ (for horizontal and vertical planes) at the entrance of the laser cavity and $108\,\mathrm{mm} \times 38\,\mathrm{mm}$ at the exit. At the location considered for the X-ray detector ($s = 6458\,\mathrm{m}$) the stay-clear region is $118\,\mathrm{mm} \times 34\,\mathrm{mm}$.

Table 7: Optical parameters at the IP in the half-cell 621.

s Azimuthal position	6451 m
$\alpha_x = -\frac{1}{2}\delta\beta_x/\delta s$	-1.549
β_x	55.32 m
D_x	2.462 m
DP_x	0.0976
$\alpha_y = -\frac{1}{2}\delta\beta_y/\delta s$	1.301
β_y	43.87 m
D_y	0.0 m
DP_y	0.0
$\sigma_{px} = \sqrt{\epsilon_x\gamma_x + (\delta p/pDP_x)^2}$	3.66×10^{-5}
$\sigma_{py} = \sqrt{\epsilon_y\gamma_y + (\delta p/pDP_y)^2}$	3.09×10^{-5}
$\sigma_x = \sqrt{\epsilon_x\beta_x + (\delta p/pD_x)^2}$	1.05×10^{-3} m
$\sigma_y = \sqrt{\epsilon_y\beta_y + (\delta p/pD_x)^2}$	8.27×10^{-4} m

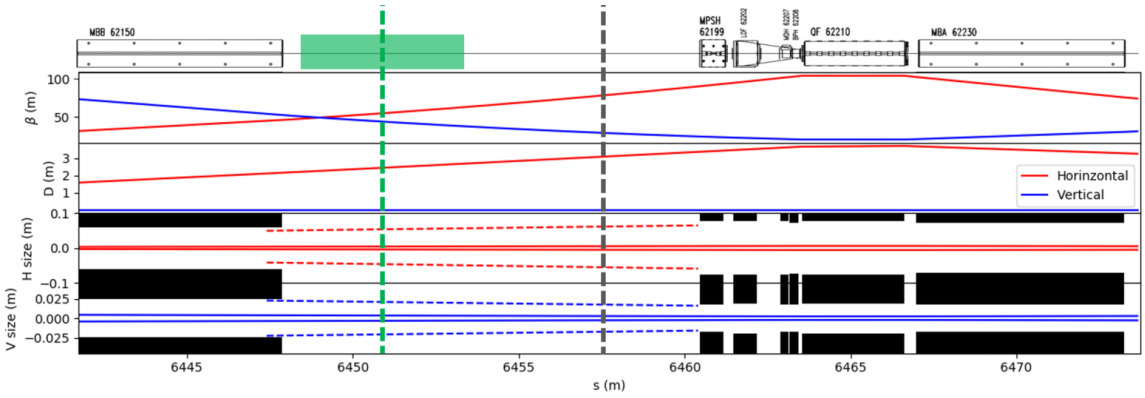

Fig. 7: Layout, optical functions and beam sizes with aperture limits around the interaction region. The IP is represented by a vertical green dotted line and the laser cavity by the green box. The vertical grey dotted line represents the location of the X-Ray detector. Note that the beam goes from left to right.

6.2.5 Beam control and diagnostics

Transverse beam position and size

Two Beam Position Monitors (BPM) will be installed upstream and downstream of the FPC in order to guarantee a good spatial overlap between the ion and the laser beams. The BPMs should be mounted on the same girder as the laser cavity mirrors and should be pre-aligned with respect to those mirrors with a precision better than $100\,\mu\mathrm{m}$ using metrology technique in the laboratory. The BPM electronic read-out system will use a CERN standard system, called 'DOROS' [51], which has already demonstrated in the SPS a few microns resolution. The existing SPS orbit corrector system is expected to effectively cover the required range of beam motion at the IP to control the spatial overlap between the ion beam and the laser pulse. At the rigidity considered for the PoP experiment, the SPS lattice correctors have modest strength. A typical range to move the trajectory of the beam in a 3-bump configuration is around $5\,\mathrm{mm}$, significantly larger than what should be needed. In case it is needed, resonant bumps with multiple lattice correctors give access to a much larger range of beam movement. In the horizontal plane the

strong dipole corrector MSPH.62199 located downstream of the FPC could also be used to move the ion beam.

The transverse beam size can be increased if needed (for example to reduce the search space for the resonance finding) by using the transverse damper for controlled emittance blow-up. This will be in an expert mode, with support from the RF experts for each set up. To reach the maximum possible beam size the blow-up takes several seconds and needs to start before the ramp. Wire scanners are generally used to measure the transverse beam size in the SPS. That will not be possible with the PSI beam as interaction with the wire would quickly strip electrons from the ions. However, beam-gas ionisation monitors [46] would provide a continuous measurement of the transverse beam size through the cycle.

Energy control

Control of the energy of the ion beam is critical to excite the PSI transition. However, in a synchrotron this can be achieved through the change of different machine parameters and with varying effects. We discuss here 3 cases referred as constant frequency, constant optics and constant field cases.

Constant frequency constraints the beam revolution frequency to be fix by maintaining the RF frequency f_{rf}. Note that the revolution frequency $f_{rev} = 1/hf_{rf}$ with $h = 4620$ the SPS harmonic number at flat-top and that the laser cavity frequency is locked to the revolution frequency:

$$f_{cav} = \frac{h}{5} f_{rev}. \tag{3}$$

We can now relate the SPS average bending field relative variation in the SPS dB/B to the relative change in momentum dp/p:

$$\frac{dB}{B} = \gamma_t^2 \frac{df_{rev}}{f_{rev}} + \frac{\gamma^2 - \gamma_t^2}{\gamma^2} \frac{dp}{p} \tag{4}$$

with γ the Lorentz factor of the PSI beam and γ_t the SPS transition energy. As we fix the RF frequency we have $df_{rev} = 0$ and the first term on the righ-hand side vanishes. Considering $dp/p = 10^{-3}$ the needed relative change in the field is $dB/B = 0.945 \times 10^{-3}$.

However, as the IP is in a dispersive region with $D_x = 2.462\,\mathrm{m}$ we also need to consider that a shift in the beam momentum will also change the beam trajectory at the IP by $dx = D_x \times dp/p \simeq 2.5\,\mathrm{mm}$ in the case we consider. Although non-negligible, such a shift can be easily compensated by the SPS orbit control, discussed in Section 6.2.5.

Constant optics constraints the beam trajectory by synchronously changing the RF frequency and the dipole magnetic field. Changes in the beam revolution frequency, momentum and average radius R are linked through:

$$\frac{df_{rev}}{f_{rev}} = \frac{1}{\gamma^2} \frac{dp}{p} - \frac{dR}{R}, \tag{5}$$

but, as we consider that the field is synchronously changed to fix the trajectory, we have a fixed average radius and $dR = 0$. Considering $dp/p = 10^{-3}$, with the conditions of the PoP $df_{rev}/f_{rev} = 1.04 \times 10^{-7}$ or $df_{rev} = 0.004\,66\,\mathrm{Hz}$.

From Eq. (3) we can see that a change in revolution frequency of the ion beam has to be followed by the optical laser cavity length:

$$L = 5 \frac{c}{h \times f_{rev}} \tag{6}$$

with c being the speed of light. Then, we can derive the relation between the cavity length and the revolution frequency variations:

$$dL = -5 \frac{c}{h} \frac{1}{f_{rev}^2} df_{rev} \tag{7}$$

and in our case we find that for $dp/p = 10^{-3}$, $dL = -804\,\mathrm{nm}$.

Constant field case fixes the magnetic field of the SPS while the RF frequency is changed to change the beam momentum. The relevant differential relation is:

$$\frac{dB}{B} = \gamma_t^2 \frac{df_{rev}}{f_{rev}} + \frac{\gamma^2 - \gamma_t^2}{\gamma^2} \frac{dp}{p}, \tag{8}$$

but as we fix $dB = 0$ it simplifies to $df_{rev}/f_{rev} = \eta dp/p$ with $\eta = 1/\gamma^2 - 1/\gamma_t^2$ the momentum compaction factor.

Considering a relative change in momentum of $dp/p = 10^{-3}$ and with the PoP specifications we find $df_{rev}/f_{rev} = -1.83 \times 10^{-6}$ or $df_{rev} = -0.0795\,\mathrm{Hz}$. But again, the most relevant quantity is the associated change in the cavity length $dL = 13.7\,\mu\mathrm{m}$.

The case of constant frequency is favoured as any change in length of the cavity beyond several nanometres would cause a loss of its internal lock and take possibly minutes to recover from (see Section 6.3.3).

Synchronisation and longitudinal beam diagnostics

The laser timing system is further described in Section 6.3.7. The control of the temporal overlap between the laser pulse and the ion bunch is critical and will be primarily controlled by the SPS RF phasing or cogging system. The implementation could be very similar to the system already in use for the synchronisation of the extracted bunch and laser of the AWAKE experiment [42]. In addition, an independent and local measurement of the temporal overlap between the ion bunch and the laser pulse will be performed close to the IP. It would rely on the simultaneous monitoring of the signals from the BPMs and from a laser diode using fast digitisers. Taking into account all cable and optical delays, a robust and direct measurements of the two beam temporal overlap can be easily obtained with an error of $\Delta t < 0.5\,\mathrm{ns}$.

The existing SPS wall current monitor would provide precise bunch length measurements. Calculations for a bunch of 10^{11} charges and $250\,\mathrm{ps}$ showed a very good accuracy of 2.5% [52]. The nominal initial conditions of the GF PSI beam are very similar and it is expected that the longitudinal cooling will can be observed using this device.

Longitudinal tomography is also being developed, but will probably only be available for reconstructing measurements, not on-line [53].

6.2.6 Uncertainties, reproducibility, ripple and noise

The standard deviation of the measured cycle to cycle orbit position for the Q26 optics around the whole machine is $200\,\mu\mathrm{m}$ in the horizontal plane and $50\,\mu\mathrm{m}$ in the vertical, measured always at maximum beta of about $109\,\mathrm{m}$ [54]. Using the optics parameters at the IP the expected standard deviation of the position of the ion beam is around $140\,\mu\mathrm{m}$ in the horizontal plane and $30\,\mu\mathrm{m}$ in the vertical plane. Those jitters are much smaller than the beam size and should therefore have only a small impact on the fraction of excited ions per crossing.

From the measurements documented in [54] the beta beating is estimated to be 25% in the horizontal plane and 10% in the vertical plane. This translates into an uncertainty on the ion beam size of around 10% in the horizontal plane and 5% in the vertical plane. Such systematic shift from the nominal conditions considered here should only have a minor effect on the fraction of excited ions and are neglected here.

The measured cycle-to-cycle stability of the beam momentum is 1.3×10^{-5}, as measured in 2015 [55]. Larger shifts and longer term drifts, for instance when the supercycle composition is changed, is of the order of 2×10^{-4}.

6.3 Optical system

Given the chosen ion species, the transition energy and the lifetime of the resonance are determined. The width of the transition of the ions in their rest frame $\Gamma = \hbar/\tau' \approx 9 \times 10^{-6}\,\mathrm{eV}$, which corresponds to a spectral bandwidth of the laser, in the laboratory frame, of $\Delta\nu \approx 1/4\pi\gamma\tau'$. It is determined by the requirement that the laser wavelength λ matches the transition energy $\hbar\omega_0' \approx 2\gamma hc/\lambda$. The choice of the laser wavelength is driven by the availability of a high average power mode-locked laser system. It is thus decided to avoid frequency doubled laser systems which would induce, de-facto, a loss of pulse energy. If a FPC is used for pulse energy enhancement at the interaction point, the choice of a green laser would additionally induce increase losses by absorption in the optical coatings, and in turn increase the issues related to high-power stacking in FPCs. It is thus decided to pursue the studies with a laser wavelength in the infrared, and as a baseline we choose $\lambda \approx 1034$ nm, though other wavelengths may be considered in the range of $1020 - 1070$ nm. This choice corresponds to a Lorentz factor $\gamma \approx 100$ and thus $\Delta\nu \approx 10$ MHz. The corresponding laser bandwidth is consequently of $\Delta\lambda \approx \lambda^2\Delta\nu/c \approx 35$ am. However, the ion energy spread $\sigma_E/E \approx 2 \times 10^{-4}$ induces large broadening of the required laser spectrum $\sigma_\lambda \approx \lambda\sigma_E/E \approx 0.2$ nm, so that most of the ions are excited by the laser pulse.

In order to excite a large fraction of ions at each turn in the SPS ring, the laser-beam must deliver a few millijoules per interaction at least. Two strategies can be considered. Either (1) interaction with a single ion bunch at a rate of about 43 kHz , or (2) interaction with all ion bunches at rates of 5 MHz to 20 MHz, corresponding to a bunch spacing of 200 to 50 ns. Both options are considered in this section.

The design of the optical system is constrained by the transition energy of the chosen ions for the PoP experiment, the ion beam size and duration, and finally by the requirement to integrate it in the SPS ring, considering both footprint and radiation levels. We first review the constraints in terms of performances of the laser system and then discuss its integration in the SPS at the end of this section.

6.3.1 Laser oscillator and amplifier

Assuming a single ion bunch interaction scenario, the laser system should deliver at least $5\,\mathrm{mJ}$ and $43\,\mathrm{kHz}$, leading to an average power exceeding $200\,\mathrm{Watts}$. Considering the installation in the SPS, with very restricted access, the laser driver can only be an industrial-proven laser system. Commercial laser systems delivering a few tens of Watts at a few tens of kHz repetition rates are available [56–60]. Nowadays, in the picosecond regime, two technologies are considered mature: one based on an Ytterbium doped thin-disk amplifier and the second one based on a large mode area Ytterbium fiber amplifier. A robust alternative is a hybrid architecture combining both technologies, with the fiber for the low-power front-end and the thin-disk amplifier for the final high-energy laser amplifier. As an example, systems delivering between 2 and $15\,\mathrm{mJ}$ are sold by TRUMPF (DIRA series of scientific systems) [61, 62]. ActiveFiber GmbH [63] or Amplitude Laser [64] sell the fiber amplifier delivering up to a few hundreds of Watts. The footprint of these laser systems does not exceed $2\,\mathrm{m}^2$. However these state-of-the-art high-power laser systems are very expensive, in the > 1 MCHF range. The TANGOR system from Amplitude Laser [65] based on the hybrid approach could deliver either a few μJ at $40\,\mathrm{MHz}$, which would be nicely suited to seed the FPC (see later) or also up to $500\,\mu\mathrm{J}$ at $43\,\mathrm{kHz}$. This is well below the initially targeted energy per pulse, but the flexibility of this system is interesting. The system allows tuning of the spectral bandwidth and thus the pulse duration [66], which maybe useful for optimisation of the interaction rate and understanding the validity of the simulations. Moreover, this system in the range of $0.5\,\mathrm{MCHF}$, being able to be used in a single shot and in an optical cavity mode may be of interest in a situation where there is a need to mitigate the experimental risk related to the implementation of the FPC in the SPS tunnel. Despite these systems are all integrated products, their operation in the SPS environment must be evaluated. Indeed, the pulse energy and duration considered here preclude any long-distance beam-transport line. However, located in the side tunnel close to LSS621, constraints related to the radiation field seem to be reduced. These systems are also expected to be relatively expensive compared to the proposal to use the FPC. In LSS621, the interaction point could be located in a long

chamber tube with a folding mirror allowing to get a small crossing angle. The laser beam could be transported under a vacuum pipe and chambers from the side tunnel where the driver laser system could be installed. The spatial matching of the laser beam to the transverse ion bunch size can be done with the help of imaging telescope along a few meters laser beam transport ensuring a stable and collimated beam in the interaction area. Instead, we propose to implement a system that can be operated with multiple bunches of PSIs and that will provide an excellent test-bench for the operation of such a system at a larger scale, for instance at the LHC. However, commercial laser systems that deliver several kilowatts at $40\,\mathrm{MHz}$ repetition rates do not exist. The use of an enhancement cavity, namely the Fabry–Pérot cavity, is thus considered. It is seeded by a lower average-power laser that would be less expensive to produce and is commercially available, depending on the required performances. This option is considered as the baseline solution, since it is expected to allow a cost reduction of the overall system. The related optical system may also be easier to tune in terms of the pulse duration and spectrum. It must be emphasised that a similar system has already been operated in accelerator environments for some time, see for instance Ref. [67].

A few milli-joules energy per pulse correspond to several tens of kilowatts of stored power in the optical resonator. The total power that can be stored in the cavity is constrained by the maximum fluence (energy per unit surface) that the intra-cavity mirrors can support and the thermally induced deformation of the mirror substrates due to residual absorption, at the level of a part per million, in the mirror coatings [68]. The former effect is limiting when the laser-beam sizes on the mirrors are relatively small. The latter induces presence of higher-order modes in the optical cavity that, in turn, induce losses and instabilities in the locking of the FPC [69]. Intra-cavity average power of $600\,\mathrm{kW}$ has been reached in optics laboratories [70] but involves the use of relatively low-finesse cavities and high-power ($500\,\mathrm{W}$) laser systems. This type of configuration is more expensive than the one considered for the GF PoP experiment which relies on maximising the finesse of the optical cavity [67].

6.3.2 Implementation of laser system

The laser system seeding the FPC must deliver about $50\,\mathrm{W}$ at $40\,\mathrm{MHz}$ with a low phase noise and, ideally, with the ability to tune the spectrum and/or the pulse duration by using Fourier limited pulses or longitudinally chirped pulses. The laser design is relying on a chirped pulse amplification scheme and is consisting of five main logical blocks, see Fig. 8.

1. The first block consists of a pulse laser oscillator, which must be equipped with a translation stage in order to adjust its repetition frequency to that of the FPC, a coarse and slow tuning based on a Peltier, and a piezo-electric for faster adaption and lock of the laser oscillator on the FPC. The laser oscillator must have low phase noise to ensure an easy locking to the FPC.

2. The second element, the front-end module, consists of three parts. First a bandwidth management module that comprises two fiber Bragg gratings thermally controlled that allow to low-pass and high-pass filter the laser spectrum that is too large to be amplified (pulse duration is too short in the amplifier). The bandwidth of the selected spectrum will determine the minimal spectral bandwidth that will be achieved at the end of the amplification stage and thus the spectrum of the laser that will interact with ions. After the two filters, a Chirped Fibre Bragg Grating, also thermally controlled will allow to tune the stretching of the pulse according to the selected bandwidth and the level of residual stretching after re-compression in the final stage of the laser system, before injecting the FPC, see Fig. 9. The actual spectrum after these elements will be precisely measured by means of a high-resolution spectrometer. Given that the group involved in the Gamma Factory has no experience with such a tunable bandwidth system, this must be tested within a dedicated R&D prior finalising the ordering of the final laser system. An electro-optic modulator (EOM) used for the locking procedure of the laser on the FPC by generating sidebands follows this bandwidth

management module. Finally, a pre-amplifier is seeded to compensate for the losses in various elements inserted in this block to get an output power at the level of $100\,\mathrm{mW}$.

3. A first amplifier based on a Ytterbium doped single-mode fiber allowing to reach up to $5\,\mathrm{W}$ is implemented after the front-end block.

4. A second large effective mode area fiber amplifier reaching up to $50\,\mathrm{W}$ will then be used to reach the required power to seed the optical cavity. One alternative, as mentioned above, is to replace the large mode area fiber by a solid-state Ytterbium:YAG amplifier to avoid non-linear effects and laser induced damage at the end of the fiber core.

5. Finally, a block containing the compressor, with fixed parameters, certainly a Chirped Volume Bragg Grating will be implemented. An additional high-power spectral filter will allow to remove the blue-side of the spectrum that must be removed to avoid heating of the ion beam by interaction with the lower energy ions. Finally, the polarisation of the beam is brought to circular and a telescope will be implemented to match the beam size and divergence on the first mirror of the FPC. Then, the beam will be stabilised by means of a dedicated set of steering mirrors and, if needed, stabilised up to few $\mu\mathrm{rad}$ (RMS) pointing by means of active analogue feedback on the position and pointing of the laser beam. A spectrometer may also be implemented in this module in order to check the spectrum before injection in the FPC.

Given that the PoP is expected to be located in LSS621, the laser system will be installed in the side tunnel. Thus, the laser-beam will be transported up to the FPC over a few meters by means of a high-vacuum laser beam transport line. Some diagnostics could be integrated in the mechanical frame of the FPC, as discussed below.

6.3.3 Fabry–Pérot cavity design

The finesse of the FPC is determined by the optical round-trip length of the cavity and the line-width of the laser. Indeed, the FPC can be understood as a frequency filter of the laser-beam spectrum. The line-width of a single peak in the laser-beam comb spectrum is difficult to measure with a sub-kHz precision. We, however, know from the past experience[2] that a few kHz line-width bulk Ytterbium laser oscillator seeding a fibre amplifiers delivering several tens of Watts can be routinely locked to a 25000 finesse optical cavity at a repetition rate of $133\,\mathrm{MHz}$. It is thus reasonable to assume that a 10000 (5000) finesse for operations at 40 (20) MHz can be implemented. The corresponding gain on the laser power would then depend on the regime in which the FPC is designed, as determined by the relation between the transmission of the coupling mirror and the product of the reflectivity of the mirrors of the FPC. At this stage of the design we can assume, for the sake of simplicity, that we can build a cavity that would deliver a gain of 5000 (2500) at $40\,(20)\,\mathrm{MHz}$. Assuming that $180\,\mathrm{kW}$ can be stored in the FPC, corresponding to $4.5\,\mathrm{mJ}$ pulse energy available in the FPC, it requires to procure a seed-laser with power of about $50\,\mathrm{W}$, assuming roughly 70% of coupling efficiency. The choice of the repetition rate of the optical cavity is mostly driven by technical constraints. Thoroughly the maximum finesse, and thus the gain, is entirely determined, for a given laser oscillator line-width (i.e. phase noise), by the repetition frequency. Thus, reducing the repetition frequency would reduce the number of non-colliding round trips in the FPC but would also reduce by the same amount the maximum available energy per photon pulse at constant seed-laser power, or would double the seed laser power at a given intra-cavity pulse energy. This would increase the cost of the seed-laser system and also the cost of the FPC that would, moreover, become more complicate to operate. We consider, in the following, that the repetition frequency of $40\,\mathrm{MHz}$ is the baseline option for the design. If the phase noise of the laser is found better than expected, the design could be upgraded to $20\,\mathrm{MHz}$ or, more simply, to a higher FPC finesse at $40\,\mathrm{MHz}$ to increase the

[2] The R&D programme within the ThomX project [71].

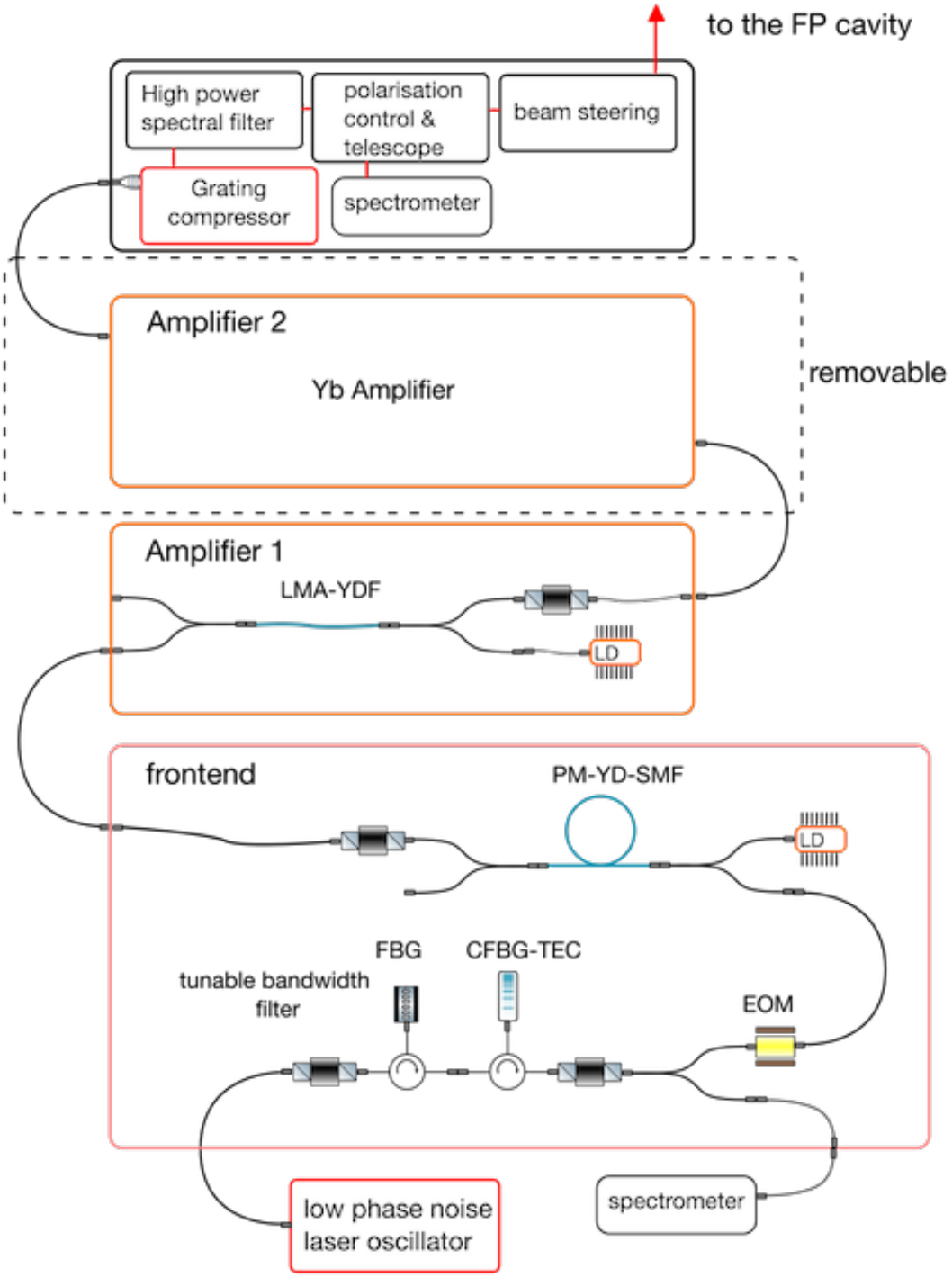

Fig. 8: Schematic description of the laser system that is expected to be used to seed the FPC. See text for details.

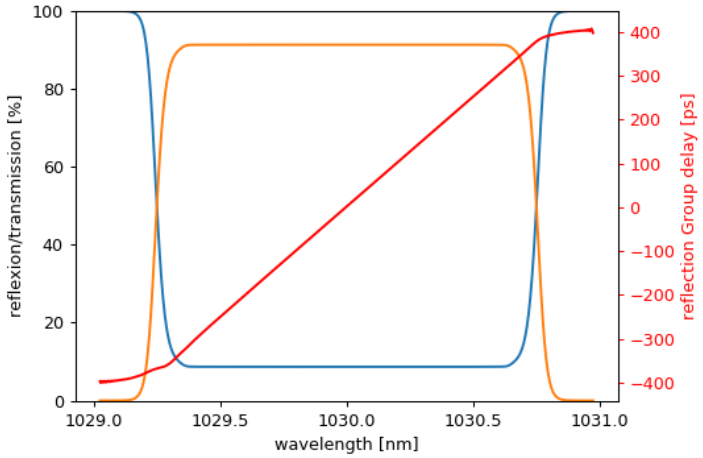

Fig. 9: On the left axis, an example of the transmission and reflection curves obtained by combining 2 fiber Bragg gratings with a compensated dispersion and a chirped fiber pulse stretcher. On the right axis the dispersion is given as function of the wavelength. These systems are commercially available at TeraXion, for example, with an integrated temperature electronic controller allowing to tune independently the blue and red edge of the filter, and the group delay dispersion.

available energy for collisions, though keeping it a reasonable level, so that the effect of thermal loading of the mirrors, due to intra-cavity losses, is kept at a reasonable level.

The length of the FPC must be tunable, so that its round-trip frequency matches a frequency equal to an integer harmonic of the bunch repetition rate and the revolution frequency. In order to achieve this, at least one of the mirrors of the FPC must be motorised, either with a stepping motor or with a piezo-electric translation stage with a large travel range to allow to set-up the cavity at the right length. This adjustment is usually done only once for a very long period of time if the reference frequency is stable enough. The choice of the actuator will depend on how frequent a tuning needs to be done, radiation harness of the components and their vacuum compatibility. An annular piezo-ceramics also equips the rear side of one the mirrors in order to electronically lock the FPC on the reference frequency. We are used to implement FUJICERAMICS [72] components which allow to tune the mechanical length of the cavity by $5\,$nm/V. Low voltages of less than $12\,$V are usually implemented in order to keep the noise low, but higher voltage up to about $150\,$V can be applied to extend the range. This higher-voltage option has to be experimentally investigated in order to ensure its viability. The corresponding maximum optical length tuning range of the cavity in the synchronisation loop of the FPC is thus of $\Delta L/L \approx 1.3 \times 10^{-8}$, which translates directly to a frequency stability of the RF reference of $\Delta f_{40} \approx 0.5\,$Hz or equivalently $5\,$Hz at $400\,$MHz.

Once the length of the cavity is fixed, the FPC geometry must be chosen. Since the atomic transition is sensitive to the angular momentum of the interacting photons, the eigen-mode of the FPC is thus required to match that of the angular momentum of the atomic transition. Assuming that the ion beam is not specifically prepared such that bound electrons take random spin projection along the beam direction (a.k.a. nearly the laser beam direction), the interaction is not expected to depend on the laser-beam helicity. This constraint implies that non-planar 4-mirror cavities with high finesse cannot be used for this purpose, since they are exhibiting helicity dependent resonance frequencies [73] due to the presence of a topological phase. The simpler choices thus reduce to either two mirror or planar, 4-mirror optical cavities. The clear advantage of 4-mirror (2 spherical, 2 planar) bow-tie optical cavities in the related context of Compton back-scattering gamma sources is their ability to provide stable geometries with a small laser-beam size (a few to several tens of micrometers) at the interaction point, while providing

independently the freedom to control the FPC optical length precisely. This ability is unnecessary in the case of the GF PoP experiment, since the ion beam size is relatively large (typically about a few millimetres). Additionally, the main drawback of this solution is that it involves a 4-mirror optical cavity which must be aligned once in the accelerator tunnel. However, highly reflective mirror coatings may be polluted by dust, and their performance might be significantly reduced. This alignment procedure must thus be performed in a highly controlled and clean (typically ISO5 class) environment. This is challenging in the accelerator tunnel of the SPS and would impose to install a laminar airflow in the accelerator tunnel. The possibility of installing the whole system in a surface clean-room and transporting it pre-aligned is in principle a possibility but the 4-mirror geometry and the required alignment precision make it difficult to preserve during installation in the tunnel. The 2-mirror geometry, however, greatly simplifies the mechanical integration of the system and, more importantly, allows sufficiently precise pre-alignment procedures to be performed on the ground before a careful installation in the tunnel, where either the alignment could be quickly corrected by manual operation or remotely performed by integrating proper motorised mounts and dedicated diagnostics. Both options needs to be investigated in terms of the risks of pollution of the FPC and increase in complexity of the mechanical implementation and potential slight vacuum degradation related to increase of motorised stages under vacuum. Finally, the choice of the 2-mirror FPC naturally allows to minimise the crossing angle between the ion and laser beams, thus the interaction rate. It is thus chosen to implement the 2-mirror FPC for the GF PoP experiment at the SPS.

The requirement on the stability of the cavity length is constrained by its finesse. Actually, any small shift of its length induce a shift of the frequency. The stability of this frequency must be within the linewidth when comparing it to the optical frequency, i.e. $\Delta L/\lambda = \Delta\nu_{\mathrm{FPC}}/(c/\lambda) < 1/\mathcal{F}$. It implies numerically that $\Delta L < 100$ pm.

6.3.4 Laser-beam parameter optimisation at IP

Using the semi-analytical approximation, a scan of the laser-beam parameters is performed, and shown in the Figs. 10–12. It has been found that it is ideal to have the RMS laser-beam size of about a 1mm or more. This will be shown to be incompatible with the optical cavity case in the next section. A more reasonable RMS beam size of about $\sigma_L = 0.65\,\mathrm{mm}$ can be implemented though. According to the 2-dimensional space optimisation given in Fig. 12, in this condition, the optimum RMS laser-beam pulse duration is about $\sigma_t = 2.8\,\mathrm{ps}$.

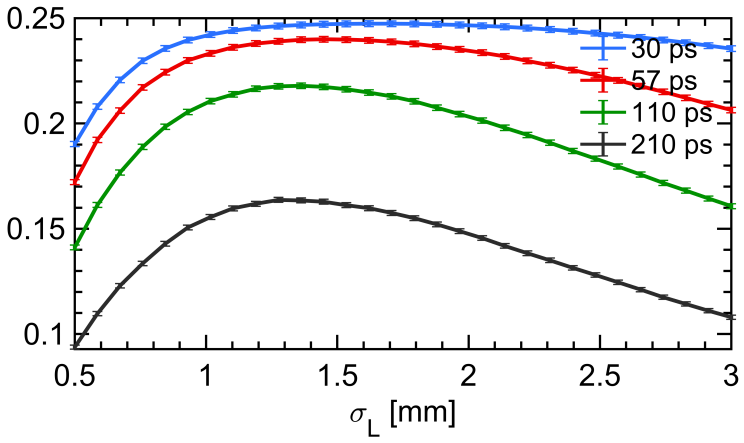

Fig. 10: The maximum fraction of the excited ions versus the transverse laser beam size σ_L. Any asymmetric choice of beam sizes can be compensated with a modification of the azimuthal angle.

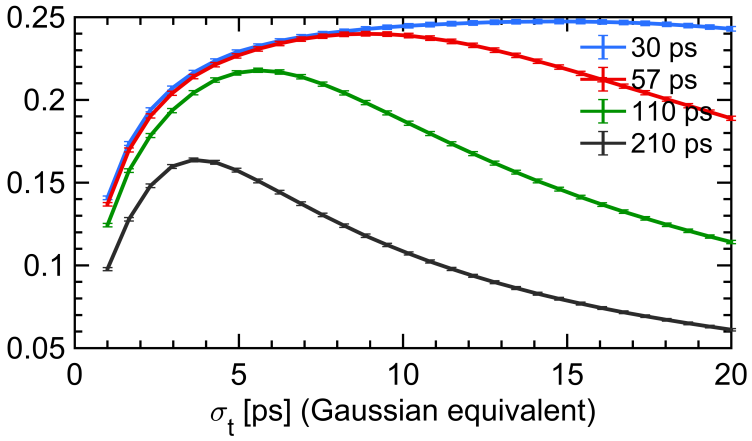

Fig. 11: The aximum fraction of the excited ions versus the laser beam pulse duration σ_t. The maximum fraction is flat meaning that a careful choice of the crossing angle θ_L and the laser beam duration can compensate for a change in σ_t.

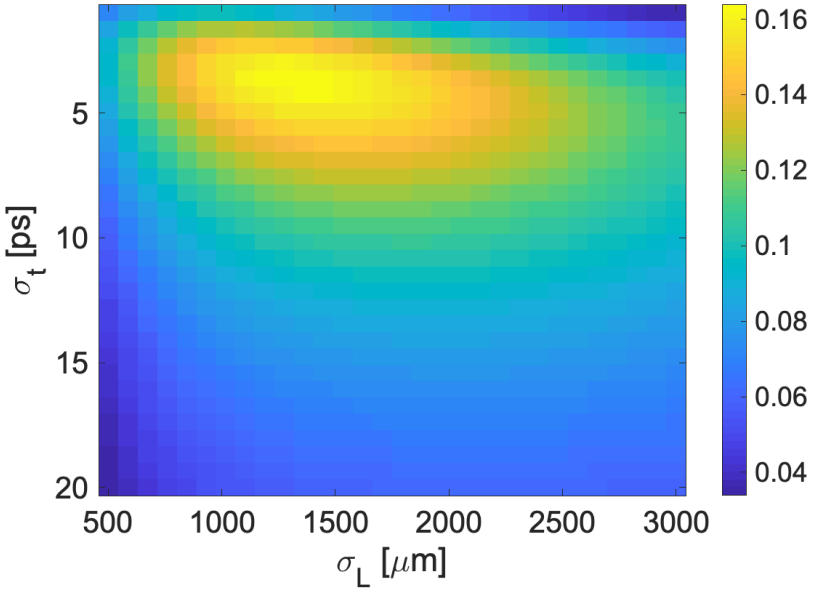

Fig. 12: The maximum fraction of the excited ions (color coded) versus the RMS pulse duration σ_t and the RMS transverse laser beam size σ_L for $\theta_L = 2.6^\circ$ and $\sigma_z = 6.3\,\mathrm{cm}$ RMS ion bunch length.

6.3.5 Optical parameters at IP

Among 2-mirror FP cavities the hemispherical or confocal geometries could be envisaged. From a practical point of view, especially for the alignment of the system, the hemispherical version seem easier to implement. Given the length of the optical cavity, driven by its synchronisation to the ion beam, the only remaining parameter is the radius of curvature R of the spherical mirror in the hemispherical geometry. The $1/e^2$ transverse size of the laser beam intensity versus the position of the plane in the FPC is shown in Fig. 13. With a 10 m radius of curvature, the divergence at the middle of the FPC is less than $100\,\mu$rad. The size of the beam at the middle point of the optical cavity is given in Fig. 15 and the fluence on the entrance mirror as a function of R is given in Fig. 14. The 10 m radius of curvature is a

baseline for the design of the FPC for the GF. This choice, however, needs some validation with some R&D studies.

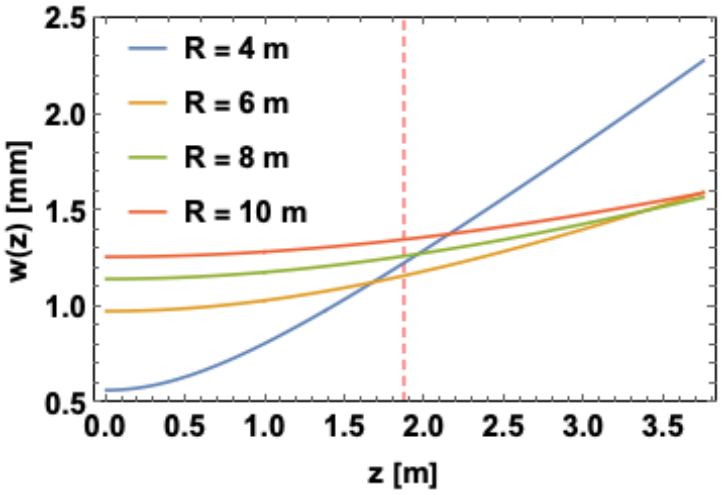

Fig. 13: The transverse size at $1/e^2$ of the intensity distribution of the laser beam inside the optical cavity. The position $z = 0$ ($z \simeq 3.75$ m) corresponds to that of the plane (spherical) mirror.

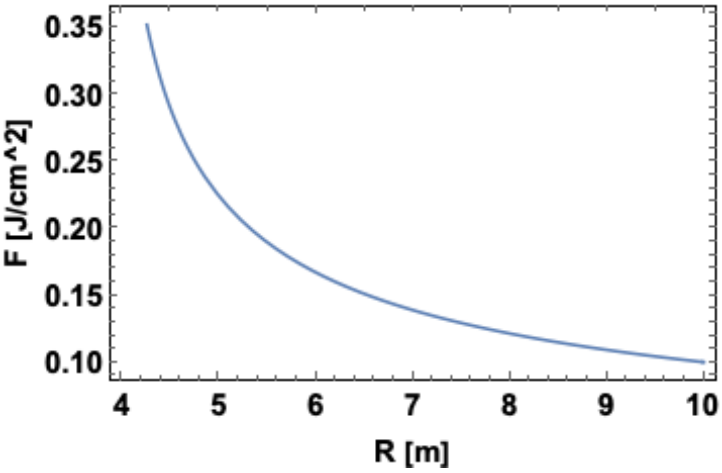

Fig. 14: The fluence $U_L/\pi w_0^2$ on the entrance mirror as a function of the radius of curvature of the spherical mirror R. A larger value of R is preferred in order to mitigate the risk of damaging the flat mirror.

6.3.6 Integration and footprint

The mechanical design is constrained by the available space in the SPS beamline and tunnel and the limited time for the installation and beam-off commissioning. The opto-mechanical and beamline design is in particular driven by the necessity of a non-disruptive integration, respecting the SPS beam impedance constraints. This particular aspect will be validated in close collaboration with the relevant CERN experts. The system is also conceived in a way that it will be pre-aligned in a "surface" clean-room and quickly realigned in-situ, with the possibility for fast change or removal of the mirrors, if required.

From our experience, a combination of granite epoxy with low thermal expansion nickel-iron alloy gives a good support for high reliability and precision Compton interaction point. In the case of the PoP experiment, the beam sizes are large with respect to usual a few tens of μm beam size. Nevertheless,

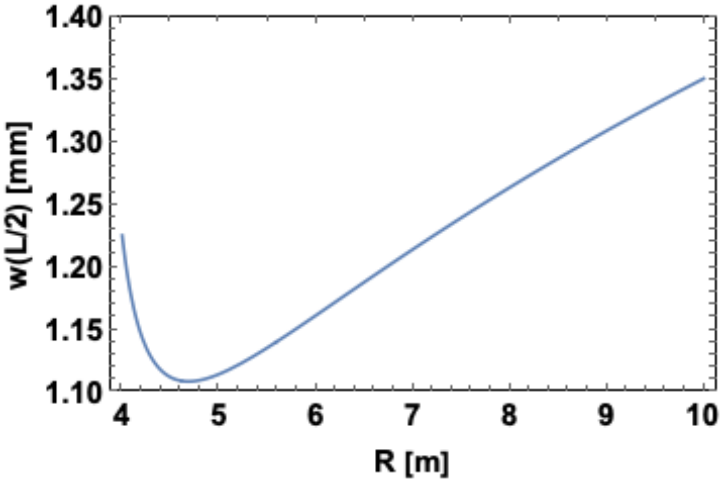

Fig. 15: Transverse size at $1/e^2$ of the intensity distribution of the laser beam at the middle point of the optical cavity as a function of the value of R. Larger values of R are preferred in order to better match the ion beam size.

the optical cavity length of $3.75\,\mathrm{m}$, the limited access and the unknown temperature variation during the machine operation constrain the interaction support stability to be in equivalent class of the Compton one, implying transverse (angular) RMS stability better than $10\,\mu\mathrm{m}$ ($10\,\mu\mathrm{rad}$) for the mirror support bases. The density of the granite epoxy is $2.3\,\mathrm{kg/dm^3}$. The granite block support is lightweight, allowing insertion of the necessary diagnostics, electronics and power supplies in the aperture with a reinforced radiation protection. In a preliminary mechanical drawing design study, a simple view of the interaction point system is given in figure Fig. 16. The integrated tools for handling of the $10\,\mathrm{tons}$ module are shown. Mechanical manual movers are not intended to be implemented at this stage since the PSI beam position will be tunable and monitored thanks to a pair of dedicated BPMs surrounding the FPC.

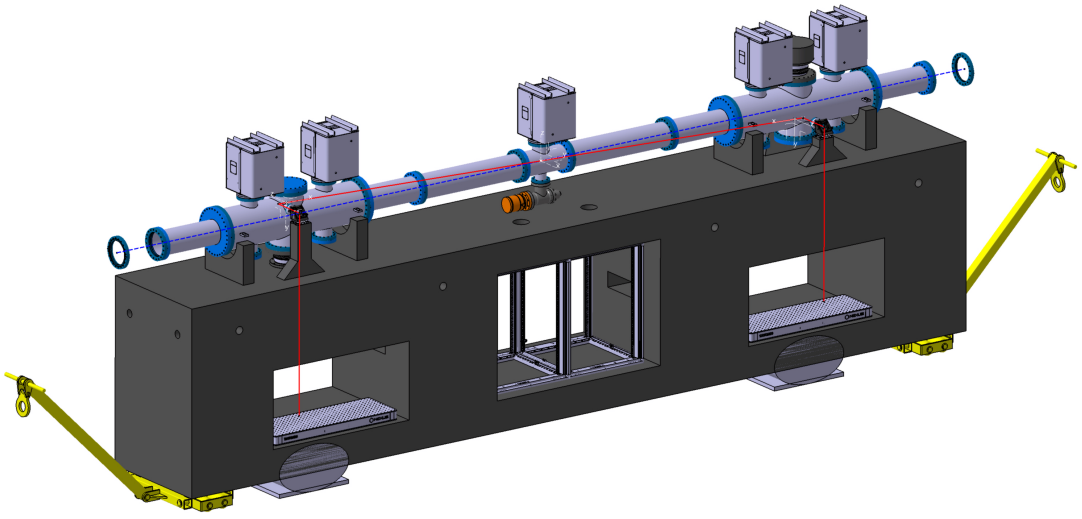

Fig. 16: Mechanical frame of the FPC including the vacuum chambers, the pumping system, the granite support. The holes in the granite allow to place the whole laser system and the associated diagnostics within the frame itself.

At the location LSS621, it is intended to equip the side tunnel with a dedicated clean optical room with air control, which will be a key aspect for the success of the experiment. This would ensure not only that the required level of cleanliness for the laser is system is simply ensured, but also that the environment is thermalized which would significantly mitigate temperature variations in the tunnel that induce performance changes of the laser system. The drawback of this location is that it requires beam transport in high vacuum from the side tunnel to the FPC entrance. This seems possible using the existing penetration in between the two tunnels. The high-vacuum laser beam transport line with moderately large aperture $\geq 50\,\mathrm{mm}$ high reflectivity dielectric multi-layer mirrors could transport the laser beam in the FPC and the reflected signal from the FPC in the side laser to get the signal in "low-radiation" environment for the PDH. The laser beam transport line could be fixed in the top-side of the SPS tunnel up to the level of the end of the section LSS621, then cross on the ceiling the walking path and turn down to the first mirror ultra-high-vacuum chamber of the FPC. As the laser waist on the input plan mirror of the cavity is relatively small, the telescope for the fine tuning of the spatial coupling can be installed in the laser room in the side tunnel.

6.3.7 Constraints on the synchronisation scheme

One of the main operational constraint on the laser system is that it must be run almost continuously over the period of data taking due to warm up drifts that are customary in laser oscillator and amplifiers. To account for this constraint, it is foreseen to lock both the laser system (including the FPC) and the proton/ion beam revolution frequency on an external clock. This will allow to maintain the laser system synchronised while operating the proton/ion beam. This will also be a convenience for realising independent tests and commissioning. Once the system is at its working point, the internal stability of the laser oscillator frequency is easily ensured in the case of the LSS621 location by implementing a laser room in the side tunnel, since it is mainly influenced by environmental drifts for a low-phase noise oscillator. Under these conditions, the choice of a state-of-the-art phase noise performance laser and a stable mechanical design of the optical cavity and beam transport will ensure that a lock of the laser pulse repetition rate on the FPC reference can be ensured without lock losses over long enough time periods (several ten minutes, maybe hours). From our past experience the main unknown here is related to additional noise brought in by the small, but still, laser-beam transport line. Lower frequency fluctuations of the FPC length will be damped by adding an overall loop to lock the optical system, as a whole, on a stable external reference. This scheme is shown in Fig. 17.

As demonstrated above, the piezo-ceramic dynamics constrains the frequency reference to be stable within $\Delta f_{40} \approx 0.5$ Hz at $40\,\mathrm{MHz}$ or equivalently $5\,\mathrm{Hz}$ at $400\,\mathrm{MHz}$. This is in order to avoid a loss of lock due to the need of moving a translation stage in the cavity. The loss of the lock would induce the need for scanning the absolute phase to retrieve the collisions. By using a synchro-loop in the SPS on flat-top would allow to avoid this inconvenience. It is thus foreseen to employ a generator synchronised with GPS timers to deliver the stable reference to the laser oscillator. The latter could be either locked on the reference frequency at the 10th sub-harmonic of the reference generator, expected to have a $400\,\mathrm{MHz}$ frequency, or directly at the reference frequency. This choice will be driven by requirements on the residual phase noise of the laser oscillator locked onto the external reference. The phasing procedure of the ion bunches with the external reference will be similar to that experienced with the AWAKE experiment. The phasing of the laser will be ensured by the use of consistent frequency-dividers for the laser and the ion bunches and a phase shifter may be also implemented in the laser locking scheme to increase flexibility.

Radial-loop or fixed field feedbacks could in principle be used, but would induce larger frequency drifts when, during the experiment, the ion beam energy will be slightly scanned in order to find the resonance and optimum energy. These frequency drifts would be too large for the range of the piezo-electric actuator that is foreseen to be implemented in the optical cavity. It must be, however, noted that

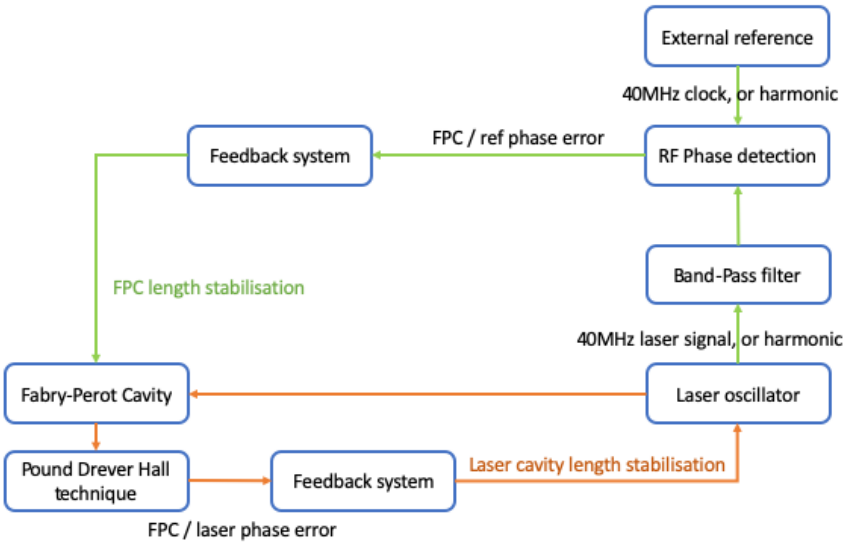

Fig. 17: Schematic drawing of the synchronisation scheme of the laser oscillator and the optical cavity on an external reference.

as far as timing jitters between the laser pulse arrival time and the ion beam arrival time (as opposed to drifts) are concerned, the system is relatively immune to such effects due to the long ion beam duration.

6.3.8 Radiation aspects

Given that the laser systems needs to be integrated in the high SPS radiation field, specific care needs to be taken in order to validate this aspect. However, this constraint is greatly relaxed thanks to the choice of integrating the critical parts of the laser system in a side tunnel and not in the SPS tunnel itself, where the typical yearly dose in LSS6 close to the beam line is of the order of magnitude of a kGy [74]. Given the limited choice of laser systems that may be used to provide the requested performance, and that these systems are not used to be implemented in high radiation field environments, the strategy that is followed relies on minimising the global dose delivered to the critical parts, namely the laser and the related electronics. The literature is indeed sparse on the topic of the radiation dose to laser oscillators and amplifiers typical of that required for the PoP experiment [75–77], especially when considering the high flux of high-energy hadrons of the SPS radiation field. These systems seem to typically survive radiation doses in the kGy range, but the tested environments are different to that of the SPS. In that respect, the choice of implementing the system in the location LSS621 is optimal since it provides a side tunnel where the radiation field is naturally shielded. A possible placement for the laser room of about $2\,\mathrm{m}$ by $3\,\mathrm{m}$ is represented by the grey rectangle on Figure 6a. If required, additional shielding materials could be installed around it by using the remaining space of about 1m between the optical room and the wall of the SPS and TI18. Access to the laser would be done through the nearby SPS tunnel and the laser system is thus meant to be fully remotely controlled. However, a detailed study of the actual radiation field in the side tunnel of the SPS still needs to be done, to validate numerically this aspect.

In the early stage of the project, before that the LSS621 location was considered, the FPC and laser system was supposed to be installed in the SPS tunnel at the location LSS616. Given the critical aspect of the radiation field on the laser and some electronics parts that are judged either impossible or extremely difficult to deport, some preliminary measurements of deposited doses at the LSS616 location were made in the last running weeks of 2018, from the September 18th to the end of the year. This

allowed to confirm the (expected) risks related to radiation field in the long straight sections of the SPS, since the inferred rates of about 1.5×10^{10} (2.1×10^{9}) high-energy hadrons per cm^2 and 1.4×10^{9} (3.8×10^{9}) thermal neutrons per cm^2 at the height (floor) $1\,\mathrm{m}$ on the side of the beam line. These figures preclude long-term use and storage of the laser system in the SPS tunnel which render the PoP operation difficult to consider and imposes specific care of single-event effects. These measurements will allow to calibrate the FLUKA simulations of the radiation field in the long straight section of the SPS up to the actual location envisioned for the PoP experiment. These will, in turn, allow to determine if further shielding is required and if additional requirements are expected on the commercial laser systems and associated electronics.

6.3.9 Required R&D and timescale for integration.

As already briefly mentioned, R&D is required to early validate a few technical choices, namely the bandwidth/pulse length management scheme with thermally controlled Bragg gratings. The optical parameters and the design of the telescope to adapt the laser to the optical cavity may also be tested early. Indeed, LAL is already engaging procurement and R&D on these two aspects, in order to validate these choices by mid-2020 in the worst case. These validations at low power may be pushed to high power to further validate the choice of the provider for the mirrors and to probe thermally induced effects in the 2-mirror optical cavity with the chosen radius of curvature and geometry. Most of the hardware required for these is already available at LAL and will allow designing the laser system for the PoP experiment by mid-2020.

Once a financial green light is obtained, one year of procurement time for the laser oscillator, additional optical parts and laser amplifier is expected. In the meantime, the mechanical design of the supporting frame for the optical cavity, the design of the laser-beam transport line and their vacuum systems with necessary safeties, the drawing of the specifications for the optical room that is intended to be located in the side tunnel will be engaged. This task is expected to last about six months, but could start at the same time as the laser system design. The increased duration is explained by necessary increased interfaces with surrounding mechanical elements and boundary conditions imposed by the existing penetrations in walls that may need some iterations. Following this design phase, procurement will be launched and is expected to last about 9 months. This implies that all elementary parts are expected to be ready 15 months after a financial approval of the project. Laboratory assembly and optimisation of the whole system and development of requested control command software will be performed in the next 9 months, with a special care given to remote operation of the whole system, including feedbacks, followed by installation in the SPS and side tunnels.

6.4 Detection of X-ray photons

6.4.1 Simulations

Photon fluxes

The features of the emitted photon beams simulated by means of the Monte Carlo programs GF-CAIN, GF-CMCC and GF-Python are reported in this section. The details of the above GF simulation tools are presented in Appendix 3. The parameters of the simulations of relevance for the PoP experiment are collected in Table 3.

Fig. 18 compares the GF-CAIN, GF-CMCC and GF-Python results for the laser (photon) pulse energy dependence of the ion excitation rate in a single ion-bunch–photon-bunch collision. This plot carries two important messages. Firstly, the results of three independent programs are in a good agreement.

Secondly, almost all the ions are excited in each bunch crossing[3]. For example, in the case of a 5 mJ laser pulse, 20.55% of ions absorb and subsequently emit a photon: this corresponds to a total flux of 1.85×10^7 photons per bunch crossing.

The GF-CAIN and GF-CMCC charactersitics of the photon flux are presented Figs. 19. As shown in the left-hand-side figure, the majority of photons coming from spontaneous emissions of excited ions are emitted in the direction of the ion beam. The angular distribution of emitted photons is peaked around 10 mrad. The most energetic photons are emitted at small angles. The maximum photon energy is 44.47 keV.

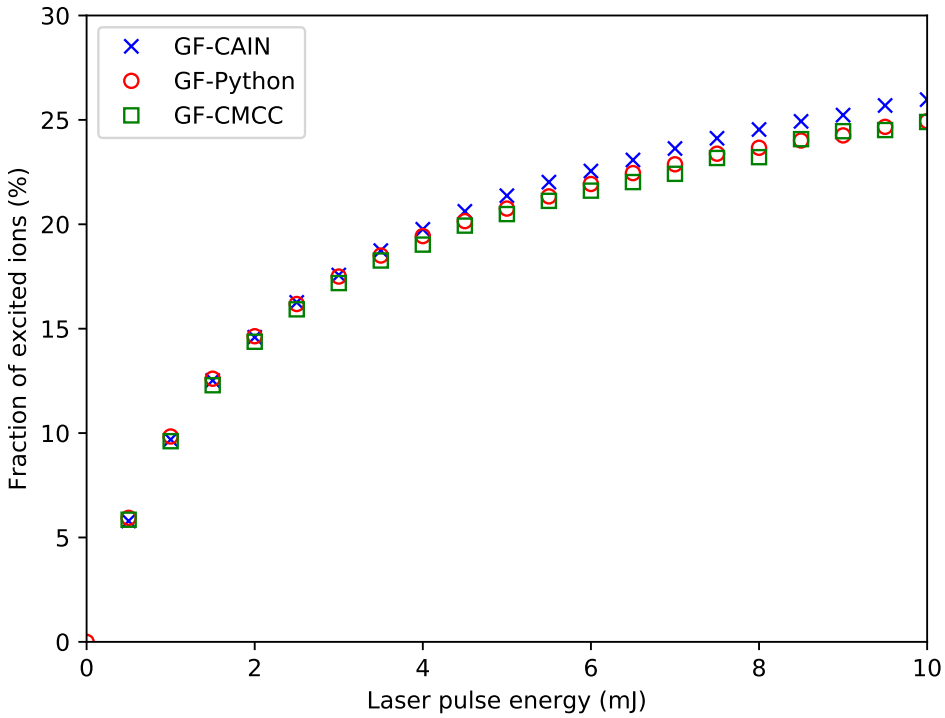

Fig. 18: The fraction of excited ions per bunch crossing as a fuction of the laser pulse energy. Predictions of the GF-CAIN, GF-CMCC [3,78] and GF-Python [79] simulation codes. The simulation parameters are given in Table 3.

As quoted in Table 3, the lifetime of the excited ions is 76.6 ps in the ion rest frame. The corresponding laboratory-frame distribution of the path-length of the excited ions (from the collision point to the photon emission point), obtained using the GF-CMCC simulation code is presented in Fig. 20. This plot shows the most important difference of the PoP experiment configuration, based on the Lamb-shift-like, l-level, atomic excitation and the future LHC implementation of the photon production scheme based on the n-level atomic excitation. The excited-state lifetime in the latter case will be shorter by up to four orders of magnitude and the photon source will be a point-like source, contrary to the former case which is specific to the SPS-based experiment, where the photon source will be distributed over a large distance. As presented in Figs. 21, the long decay-path, specific to the SPS PoP experiment, gives rise to a loss of the correlation between the radial position of the photon impact point on the detector plane, perpendicular to the beam axis, and the photon energy. The degree in which such a correlation is smeared out will allow us to measure the lifetime of the excited state in the SPS PoP experiment. In Fig. 22 we present the expected energy spectra of photons intercepted by a ring-shaped flat detector, placed at $z = 7$ m from IP, within the radial distances of $4\,\text{cm} < r < 6\,\text{cm}$. The low-energy tail of the photon energy distribution for $\tau' = 76.6$ ps carries the precise information on the value of the excited-state lifetime.

[3]In our case, in which the excited-state lifetime is significantly longer than the duration of the laser pulse, and the maximal number of excited ions, in the presence of saturation effects discussed in Appendix 2, is 50%.

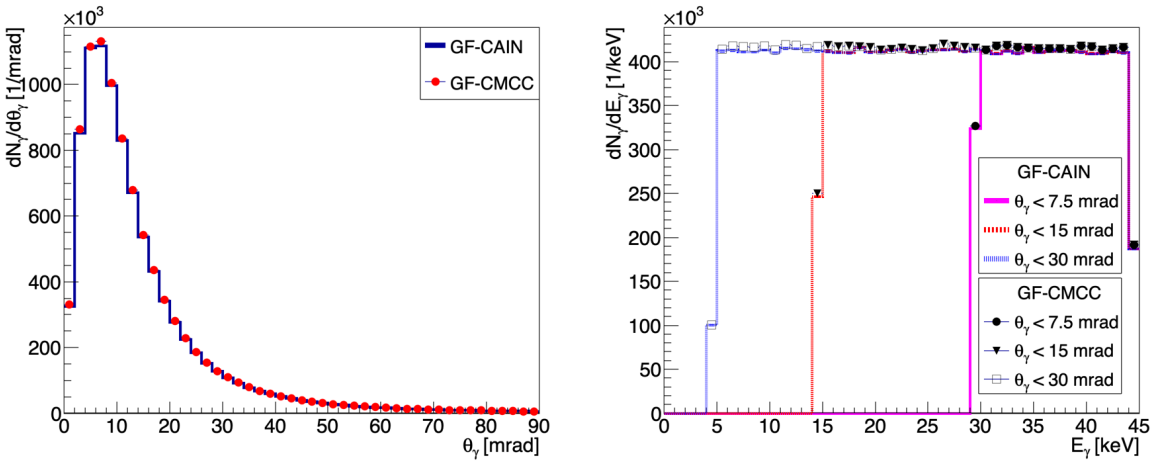

Fig. 19: The `GF-CAIN` and `GF-CMCC` simulation results for a single PSI-bunch–laser-pulse collision. Left: the angular distribution of emitted photons. Right: the energy spectra of the emitted photons within the three cones centred at the ion beam direction and delimited by $\theta_\gamma^{max} = 30, 15, 7.5$ mrad.

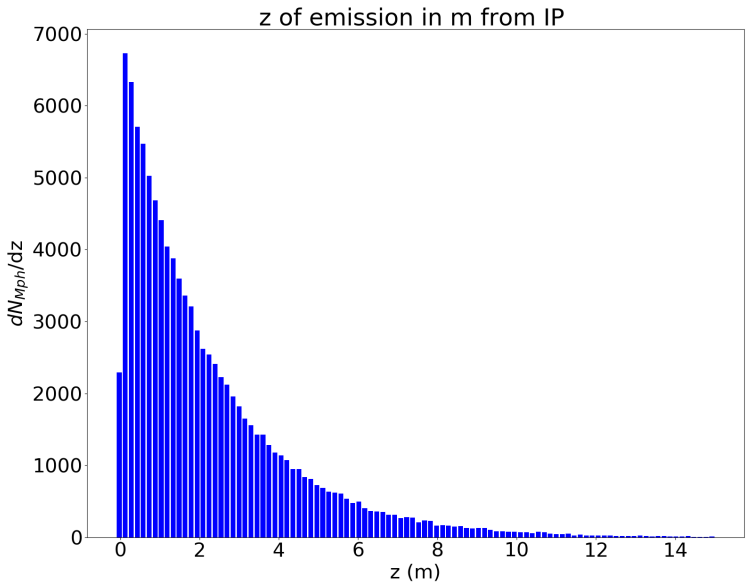

Fig. 20: The distribution of the path-length of the excited ions (from the collision point to the photon emission point) in the laboratory reference frame – the `GF-CMCC` simulation.

Excitation rates and sensitivity to imperfections/errors

For the initial “resonance finding" stage of the PoP experiment an evaluation of the sensitivity of the ion excitation rate and the resulting photon fluxes to a possible initial mismatch of the expected and observed parameters of the photon pulses and ions bunches is of primordial importance.

In Section 6.1.4, the maximum *expected* offsets of the bunch-crossing parameters were discussed and listed Table 4. For the worst-case offsets, the predicted fraction of the excited ions will be reduced down to $2.7\,\%$ from around $20\,\%$ in perfect conditions.

In order to be protected against a significantly larger absolute offset of the beam momentum with

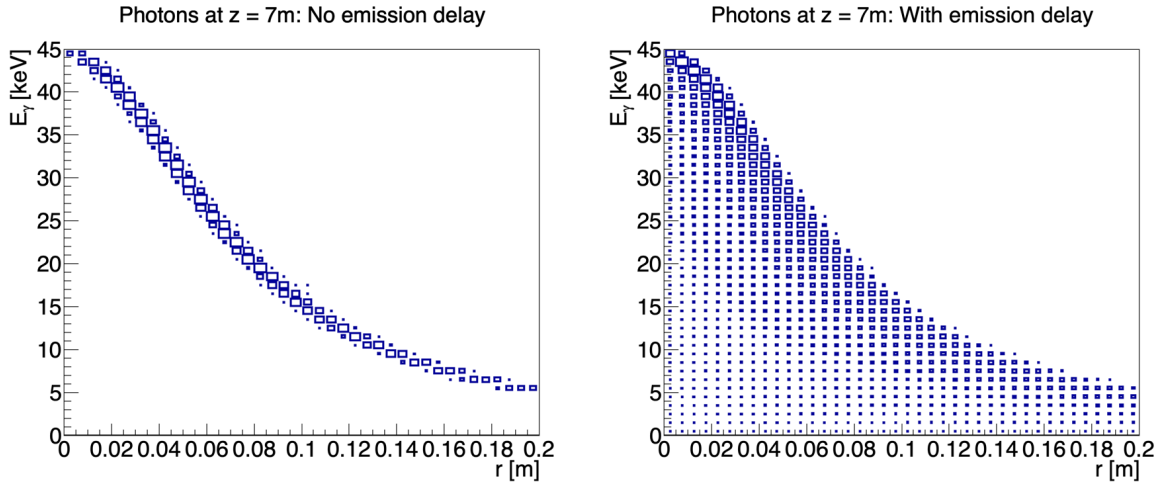

Fig. 21: The energy distribution of emitted photons as a function of the radial position of the photon impact point on the detector plane. The detector plane is perpendicular to the beam axis and placed at $z = 7\,\mathrm{m}$ from IP. Left: the lifetime of the excited ion $\tau' = 0\,\mathrm{ps}$ (no decay delay). Right: the lifetime of the excited ion $\tau' = 76.6\,\mathrm{ps}$. Simulations were made using `GF-CAIN`.

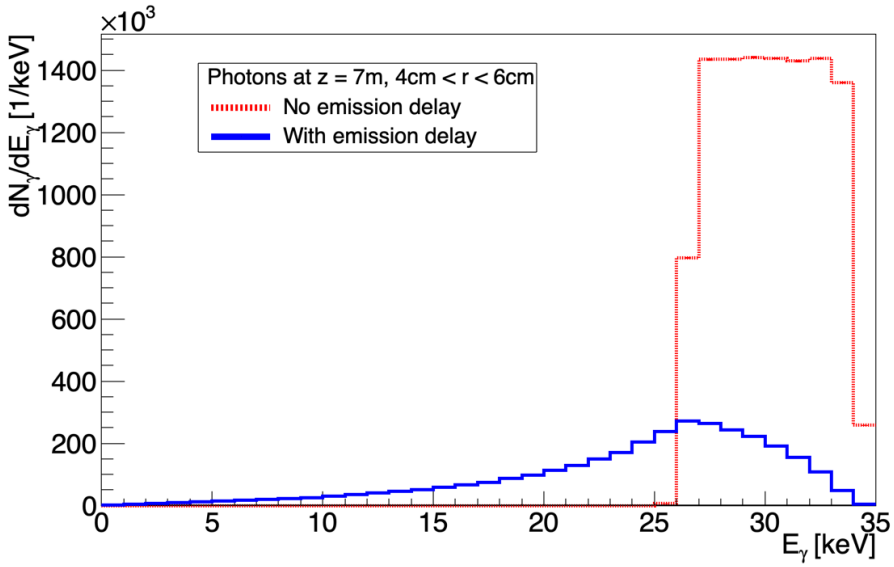

Fig. 22: Photon energy spectra for photons intercepted by a ring-shaped flat detector, placed at $z = 7\,\mathrm{m}$ from IP, within the radial distances of $4\,\mathrm{cm} < r < 6\,\mathrm{cm}$, as predicted by `GF-CAIN`. Dashed red line: the lifetime of the excited ion $\tau' = 0\,\mathrm{ps}$ (no decay delay). Solid blue line: the lifetime of the excited ion $\tau' = 76.6\,\mathrm{ps}$. The spectra are presented for a single PSI-bunch–laser-pulse collision.

respect to the assumed value, we consider a systematic scan of the PSI beam momentum setting. Fig. 23 shows the dependence of the fraction of the excited ions as a function of the relative momentum offset.

This plot shows that we will be able to handle even larger that expected initial offsets of the absolute scale of the beam momentum.

For possible horizontal and vertical offsets, the local FP associated BPMs are expected to ensure the alignment of the ion bunches and photon pulses to a much better precision than the laser or PSI beam sizes. Therefore, those offsets are expected to have only minor effects on the fraction of the excited ions.

The relative ion-bunch an photon-pulse timing offset has a large effect on the fraction of the excited ions due to the non-zero crossing angle of laser pulses and ion bunches. The timing monitoring system

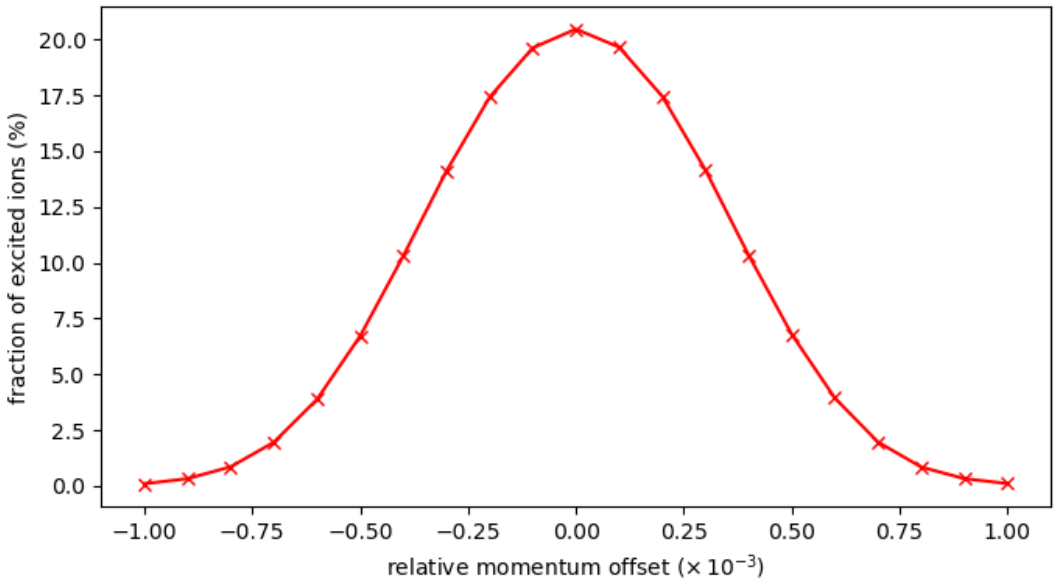

Fig. 23: Fraction of excited ions as a function of the relative beam momentum offset with respect to the expected value as predicted by the Monte Carlo event generator `GF-CAIN`.

discussed in Section 6.1.4 and the RF synchronisation stability will ensure the maximal timing offset well below $0.5\,\mathrm{ns}$ which is by a factor of 2 larger that the duration of the PSI bunch and sufficient for the initial timing adjustment.

6.4.2 Photon detectors

The detection and characterisation of the emitted X-ray photons is crucial for the GF PoP experiment for several reasons. First, it should provide a clear demonstration of the photon beam properties, i.e. photon flux, density and spectrum, that will pave the way for the future implementation of the Gamma Factory photon production scheme at the LHC. Secondly, and even more importantly for the experiment at the SPS, the produced photon beams will be the main observable for the set-up and for the optimisation of the interaction region.

Detector constraints

Simulations of the interaction between the laser beam and the PSI beam have been performed using different codes, as described in detail Section 6.4.1. The photon fluxes have been transported downstream of the interaction point along the SPS ring and the results of these simulations show important geometrical constraints:

- At the location under consideration in the SPS the extraction of produced X-rays out of the vacuum beam line is not possible. The downstream cell of dipoles that curves the PSI trajectory away from the produced photons is very dense and the addition of the X-ray extraction system would be complcated. Further study could identify a possible extraction scheme of slightly off-axis photons, in particular downstream of the 622 cell.
- A hollow-shaped detector can be envisaged to detect outgoing photons. The inner size of the hole should, however, be large enough not to interfere with the PSI beams.
- Due to geometrical constrains in the machine, the distance between the interaction point and the detector cannot be larger than $9\,\mathrm{m}$.

The detector should have a large dynamic range and good sensitivity. It will be crucial to be able to measure a low flux when the PSI beam position, timing and energy are not perfect. Also, it has to be able to resolve relatively small variations in the photon flux to achieve the PoP R&D goals.

More practical considerations should also guide the choice of the detector. It should be cost-effective by relying on existing technology and possibly existing integration design. It should also be simple and reliable enough for a fast implementation and commissioning.

Proposed detector system

As a first step, a simple and cost-effective solution is envisaged to measure the X-ray photons using a scintillating material and a camera. Such systems, known as BTV [80], are available at CERN and could be installed in the SPS at the desired location. This device typically includes a remotely controlled manipulation system that can insert in the beam pipe up to 2 screens. This system can be placed $7\,\mathrm{m}$ downstream of the proposed IP. The screen itself is a $100\,\mathrm{mm}$ square on the side of the beam axis and with an elliptical hole in the central part.

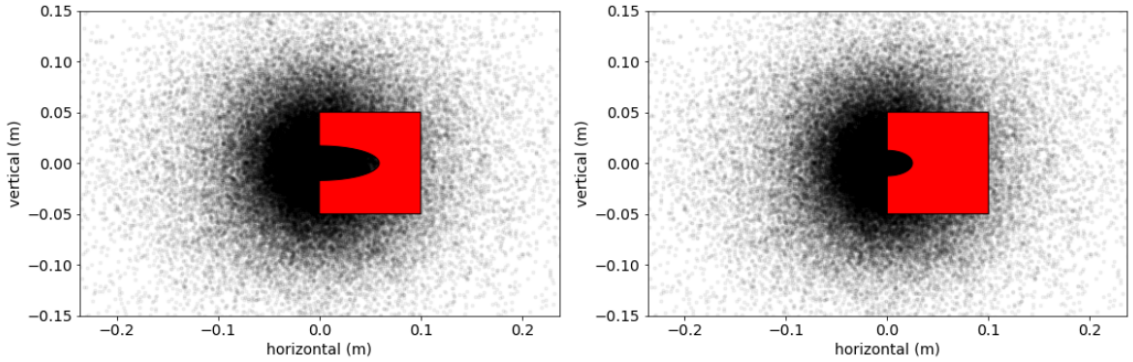

Fig. 24: Detector screens considered with elliptical holes and referred to as the large aperture, on LHS, and the small aperture, on RHS. The transported photons in the ideal conditions are shown as black dots.

Fig. 24 shows the two detector screens considered with the transported simulated photons. The large aperture screen has a hole with an elliptical shape and the semi-major axis of $59\,\mathrm{mm}$, and $17\,\mathrm{mm}$ in the horizontal and vertical planes, respectively. This shape follows the stay-clear, discussed in Section 6.2.4, and can be used in the cycled SPS operation, as the screen surface is outside the required aperture.

A second screen with a smaller aperture of $25\,\mathrm{mm} \times 12.5\,\mathrm{mm}$ could also be installed in the same vacuum tank to be used during commissioning to maximise the measured signal. Its smaller aperture would only allow injection and acceleration of the PSI beams.

The screen, made out of a thin scintillating crystal or an assembly of crystals, would be mounted on a rigid frame. Yttrium Aluminium Garnet doped with Cerium (YAG:Ce) is a common material, typically used for the detection of low-energy X-rays. Non-hygroscopic, it is compatible with the vacuum environment of the SPS. From a tabular specification a reasonable thickness of $3\,\mathrm{mm}$ would absorb $\sim 100\%$ of incoming photons in the relevant energy range, i.e. up to $45\,\mathrm{keV}$. A typical light output for this material is 8 photons per keV of the incident photon energy [81]. Other scintillating materials, such as LuAg:Ce, recently developed for detection of low-energy X-rays could also be used alternatively, providing a higher light yield [82].

Simulations were performed to model the efficiency of the detector system proposed above. The expected photon distribution on the scintillating screen, $7\,\mathrm{m}$ downstream the IP, has been calculated

assuming the ideal conditions, i.e. at resonance and with a perfect overlap between the laser and the particle beams. The results are presented in Fig. 25 showing the X-ray density on the screen and the resulting number of visible photons, expressed in photons per mm^2, that will be produced by a $3\,\mathrm{mm}$ thick YAG:CE scintillating screen.

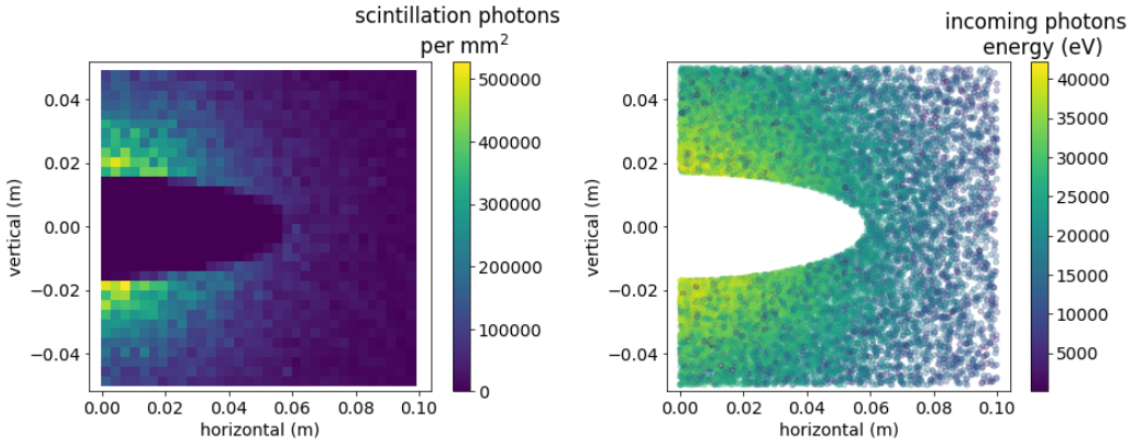

Fig. 25: A typical image of the X-ray beams measured using a scintillating screen (LHS). The spatial distribution of the incoming X-ray photon energy on the screen (RHS)

The simulation results from the laser-photon–PSI interaction in perfect conditions and with the `GF-CAIN` code predicts the production of 1.8×10^7 photons, totalling $4.1 \times 10^{11}\,\mathrm{eV}$. Transport and interaction with the two different detectors provide the fraction of those X-ray photons that interact with the screen.

- The large aperture detector captures $19.1\,\%$ of produced X-ray photons, $21.5\,\%$ of their total energy and produces 7×10^8 scintillation photons per bunch collision.
- The small aperture detector captures $25.3\,\%$ of produced X-ray photons, $30.4\,\%$ of their total energy and produces 9.9×10^8 scintillation photons per bunch collision.

Taking the case of the large aperture detector, the total photon flux emitted by the screen is 3×10^{13} $\mathrm{photons/s}$, equivalent to $1\,\mu\mathrm{W}$ when considering that scintillation occurs mainly at a wavelength of $550\,\mathrm{nm}$. As scintillation light is emitted isotropically, the number of photons recorded by a camera that is located at a distance of $50\,\mathrm{cm}$ from the screen would be then further reduced by a factor 150. This is assuming a realistic angular acceptance of $40\,\mathrm{mrad}$ for the optical detection system. The corresponding flux of photons on the camera is then $2 \times 10^{11}\,\mathrm{photons/s}$ which is typically one order of magnitude larger than the sensitivity limit of standard digital camera [83]. Furthermore, an intensified camera [83] would be able to increase the sensitivity by 2 to 3 orders of magnitude. This would allow to compensate for further reductions in the produced X-ray flux while considering possible spatial and temporal offsets between the ion and laser beams as well as a shift of the incoming photon energy out of resonance.

Future developments

In the phase 2 of the PoP experiment, pixel detectors, e.g. `timepix3` [84], already developed for beam instrumentation purpose [46] could be used for more precise characterisation of the X-ray flux. They will have the advantage to be sensitive to single photons with high spacial and energy resolution. They are expected to provide better energy resolution, more precise measurement of the lifetime of the ion's excited state and of the atomic transitions energies.

6.5 Cooling

The turn-by-turn simulation of longitudinal cooling of the Li-like Pb beam in the SPS is described in the dedicated Python notebook [85].

The longitudinal phase-space distribution of the ion beam is shown in Fig. 26. In order to speed-up the cooling process, we choose to excite ions in the upper part of the ion beam energy distribution, so that the energy loss due to the photon emission for ions with energy deviation $\Delta E > 0$ is significantly larger than the energy loss for the ions with $\Delta E < 0$, and this is true for a large fraction of the ion beam. This is achieved by setting the relative frequency spread in the laser pulse to be equal to the half of the relative energy spread in the ion beam

$$\frac{\sigma_\lambda}{\lambda} = \frac{1}{2}\frac{\sigma_E}{E}. \tag{9}$$

In this simulation we assume the Gaussian Fourier-limited laser pulses with $\sigma_t \sigma_\omega = 1$. Then, the relative energy spread $\sigma_E/E = 2 \times 10^{-4}$ corresponds to the laser pulse duration $\sigma_t = 5.5\,\mathrm{ps}$.

Fig. 26 shows that over the first 20 seconds of beam–laser interaction the peak current in the ion beam increases by a factor of three due to the longitudinal cooling of the beam – this should be visible in the longitudinal beam current profile monitor of the SPS.

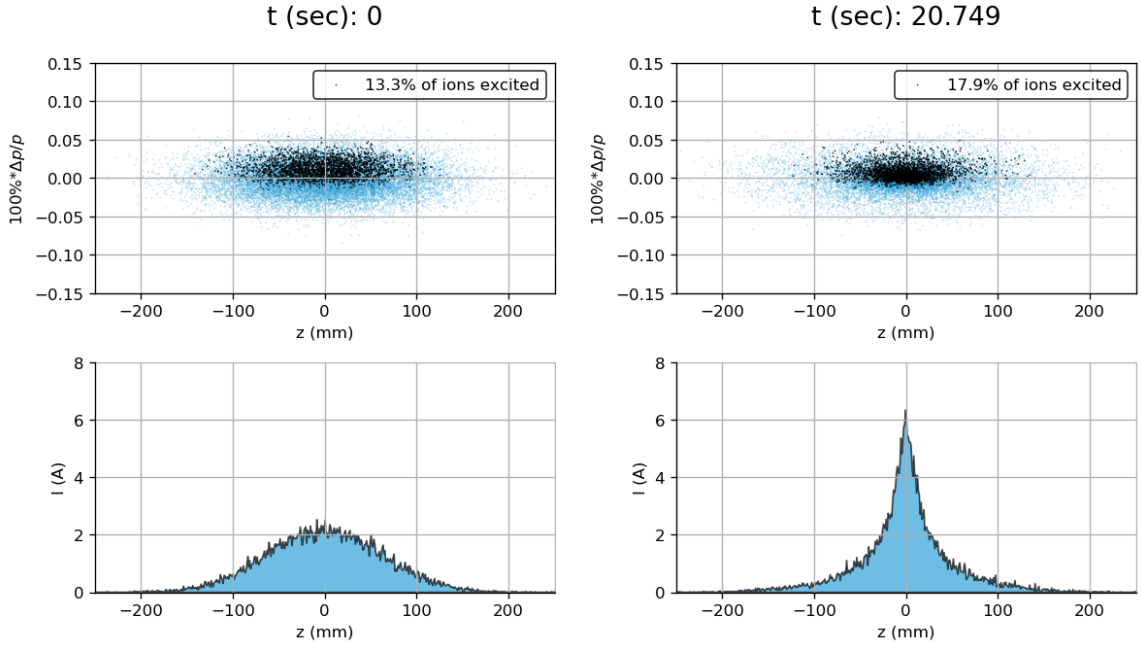

Fig. 26: Simulation of longitudinal laser cooling of the Li-like Pb beam in the SPS [85]. Excited ions are marked by black dots, while unperturbed ions are shown as blue dots. The LHS pictures show the initial ion beam distribution, the RHS pictures show the beam after 20 seconds of cooling.

Simulating a longer cooling process produces even a higher peak current in the ion beam. However, for the large peak current the collective effects will become important and still have to be included into the simulation.

In this simulation the only clearly observable effect is in the longitudinal ion beam distribution. However, since at the laser–ion beam interaction point there is a significant value of the horizontal dispersion function ($D_x = +2.4$ m), we can also use the effect of dispersive coupling (see Section 3.2) in order to transfer the cooling into the transverse plane. This can be achieved by simply shifting the horizontal position of the laser focal point by 1 mm (towards negative x, as explained in Fig. 2). Such simulations are performed in a similar Jupyter notebook [86]. The results are shown in Fig. 27. We can see that the small shift of the laser focal point by -1 mm reduces the number of excited ions from 16.2%

to 12.4% which, in turn, reduces the rate of the longitudinal cooling, but there is a dramatic increase in the rate of the transverse cooling instead.

Shifting the laser focal point into the positive direction in x will result in the blow-up instead of the reduction of the horizontal emittance.

Understanding and control of these cooling/heating effects are very important for the LHC-based Gamma Factory, where the rates of the laser cooling are greatly increased compared to the SPS Proof-of-Principle experiment.

7 Timeline, resources and organisation

7.1 Timeline

The timeline for the SPS proof-of-principle experiment has been developed within the timeline of the overall Gamma Factory R&D studies and is presented below in this context.

The overall Gamma Factory initiative R&D has been conceived and set up in three main phases:

- Phase 1: Initial Study;
- Phase 2: SPS Proof-of-Principle Experiment;
- Phase 3: LHC Demonstrator Application.

The scheduling for these phases is constrained by the already approved operation schedule of the CERN accelerators [87]. The GF R&D timeline planning is defined to minimise interference with the ongoing CERN research programme.

7.1.1 Phase 1: Initial Studies

The first phase of initial studies started in February 2017, with the creation of the GF study group embedded within the Physics Beyond Colliders (PBC) framework. It included the exploration of the different concepts, theoretical studies and simulations, and preparation and execution of dedicated SPS and LHC accelerator tests performed over the years 2017–2018. This phase is now approaching completion with the present LoI for the GF PoP SPS experiment. The timeline of this Initial Study phase, together with its key achievements and remaining milestones superimposed on the LHC and SPS operation roadmap, is summarised in Fig. 28.

7.1.2 Phase 2: SPS Proof-of-Principle Experiment

The proposed second phase of the GF initiative is the SPS Proof-of-Principle experiment with the objectives described in details above. This phase will demonstrate the feasibility of resonant laser atomic excitation of relativistic atoms, and is the essential precursor for future higher-energy GF developments. The phase will need to be approved as a Project to construct, install and operate the experiment. The identified planning of this PoP phase includes:

1. Procurement and laboratory tests of the vacuum vessel, laser-system, FPC and remote controls;
2. Procurement and tests of the photon-detector components;
3. Construction and installation (or upgrade) of the TT2 stripper;
4. Installation of the room for the laser in the SPS tunnel;
5. LSS6 installation of the vacuum vessel, the laser system, the FPC and the photon detection system;
6. Overall experiment commissioning: hardware commissioning, beam commissioning, resonance finding, measurements, photon detection, etc.

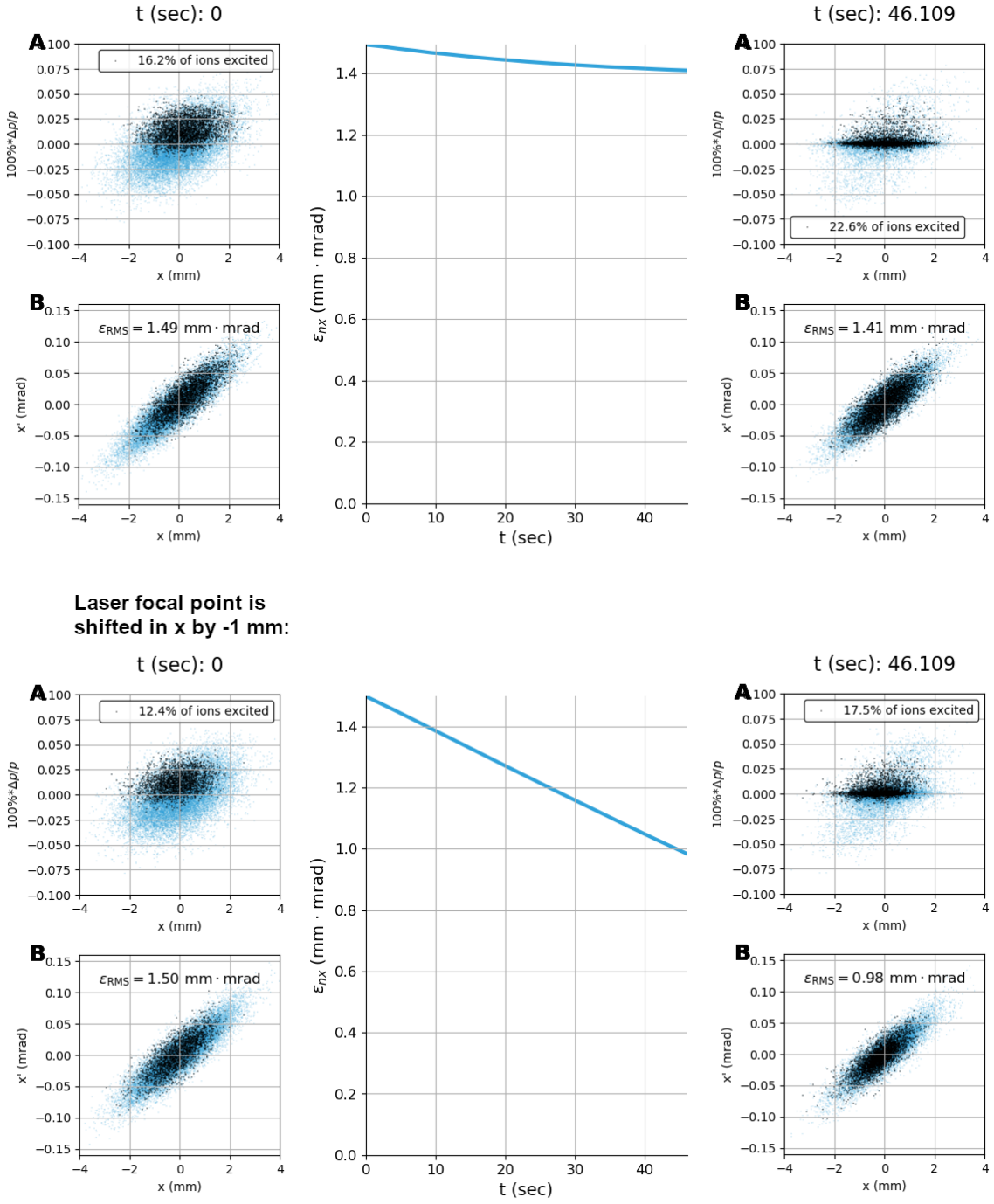

Fig. 27: Simulated evolution of transverse emittance in two regimes of the laser cooling: top pictures show the case when the ion beam and the laser are aligned in the interaction point, while the bottom pictures show the case when the laser pulse is misaligned by -1 mm with respect the the ion beam center in order to achieve the fast transverse cooling via the dispersive coupling (see Section 3.2 for details). Excited ions are marked by black dots, while unperturbed ions are shown as blue dots. For details see the dedicated Jupyter notebook [86].

The overall timeline of the PoP phase of the GF studies in the period 2020–2024, together with its milestones, is presented in Fig. 29. The installation of the infrastructure and sub-systems are foreseen to take place during the 2021/22 and 2022/23 winter Year End Technical Stops (YETS). The laser room is one of the critical points in the planning, since this infrastructure needs to be completed before any of the laser sub-systems can be installed. For this reason, the present planning is conservative in that it assumes: (1) that no works are possible in LS2, (2) that the YETS 2021/2022 is fully dedicated to the laser room and other infrastructure, and (3) that the laser system can only be installed and commissioned in the YETS 2022/2023. If some preparatory works can still be accommodated at the end of LS2, then the more margin could be generated in the critical path activity of the laser room installation.

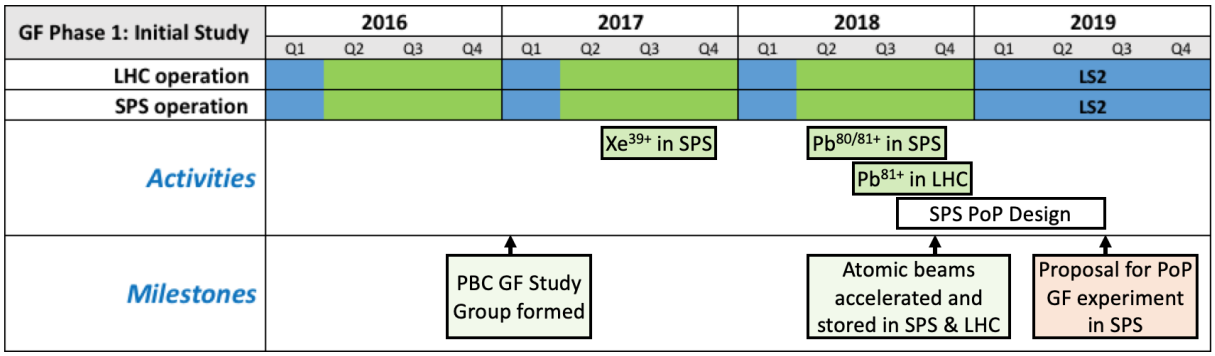

Fig. 28: The timeline of the Gamma Factory Initial Study, Phase 1 activities – years 2016–2019.

In 2021 the beam tests in the SPS will use the existing stripper (in a dedicated mode) and will focus on establishing and characterising the SPS cycle and the beam, as well as investigating the energy calibration methods.

In 2022, with the new stripper available, the beam tests in SPS can take place inside a supercycle with other beams. It is planned to commission the photon detector and to finalise the SPS beam characterisation and energy matching, as well as measurement of the performance with the new stripper.

In 2023 and 2024, after the installation of the laser and the FPC, the plan is to have a series of PoP runs totalling about 5 weeks per year, which would be split between (mostly) experimental time for commissioning and measurements with the experiment proper, and MD for beam improvement and technical aspects, like BPM commissioning. It is expected that most of this time will be in parallel operation. This scenario assumes that the TT2 stripper is configured in the 2021/2022 YETS to allow the foil to be inserted for the ion cycles, and that in consequence the PoP experiment will use the SPS ring in a parasitic mode with minimal interference with the canonical SPS operation. A few dedicated periods of experiment or MD for stand-alone runs with the SPS Pb^{79+} beam in a coast mode may be required, e.g. to optimise the photon beam production efficiency or perform long lifetime or blowup measurements.

Beyond 2024, there will be the opportunity to improve the experiment in LS3 on the basis of the results from Run 3, for example with the improved detector(s) or laser system, and it is expected that the experiment will remain in the SPS for the LHC Run 4 period scheduled from 2026 to 2029.

The SPS PoP programme therefore covers about a decade. The operational experience with the experiment, its results and their extrapolation to the LHC running conditions will be essential to assess the feasibility of an LHC-based photon-beam production scheme. In parallel to running the PoP experiment, we plan prepare over the years 2023 and 2024, a GF Technical Design Report (TDR) for an LHC Demonstrator Application.

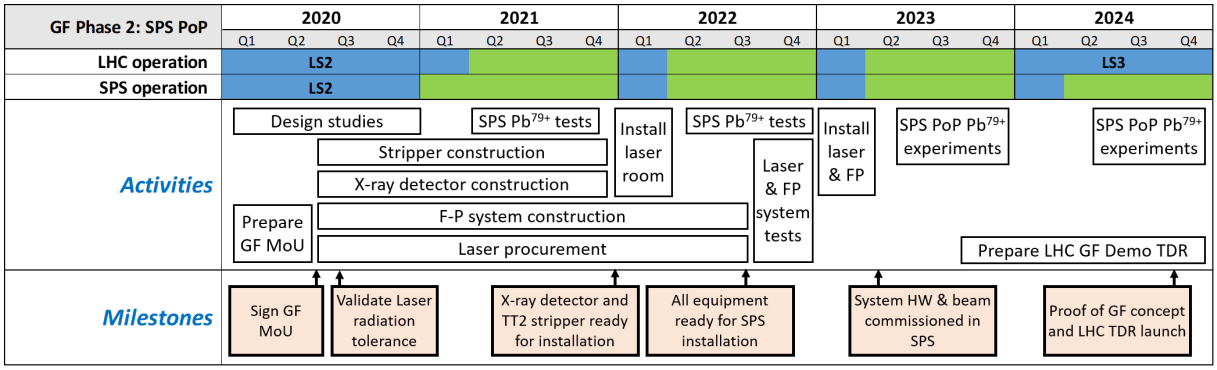

Fig. 29: The timeline of the Gamma Factory SPS PoP experiment, Phase 2 activities, for the years 2020–2024. Beyond this timeframe an upgrade of the system in LS3 will be possible for a second run in the years 2026–2029.

7.1.3 Phase 3: LHC Demonstrator Application

The SPS PoP experiment will give key input for the third phase: a demonstration of a Gamma Factory Application in the LHC, with the much higher Lorentz-γ boost factor.

The detailed technical scope, timeline and cost of the LHC Demonstrator Application phase of the studies are hypothetical, as long as the PoP experiment and the specific LHC applications are not finalised. A possible and logical application would be to use the Li-like Pb^{79+} in the LHC and to excite either the $2s \to 3p_{1/2}$ or $2s \to 2p_{3/2}$ transitions. This scenario would represent a "minimal investment" option, cover large domain of photon beam energies from 15 to 87 MeV, use the well-studied Pb^{79+} beam already foreseen for the running period following LS3 and could also directly re-use the laser and FP system of the SPS PoP experiment. The LHC experiment would allow to study the new technical aspects of γ-photon extraction, ionisation from double-photon absorption and γ-ray detectors. In addition, it would open the possibility of new Atomic Physics measurements (combined measurement of the spin 3/2 state (LHC) and 1/2 state (SPS), measurement of the neutron skin of the nuclei in dedicated runs using different lead isotopes), a possible light-shining-through-the-wall demo experiment and characterisation of the secondary beams of polarised positrons and neutrons.

The timeline of the design, construction and installation of an eventual Phase 3 LHC Demonstrator will begin around 2025 and is expected to last around 4–5 years, depending on the scope.

7.2 Project resources

The initial study (Phase 1) of the GF R&D programme was accomplished without a dedicated budget line, since there was no material expenditure and the required financial support for studies was very kindly found within the Physics Beyond Colliders envelope. Manpower was found within the CERN Physics Beyond Colliders community and from external institutes.

The cost and manpower needs for the LHC Demonstrator Application (Phase 3) will depend heavily on the specifics of the application tools chosen, since this will determine the laser technology, the interaction region design, the beam extraction and γ-ray transport design. The scope definition and detailed costing of this Phase 3 will be a key part of the TDR stage, which will be finalised, at the earliest, before the end of the year 2024.

The SPS PoP experiment requires a modest but tangible level of financial and manpower investment for the design, construction, installation and execution of the experiment. The financial estimates are relatively well defined, since the costs for the technical sub-systems are based on similar systems for which the costs have been well established. The manpower estimates have been made for each of the subsystems (activity) and intrinsically have more uncertainty. However, the totals obtained are fully

coherent with the manpower costs of similar size projects at CERN, for developments of similar technologies, in terms of the kCHF per FTE of effort. The finalisation of these estimates with the responsible teams and the collaboration will be one of the first activities of the project after approval.

The manpower for the project will rely heavily on the collaborating institutes, as well as CERN. The present members of the GF study group and their institutes are listed in Appendix 1.

7.2.1 Budget estimate

The estimated financial cost and manpower needs for the Phase 2 of the project – the SPS PoP experiment – are outlined in the following sections. The cost estimates are based on the scope described above, with the new stripper foil and the dedicated laser system to be installed, together with the FPC, the X-ray detector and all the experiment infrastructure. The main cost drivers are:

1. The new stripper in the PS–SPS transfer line, with changes to the local vacuum layout, controls and cabling;
2. The laser system in the SPS tunnel, with the laser room, the transport beamline, the infrastructure and cabling;
3. The vacuum vessel and the FPC in the SPS ring, together with controls, cabling and changes to the local vacuum layout;
4. The photon detection system and readout in the SPS ring, together with controls, cabling and changes to the local vacuum layout.

The preliminary cost estimates for the different sub-systems and other required expenditures are summarised in Table 8. The costs associated with the controls, infrastructure and services needed for the ion stripper, the laser and the diagnostics (e.g. cabling, shielding) are included in the estimates, as well as some costs for the collaboration for the design study. Manpower (Doctoral students and Post-Doctoral Research Assistants) which needs financing from the project budget is also specified explicitly in this material budget table.

Table 8: Preliminary material cost estimates for the Gamma Factory SPS PoP experiment.

	Item	**Cost [kCHF]**
1	**Stripping foil** unit (design, assembly, tests, installation – in synergy with a foreseen stripper upgrade)	125
2	**FPC** (optics, support, interface, vacuum system)	180
3	**Laser system** (oscillator, amplifier, electronics, controls, assembly, lab tests, shipping, installation)	800
4	**Laser clean room and UHV transport line** (in SPS tunnel)	600
5	**Photon detection system** (design, detector, controls, vacuum chamber, assembly, tests, installation)	100
6	**Beam position monitor** (detector, cabling, electronics)	50
7	**Infrastructure and services** (cabling, supports, shielding)	80
8	**Manpower** (Doctoral Student/PDRA subsistence)	350
9	**Collaboration support** (travel, subsistence)	80
	Total	2365

7.2.2 Manpower estimate

The provisional estimates for manpower needed for the provision or integration of the different subsystems is given in Table 9. The numbers are total integrated FTE.years, and are divided into the CERN Staff or the GF collaboration. The CERN manpower will cover site-specific aspects, such as controls integration, tests, synchronisation and also contribute to experimental commissioning and tests. It will be distributed between the CERN accelerator departments. The GF collaboration manpower is mainly for the bulk of the activities for the laser system, the FPC and the detector and will need to be provided by the collaborating institutes.

A breakdown of the expected costs and manpower profiles per year is made in Table 10.

Table 9: Preliminary manpower estimates for the Gamma Factory SPS PoP experiment.

Item	**Collaboration [FTE.y]**	**DOCT/PDRA [FTE.y]**	**CERN [FTE.y]**
Stripping foil unit	0.2		1.0
FPC	2.5	1.0	0.5
Laser system	2.5	3.0	0.5
Laser beamline	1.0		0.1
Photon detection system	2.0		2.0
Infrastructure and services	0.5		2.5
Collaboration support	0.2		0.5
Commissioning, measurements, analysis	1.8	1.5	2.3
Total	10.7	5.5	9.4

Table 10: Preliminary resource profile for the Gamma Factory SPS PoP experiment.

Year	**Cost [kCHF]**	**Manpower [FTE]**		
		Collaboration	**DOCT/PDRA**	**CERN**
2020	510	1.5	0.5	0.9
2021	705	2.6	1.0	2.5
2022	680	2.2	1.2	2.0
2023	260	2.2	1.4	2.0
2024	210	2.2	1.4	2.0
Total	2365	10.7	5.5	9.4

7.3 Organisational aspects and task list

The SPS Implementation of the GF PoP experiment will require a defined Work Breakdown Structure (WBS) and responsibilities allocated to the CERN groups for the cases where equipment is to be installed in the accelerator or integrated into the SPS control system, and for other crucial machine activities. The responsibility will be on the side of the GF collaboration for provision of specific subsystems, simulation efforts and other deliverables.

A preliminary list of tasks that will form the basis for the WBS is shown below, where the expected responsibility sharing between CERN and the GF collaboration is indicated. Each task will have a task leader, selected once the LoI is approved, the collaboration is consolidated and we move to the

technical design phase of the project. One of the first activities at the start of the project execution will therefore be to finalise the technical organisation and to define the responsibilities of CERN and of the GF collaboration, based on this task list.

A formal collaboration agreement will be needed for the responsibility definition and to agree the milestones and deliverables. An important initial milestone will be the formulation and signature of a Memorandum of Understanding (MoU) to formalise the collaboration and the various contributions of the different partners, including CERN. This should be done within 6 months of the project start.

7.3.1 Task breakdown

Atomic Physics input

The calculations of the atomic resonance energy levels, cross sections and lifetimes will come from the contributing GF collaborators. This topic will also include input and calculations for the design of the Atomic Physics measurements and contribution to the analysis of the measurement data.

Simulation and data analysis

The simulations of the laser-photon interactions will be largely carried out by the contributing GF collaborators, while the accelerator physics simulations will be shared between CERN and the GF collaboration. Other more specific topics, like the beam stability and impedance effects of the installed components, will be carried out by CERN. The analysis of the experimental data and the comparison with the theoretical calculations will be a joint effort depending on the specific topic.

SPS PSI Beams

CERN will be responsible for the preparation, provision and characterisation of the PSI beams. This also includes the description of the accelerator optics and beam distribution characteristics at the interaction region and the detector.

Stripper foil and stripper unit

The contributing GF collaborators will be responsible for the simulations of the stipping efficiency and specification of the foil, while CERN will provide the foil and the stripper system together with its controls, and install it into the PS-to-SPS transfer line.

SPS Beam Diagnostics

The beam diagnostics will be needed for the characterisation of the PSI beam transverse and longitudinal distributions, as well as the read-out of the beam position and intensity. In addition, the information on the beam momentum centroid and distribution will be required. These aspects will be the responsibility of CERN, although the incorporation of the BPMs in the vacuum vessel around the FPC will need close collaboration.

Laser–PSI beam synchronisation

The synchronisation between the laser and PSI beams will be under the responsibility of CERN, using the existing technology. The key aspect of the definition of the interfaces needs to be closely coordinated between CERN and the laser and FPC experts.

Laser system and Fabry–Pérot cavity

The design and procurement of the laser system and the FPC including the vacuum vessel will be the responsibility of the contributing GF collaborators, complete with the local controls and infrastructure.

The details of the interfaces to the vacuum system, the support structures and the integration of the system into the CERN control system will need to be a joint effort.

Laser room and beamlines

The laser room with controlled environment and the beamlines to transport the laser beam to the FPC will be the responsibility of the contributing GF collaborators to provide, while the design, detailed integration and installation into the SPS tunnel will be performed in close synergy with CERN.

Physical Integration in SPS tunnel

CERN will perform the verification of the physical integration of the various systems into the SPS tunnel, with updates of databases, layouts and optics files. Any detailed drawings for this integration will be provided by the collaboration as part of the design.

Integration into CERN control system

Control of laser timing, power and other parameters will need to be included in the CERN control system, together with the acquisition of the laser and FPC parameters, and data from the photon detector. The data acqusition and control hardware will be a part of the detector and laser/FP systems procured by the collaboration, while the middleware layer and high-level software (including APIs, GUIs, logging) will be provided by CERN.

Photon detection system

The design, construction and installation of the X-ray photon detection system will be the responsibility of CERN. It is assumed that the existing technical solutions will be reused. The GF collaboration will support this with simulations and specifications needed for the system definition.

SPS vaccum

The responsibility for the SPS vacuum in terms of changes local to the FPC and detector, as well as information needed for calculations of the PSI lifetimes, will be the responsibility of CERN. Specifications for the pumping and instrumentation will be needed from the contributing GF collaborators for the FPC vacuum vessel.

Radiation and beam loss simulations and effects

The provision of radiation field estimates including simulations of the effectiveness of shielding will be from CERN, on the basis of existing information on beam losses and expected distributions with the PSI beams. Radiation tests on specific critical electronics and optical components will need to be jointly organised with CERN and the contributing GF collaborators.

Impedance

The impedance of the proposed devices to be installed on the SPS ring will need to be formally validated by CERN, on the basis of the detailed design (geometries and materials) provided by the contributing GF collaborators. CERN will need to give an input at the design time to make sure the impedance constraints are respected.

Shutdown scheduling and planning

The planning of the inspection and installation works in the CERN shutdowns will be managed by CERN with the input of the contributing GF collaborators on the duration and conditions of the various interventions.

Radiation protection and safety

Radiation protection and safety will be organised by CERN as part of the project safety file.

Infrastructure

Infrastructure such as cables, cooling, ethernet or optical fibres in SPS LSS6 (for the laser, the FPC and the detector) and in TT2 (for the stripper) will be the responsibility of CERN, although the specification will need to be provided by the contributing GF collaborators for the laser and the FPC.

8 Summary

We propose an SPS experiment to study a novel accelerator-based production scheme of high-intensity photon beams in an energy range inaccessible for present FEL technology. Our goal is to test this scheme at the SPS prior to its possible future implementation at the LHC. We plan to collide an atomic beam of lithium-like lead, $^{208}\mathrm{Pb}^{79+}$, circulating in the SPS, with a laser beam. The laser beam power will be enhanced in an optical resonator incorporated into the SPS ring, and the laser beam wavelength tuned with respect to the atomic beam momentum to maximise the rate of the resonant, $2s \rightarrow 2p_{1/2}$, atomic transitions of the $^{208}\mathrm{Pb}^{79+}$ ions. In addition to the basic feasibility, one of the goals of the proposed experiment is to demonstrate that atomic beams can be efficiently cooled, both longitudinally and transversely, at ultra-relativistic energies.

The ultimate aim of the Gamma Factory initiative is to create and to exploit new type of particle beams characterised by a significant leap in their intensity, purity, energy range, and plug-power efficiency. The primary beam of γ-rays is proposed to be generated by storing atomic beams of partially stripped ions in the LHC ring(s) and by exciting their atomic degrees of freedom by laser beams. The secondary beams of polarised charged leptons, neutrinos, neutrons and radioactive ions would be produced in collisions of the high-intensity γ-ray beams with external target(s). These primary and secondary beams, if produced by the Gamma Factory, could open new perspectives for the High Energy Physics community and new cross-disciplinary research domains at CERN by re-using its existing accelerator infrastructure in unconventional but innovative way. The Gamma Factory Proof-of-Principle experiment in the SPS is an important and necessary R&D step for a future Gamma Factory research programme, and a realistic evaluation of the achievable photon beam intensities is the primary target of the proposed experiment.

The Gamma Factory R&D studies have already made real progress and have attracted the interest of many research groups from around the world, representing diverse physics communities. The demonstration of efficient production, acceleration and storage of atomic beams in the CERN accelerator complex has been already achieved during the past two years, and the design of the SPS Proof-of-Principle experiment has been defined. If the proposed SPS experiment is approved, it will provide, at a modest cost and a negligible interference with the ongoing CERN research programme, the necessary input data for the quantitative evaluation of the Gamma Factory research potential.

Appendices

1 GF community and expected participation in SPS PoP experiment

The GF initiative is of general interest for the following scientific communities:

- the accelerator physics community;
- the particle physics community;
- the laser physics community;
- the atomic, molecular and optical physics community;
- the nuclear physics community;
- the applied physics community.

The GF study group was formally created in February 2017 and now includes scientists representing all the above communities. The group is, at present, composed of 65 researchers affiliated to 24 institutes from 10 countries, and it is steadily expanding. Its present members are listed below. The composition of the group actively involved in the SPS PoP experiment will evolve from this community, with emphasis on the laser, accelerator and atomic physics communities for the realisation and execution of the experiment. It will be open to new research groups and individuals willing to join the GF initiative, or just to participate in its PoP experiment. In particular, as the concepts for the LHC demonstration experiment develop with the progress in the SPS, it is expected that the group will expand in the appropriate specific directions.

Members of Gamma Factory Study Group

A. Abramov[1], S.E. Alden[1], R. Alemany Fernandez[2], P.S. Antsiferov[3], A. Apyan[4], H. Bartosik[2], E.G. Bessonov[5], N. Biancacci[2], J. Bieroń[6], A. Bogacz[7], A. Bosco[1], R. Bruce[2], D. Budker[8,9,10], K. Cassou[11], F. Castelli[12], I. Chaikovska[11], C. Curatolo[13], P. Czodrowski[2], A. Derevianko[14], K. Dupraz[11], Y. Dutheil[2], K. Dzierżęga[6], V. Fedosseev[2], N. Fuster Martinez[2], S.M. Gibson[1], B. Goddard[2], A. Gorzawski[15,2], S. Hirlander[2], J.M. Jowett[2], R. Kersevan[2], M. Kowalska[2], M.W. Krasny[16,2], F. Kroeger[17], D. Kuchler[2], M. Lamont[2], T. Lefevre[2], D. Manglunki[2], B. Marsh[2], A. Martens[11], J. Molson[2], D. Nutarelli[11], L.J. Nevay[1], A. Petrenko[18,2], V. Petrillo[12], W. Płaczek[6], S. Redaelli[2], Y. Peinaud[11], S. Pustelny[6], S. Rochester[19], M. Sapinski[20], M. Schaumann[2], R. Scrivens[2], L. Serafini[12], V.P. Shevelko[5], T. Stoehlker[17], A. Surzhykov[21], I. Tolstikhina[5], F. Velotti[2], G. Weber[17], Y.K. Wu[22], C. Yin-Vallgren[2], M. Zanetti[23,13], F. Zimmermann[2], M.S. Zolotorev[24] and F. Zomer[11]

[1] *Royal Holloway University of London Egham, Surrey, TW20 0EX, United Kingdom*
[2] *CERN, Geneva, Switzerland*
[3] *Institute of Spectroscopy, Russian Academy of Sciences, Troitsk, Moscow Region, Russia*
[4] *A.I. Alikhanyan National Science Laboratory, Yerevan, Armenia*
[5] *P.N. Lebedev Physical Institute, Russian Academy of Sciences, Moscow, Russia*
[6] *Marian Smoluchowski Institute of Physics, Jagiellonian University, Kraków, Poland*
[7] *Center for Advanced Studies of Accelerators, Jefferson Lab, USA*
[8] *Helmholtz Institute, Johannes Gutenberg University, Mainz, Germany*
[9] *Department of Physics, University of California, Berkeley, USA*
[10] *Nuclear Science Division, E.O. Lawrence National Laboratory, Berkeley, USA*
[11] *LAL, Univ. Paris-Sud, CNRS/IN2P3, Université Paris-Saclay, Orsay, France*
[12] *Department of Physics, INFN–Milan and University of Milan, Milan, Italy*
[13] *INFN–Padua, Padua, Italy*
[14] *University of Nevada, Reno, Nevada 89557, USA*
[15] *University of Malta, Malta*
[16] *LPNHE, University Paris Sorbonne, CNRS–IN2P3, Paris, France*

[17] *HI Jena, IOQ FSU Jena and GSI Darmstadt, Germany*
[18] *Budker Institute of Nuclear Physics, Novosibirsk, Russia*
[19] *Rochester Scientific, LLC, El Cerrito, CA 94530, USA*
[20] *GSI, Helmholtzzentrum für Schwerionenforschung, 64291 Darmstadt, Germany*
[21] *Braunschweig University of Technology and Physikalisch-Technische Bundesanstalt, Germany*
[22] *FEL Laboratory, Duke University, Durham, USA*
[23] *University of Padua, Padua, Italy*
[24] *Center for Beam Physics, LBNL, Berkeley, USA*

2 Photon absorption and emission by ultra-relativistic partially stripped ions

The interaction of a photon with an ultra-relativistic partially stripped ion propagating in the opposite direction is the key phenomenon exploited by the GF PoP experiment to produce high-energy gamma-rays. Due to a relativistic Doppler shift, the ion experiences in its rest frame the photon of much higher energy which, if resonant with its atomic-levels transition, is able excite it. The excited ion eventually decays into its ground state emitting a photon. Due to the ultra-relativistic motion of the ion, the secondary photon energy is increased with respect to the primary photon. This process is shown in Fig. 30.

In the laboratory reference frame:

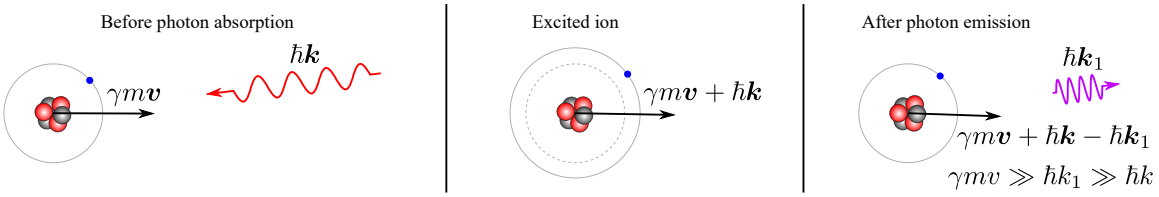

In the initial ion reference frame:

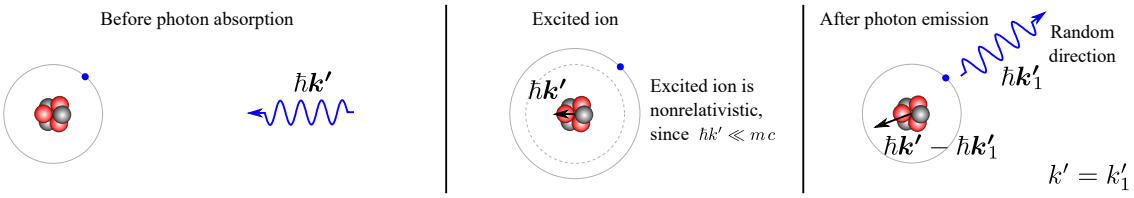

Fig. 30: The process of photon scattering in the laboratory and rest reference frames.

For ultra-relativistic ions, the scheme enables conversion of infra-red, visible or near-ultraviolet photons into X-ray or gamma-ray photons. Moreover, it also provides control over the secondary-photon frequency by adjusting the ion energy.

To consider the process quantitatively, we utilise 4-vectors $(E/c, \boldsymbol{p})$ for the Lorentz transformation. The ion 4-momentum is given by $(\gamma mc, \gamma m\boldsymbol{v})$ and the photon 4-momentum is $(\hbar\omega/c, \hbar\boldsymbol{k})$. If the z-axis is aligned with the direction of the ion motion, then the Lorentz transformation can be written as

$$\begin{pmatrix} E'/c \\ p'_x \\ p'_y \\ p'_z \end{pmatrix} = \begin{pmatrix} \gamma & 0 & 0 & -\beta\gamma \\ 0 & 1 & 0 & 0 \\ 0 & 0 & 1 & 0 \\ -\beta\gamma & 0 & 0 & \gamma \end{pmatrix} \begin{pmatrix} E/c \\ p_x \\ p_y \\ p_z \end{pmatrix}, \tag{10}$$

where prime quantities are given in the ion rest frame (Fig. 31). Here, $\gamma = 1/\sqrt{1-\beta^2}$ is the Lorentz factor and $\beta = v/c$ with v being the speed of the particle and c being the speed of light.

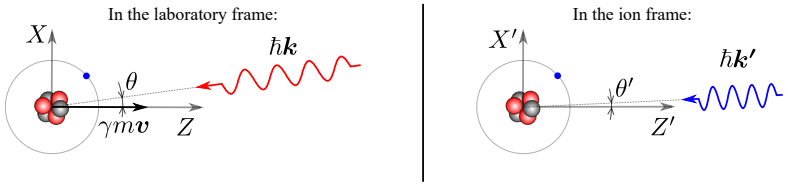

Fig. 31: Transformation of the process of photon scattering between the laboratory frame and the ion rest frame.

Since a photon momentum $\boldsymbol{p}$ relates to the light's wave-vector $\boldsymbol{k}$ through $\boldsymbol{p} = \hbar\boldsymbol{k}$, where $\hbar$ is the

reduced Planck constant, $k_x = -k\sin\theta$, $k_y = 0$, $k_z = -k\cos\theta$ and $k = \omega/c$ (Fig. 31), one can rewrite Eq. (10) into

$$\begin{pmatrix} 1 \\ -\sin\theta' \\ 0 \\ -\cos\theta' \end{pmatrix} \omega' = \begin{pmatrix} \gamma & 0 & 0 & -\beta\gamma \\ 0 & 1 & 0 & 0 \\ 0 & 0 & 1 & 0 \\ -\beta\gamma & 0 & 0 & \gamma \end{pmatrix} \begin{pmatrix} 1 \\ -\sin\theta \\ 0 \\ -\cos\theta \end{pmatrix} \omega, \tag{11}$$

and hence the relation between the photon frequency in the two frames is given by

$$\omega' = (1 + \beta\cos\theta)\gamma\omega \approx \left(1 + \beta - \beta\frac{\theta^2}{2}\right)\gamma\omega \approx 2\gamma\omega. \tag{12}$$

Eq. (12) shows that the frequency of the photon in the ion frame is 2γ-times larger than in the laboratory frame, and hence it can excite transitions inaccessible to the light.

An important issue seems to be a spread of the angle $\Delta\theta$, as ions would experience photons of different frequencies. However, from the Lorentz transformation

$$\omega' \sin\theta' = \omega \sin\theta, \tag{13}$$

one can show that

$$\Delta\theta' \approx \frac{\Delta\theta}{2\gamma} \tag{14}$$

and the spread is significantly suppressed. In particular, a spread on the order of $\Delta\theta \approx 1$ mrad corresponds to an ion-frame frequency spread of only $\sim 10^{-6}$. This shows that the angular misalignment is not a serious problem. At the same time a much more significant contribution comes from the energy spread in the ion beam (typically $\approx 10^{-4}$). Because of this spread, in order to excite a large fraction of the ions in the beam the relative frequency spread of the laser pulse should be comparable to the relative energy spread in the ion beam.

After a finite time, an excited ion returns to the ground state emitting a secondary photon. This process is depicted in Fig. 32 in both the laboratory and ion rest frames. At this level, it can be assumed

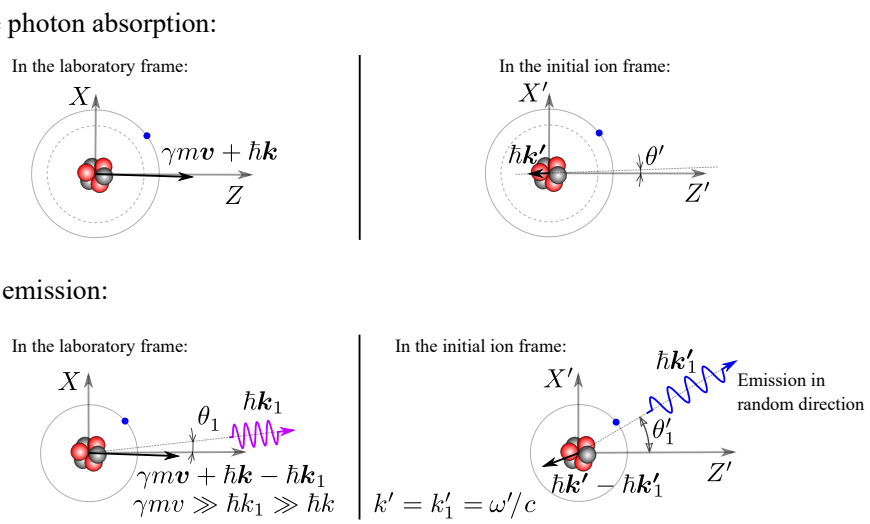

Fig. 32: The excited ion after the photon absorption and the ion after the photon emission.

that the emission of the photon in the ion rest frame is isotropic. This is, however, strongly modified when transferring the system into the laboratory frame.

Let us consider now the process where the secondary photon is emitted in the same plane as the absorbed photon (the $x'z'$-plane) at a random angle θ_1'. In such a case, the wave-vector components are

given by $k'_{1x} = k' \sin\theta'_1$ and $k'_{1z} = k' \cos\theta'_1$ and the inverse Lorentz transformation gives us the relation between the emitted-photon parameters in the two frames

$$\begin{pmatrix} 1 \\ \sin\theta_1 \\ 0 \\ \cos\theta_1 \end{pmatrix} \omega_1 = \begin{pmatrix} \gamma & 0 & 0 & \beta\gamma \\ 0 & 1 & 0 & 0 \\ 0 & 0 & 1 & 0 \\ \beta\gamma & 0 & 0 & \gamma \end{pmatrix} \begin{pmatrix} 1 \\ \sin\theta'_1 \\ 0 \\ \cos\theta'_1 \end{pmatrix} \omega'. \tag{15}$$

Hence, the secondary-photon frequency is given by

$$\omega_1 = \gamma(1 + \beta\cos\theta'_1)\omega' \approx 2\gamma^2(1 + \beta\cos\theta'_1)\omega. \tag{16}$$

The laboratory-frame emission angle θ_1 can be also calculated using the inverse Lorentz transformation

$$\omega_1 \sin\theta_1 = \omega' \sin\theta'_1 \;\Rightarrow\; \sin\theta_1 = \frac{\sin\theta'_1}{\gamma(1 + \beta\cos\theta'_1)}, \tag{17}$$

yielding a typical of emission spread $\Delta\theta_1 \sim 1/\gamma$.

A small fraction of photons is emitted with $\theta_1 \sim 1$ and in this case to separate the forward and backward emissions it is important to know $\cos\theta_1$:

$$\omega_1 \cos\theta_1 = \omega'\gamma(\beta + \cos\theta'_1) \;\Rightarrow\; \cos\theta_1 = \frac{\beta + \cos\theta'_1}{1 + \beta\cos\theta'_1}. \tag{18}$$

The typical transverse kick obtained by the ion due to the photon emission is very small compared to the typical angular spread in the ion beam. Therefore, the main effect of the photon emission on the ion motion is the small loss of the ion total momentum.

2.1 Photon absorption cross section

The cross section of the ion excitation by a photon with the frequency ω' is given by [88, 89]

$$\sigma = 2\pi^2 c r_e f_{12} g(\omega' - \omega'_0), \tag{19}$$

where r_e is classical electron radius, f_{12} is the oscillator strength, ω'_0 is the resonance frequency of the ion transition, $g(\omega' - \omega'_0)$ is the Lorentzian

$$g(\omega' - \omega'_0) = \frac{1}{2\pi} \cdot \frac{\Gamma}{(\omega' - \omega'_0)^2 + \Gamma^2/4}, \tag{20}$$

where Γ is the resonance width defined by the lifetime of the excited ion τ':

$$\Gamma = \frac{1}{\tau'}. \tag{21}$$

Also

$$\Gamma = 2 r_e \omega'^2_0 f_{12} \frac{g_1}{c g_2}, \tag{22}$$

where g_1, g_2 are the degeneracy factors of the ground state and the excited state. Therefore,

$$\sigma(\omega' - \omega'_0) = \frac{\sigma_0}{1 + 4\tau'^2(\omega' - \omega'_0)^2}, \tag{23}$$

where

$$\sigma_0 = \frac{\lambda_0'^2 g_2}{2\pi g_1}. \tag{24}$$

$\lambda_0' = 2\pi c/\omega_0'$ is the transition wavelength.

2.2 Estimate of the required laser energy

We can estimate the energy of the laser pulse required to excite significant fraction of ions in the bunch. If the laser wavelength perfectly matches the ion level we would need one photon per every σ_0 cross section, i.e.

$$N_{\hbar\omega_0} \sim \frac{w_L^2}{\sigma_0}, \tag{25}$$

where w_L is the laser beam transverse size (assumed to match the size of the ion beam). However, since the energy spread σ_E/E in the ion bunch is larger than the width of the resonance we need $N_{\hbar\omega_0}$ photons for all possible frequencies, i.e.

$$N_{\hbar\omega} \sim N_{\hbar\omega_0} \frac{\sigma_E}{E} \Big/ \frac{\Gamma}{\omega_0} \sim \frac{w_L^2}{\sigma_0} \frac{\sigma_E}{E} \omega_0 \tau'. \tag{26}$$

And the energy of the laser pulse should be

$$U \sim \hbar\omega \frac{w_L^2}{\sigma_0} \frac{\sigma_E}{E} \omega_0 \tau'. \tag{27}$$

This expression is an order of magnitude estimate neglecting geometric factors of overlap between the laser and the ion bunch.

2.3 Saturation effect

The number of excitation events for every ion (or probability of its excitation) can be found as

$$N_{exc} = \frac{dN_{\hbar\omega}}{dS} \bar{\sigma}, \tag{28}$$

where $\bar{\sigma}$ is the excitation cross section averaged over the laser frequency distribution and, as we have already seen, $\bar{\sigma} \ll \sigma_0$.

In our model here, we assume that if $N_{exc} \ll 1$, then N_{exc} is the probability of the ion excitation. For $N_{exc} \sim 0.1$ we should take into account the saturation effects. This can be done by solving the rate equation

$$\frac{dP_2}{dt} = m_2 P_1 - m_2 B P_2, \tag{29}$$

where P_2, P_1 are the probabilities of the ion to be in the excited and non-excited state, respectively ($P_1 + P_2 = 1$). The rate of excitation events $m_2 P_1$ is proportional to the population of the lower level P_1, the photon density and the absorption cross section, while $m_2 B P_2$ is the rate of stimulated emission events ($B = g_1/g_2$). Before the ion enters into the laser pulse: $P_1 = 1$ and $P_2 = 0$.

To solve the rate equation we need to separate the variables:

$$\frac{dP_2}{1 - (1+B)P_2} = m_2 dt. \tag{30}$$

m_2 depends on time during the passage of the ion through the laser pulse, but we already know the answer in the case of small $P_2 = N_{exc} \ll 1$, hence

$$\int_t m_2(t)dt = \frac{dN_{\hbar\omega}}{dS}\bar{\sigma}. \tag{31}$$

Therefore the result of integration

$$N_{exc} = P_2 = \frac{1 - \exp\left[-(1+B)\int_t m_2(t)dt\right]}{1+B} = \frac{1 - \exp\left[-(1+B)\frac{dN_{\hbar\omega}}{dS}\bar{\sigma}\right]}{1+B}. \tag{32}$$

As one can see, if $\frac{dN_{\hbar\omega}}{dS}\bar{\sigma}$ is small it equals N_{exc}, while for large $\frac{dN_{\hbar\omega}}{dS}\bar{\sigma}$ the result is limited by $1/(1+B)$.

3 Simulation tools

New simulation codes had been developed within the Gamma Factory study group to implement the theory of collisions of bunched ultra-relativistic atomic beams with laser pulses. The simulation results presented in this LoI have been obtained using these independent frameworks. A short description of the codes is presented below.

3.1 GF-CMCC

`CMCC` is a Fortran event generator dedicated to simulations of asymmetric electron–photon or proton–photon collisions [90]. The code has been adapted to simulate PSI–laser-photon interaction and it has been named `GF-CMCC` [3, 78]. The interaction is simulated in a static way, without propagation of the beams through each other (no time steps). Given the ion mass and the state-degeneracy factors g_1, g_2, the beam is sampled according to the Gaussian distributions of position and momentum. The program loops over the macro-particles in which the beam is clustered in order to reduce the computational time. For every macro-particle the energy of the interacting photon is sampled around a mean value corresponding to the mean value of the desired resonance, and the resonant absorption cross section is calculated.

In order to define the total number of PSIs excited thanks to absorption of photons from the laser, the program uses a Monte Carlo rejection method. The spatial, energy and density distributions of the laser and the interaction angle are taken into account. The ion de-excitation occurs at a distance from the interaction point depending on the mean lifetime of the spontaneous emission. The emitted photon is generated in the centre-of-mass frame and then Lorentz boosted in the laboratory frame. We are considering an isotropic photon emission in the PSI rest frame.

A depletion of the number of spontaneous emitted photons can be caused by stimulated emission of low energy photons occurring if the excited ion absorbs a second photon from the laser beam. Stimulated emission is more probable when the laser density is higher and the spontaneous emission decay time is longer. Disregarding stimulated emission, the code provides also a calculation of the total number of emitted photons based on the luminosity formula.

3.2 GF-CAIN

`GF-CAIN` [91] is a stand-alone Monte Carlo event generator for collisions of PSI bunches with laser-photon pulses including processes of resonant atomic photon absorption and subsequent spontaneous as well as stimulated photon emissions. It is based on the program `CAIN` for simulations of beam–beam interactions involving high energy electrons, positrons and photons developed by K. Yokoya et al. [92] at KEK-Tsukuba, Japan, and dedicated to the ILC project.

In the current version of `GF-CAIN` two species of PSI are included:

1. The hydrogen-like lead ion $^{208}\mathrm{Pb}^{81+}$ with the transition: $1s^1\ ^2S_{1/2} \rightarrow 2p^1\ ^2P_{1/2}$ as an example for the LHC-based GF.
2. The lithium-like lead ion $^{208}\mathrm{Pb}^{79+}$ with the transition: $1s^2 2s^1\ ^2S_{1/2} \rightarrow 1s^2 2p^1\ ^2P_{1/2}$ for simulations of the GF PoP experiment at the SPS.

In the Monte Carlo simulations of `GF-CAIN`, first the PSI bunch and the laser-photon pulse are placed at some distance from each other in the time moment t_0 – usually the time $t = 0$ corresponds to the moment when the centres of the PSI bunch and the laser pulse overlap. Then, the simulation of the collision between the PSI-bunch and the photon-pulse is performed in time steps Δt according to the scattering probability

$$P(\vec{r}, \vec{p}, \vec{k}, t; \Delta t) = \sigma_{\mathrm{tot}}(\vec{p}, \vec{k})\,(1 - \vec{\beta} \cdot \vec{k}/|\vec{k}|)\,n_p(\vec{r}, \vec{k}, t) c \Delta t, \tag{33}$$

where $\vec{r}$, $\vec{p}$ and $\vec{\beta}$ are the PSI position, momentum and relativistic velocity, respectively, $\vec{k}$ – the photon wave-vector, $n_p(\vec{r},\vec{k},t)$ – the local photon density of the laser beam, and $\sigma_{\rm tot}(\vec{p},\vec{k})$ is the total cross section for a single PSI–photon scattering, i.e. photon absorption by PSI corresponding to its transition to an excited atomic state. The time interval Δt is adjusted such that $P \leq 1$.

The Monte Carlo event generation is done in two stages:

1. According to the probability $P(\vec{r},\vec{p},\vec{k},t)$ a scattering event is sampled using the von Neumann rejection method.

2. When scattering event occurs, an emitted photon is generated, i.e. its energy and emission angles are generated in the PSI rest frame according to the differential cross section, and then an event is Lorentz-transformed to the laboratory (LAB) frame.

The above is repeated for each PSI macroparticle, and then generation moves to the next time moment, i.e. $t + \Delta t, \ldots$. The simulation is finished when the final time moment t_1 is reached. The generated event is represented by three lists of final-state macroparticles, i.e. the emitted photons, the excited and de-excited ions, together with their space-time coordinates, four-momenta and weights. This data can be written to a disk-file or transmitted to an appropriate data-analysis program.

In `GF-CAIN` the stimulated emission is implemented in the following way. First, the spontaneous-emission time-delay is generated from the exponential distribution with the mean value corresponding to the lifetime of the excited state. If the PSI is in the excited state, the stimulated emission is generated according to the probability

$$P'(\vec{r},\vec{p}) = \frac{g_1}{g_2}\, P(\vec{r},\vec{p}), \tag{34}$$

where $P(\vec{r},\vec{p})$ is given in Eq. (33) and $g_{1,2}$ are the state-degeneracy factors. This is done with the use of the von Neumann rejection method, and when the event is accepted the ion returns to the unexcited (ground) state while the two photons are discarded. The unexcited ion can be excited again via the laser-photon absorption according to Eq. (33), and so on. The excited ions can emit photons not only during the time of the collision between the PSI-bunch and the laser-pulse, but also afterwards when they travel in the beam pipe. In `GF-CAIN` this is done with the help of special 'drift' routines which can propagate all final-state particles forward to an arbitrary time moment or z-axis coordinate, de-exciting the excited ions on the way via the spontaneous photon emission according to their lifetimes.

3.3 GF-Python: Python-based simulation toolkit

In order to do the first simulations of the Gamma Factory PSI beam dynamics, several Python scripts and Jupyter notebooks were written and combined into a single comprehensive notebook addressing the PSI beam excitation with the laser pulse, photon emissions and turn-by-turn PSI beam dynamics. The code with detailed description is available on-line [85] (the theoretical part is described in Appendix 2).

The main Python notebook describes the process of longitudinal cooling in the SPS [85]. This is a Monte Carlo code which performs turn-by-turn simulation of PSI beam dynamics including interactions with the laser beam, namely the excitation of ions and emission of photons, resulting in the recoil effect which is reducing the total momentum of the ion. No collective effects are taken into account here.

Also, there are several variants of this notebook, addressing different aspects of the proposed experiment: distributions of emitted photons [93, 94], transverse cooling [86], optimisation of laser parameters [79].

The comparison of the ion excitation rates calculated by `GF-Python`, `GF-CAIN` and `GF-CMCC` is shown in Fig. 18.

3.4 Semi-analytical approach

In order to perform quick optimisation of the laser beam parameters, a semi-analytical approach has been developed. The PSI beam 3D direct space is randomly sampled. The momentum-space correlations are neglected. The laser-beam is assumed to be Fourier limited with a flat spectrum. The related sine-cardinal temporal distribution is approximated with a Gaussian distribution to allow analytical calculations. This approximation induces a loss of about 3.3% of the laser beam pulse energy in the tails that are not described by the Gaussian approximation.

The interaction probability for each ion averaged over the spectrum is

$$p_i = \frac{p_{\max}}{1+B}\left(1-\exp(-(1+B)\widetilde{\mathcal{L}}_i\widetilde{\sigma}/p_{\max})\right), \tag{35}$$

where

$$p_{\max} = 0.5\,\mathrm{erf}\left(\frac{\hbar\omega_0'\lambda}{hc(1+\beta\cos\theta_L)}\frac{\Delta\lambda}{\lambda}\frac{E}{\gamma\sigma_E\sqrt{2}}\right) \tag{36}$$

which accounts for the fact that only a fraction of the upper part of the ions spectrum match the laser bandwidth $\Delta\lambda$ (assumed flat) and for the saturation effect. The choice to only match the upper part of the ion spectrum is justified in Section 6.5 where the cooling of the ion beam is discussed. Averaging the single probabilities p_i over the Monte-Carlo samples provides the fraction of ions that is expected to interact in average. In these expressions the parameters $\widetilde{\mathcal{L}}_i$ and $\widetilde{\sigma}$ denote the spatial and the spectral overlaps of the laser and ion beams, respectively. These two quantities correspond to the luminosity and the cross section in absence of saturation effects.

The spatial overlap term for a given ion identified by its position (x_i, y_i, z_i) in the ion beam frame

$$\widetilde{\mathcal{L}}_i = 2n_L c\cos^2(\theta_L/2)\int dx\int dy\int dz\int dt\; n_{\mathrm{laser}}(x_{\mathrm{L}}, y_{\mathrm{L}}, z_{\mathrm{L}}-ct)\,\delta^{(3)}(x-x_i, y-y_i, z-\beta ct-z_i), \tag{37}$$

reduces to

$$\widetilde{\mathcal{L}}_i = \frac{n_L}{2\pi\sigma_L^2\sqrt{1+\sigma_z^2/\sigma_L^2\tan^2(\theta_L/2)}}\exp\left(-\frac{x_i^2}{2\sigma_L^2}-\frac{(z_i\tan(\theta_L/2)+y_i)^2}{2\sigma_L^2(1+\tan^2(\theta_L/2)\sigma_z^2/\sigma_L^2)}\right), \tag{38}$$

where n_L is the number of photons in a laser pulse, $\sigma_z = c\sigma_t$ is the longitudinal laser-beam size. The choice of the vertical crossing plane allows to minimise the crossing angle between the two beams and, in turn, maximises the overall interaction probability.

The spectral term reads

$$\widetilde{\sigma} = \sigma_{\max}\frac{\Gamma\pi}{4}\frac{\lambda^2}{hc\Delta\lambda\gamma(1+\beta\cos(\theta_L/2))}, \tag{39}$$

where in the spatial overlap the error function term is removed, since it is included through the saturation probability $p_{\max}$. The resulting interaction probabilities were benchmarked against the results of the numerical models, described above.

References

[1] M. W. Krasny, "The Gamma Factory proposal for CERN", 1511.07794.

[2] M. Krasny *et al.*, "The CERN Gamma Factory Initiative: An Ultra-High Intensity Gamma Source", in *Proceedings, 9th International Particle Accelerator Conference (IPAC 2018): Vancouver, BC Canada*, p. WEYGBD3, 2018.

[3] C. Curatolo *et al.*, "Novel high intensity gamma-source at CERN: the Gamma Factory Initiative", *PoS (LHCP2018) 089* (2018).

[4] W. Placzek *et al.*, "Gamma Factory at CERN – novel research tools made of light", *Acta Phys. Pol. B* **50** (2019) 1191–1203, 1903.09032.

[5] S. Baudrand *et al.*, "A High Precision Fabry-Perot Cavity Polarimeter at HERA", *JINST* **5** (2010) P06005, 1005.2741.

[6] J. Bonis *et al.*, "Non-planar four-mirror optical cavity for high intensity gamma ray flux production by pulsed laser beam Compton scattering off GeV-electrons", *JINST* **7** (2012) P01017, 1111.5833.

[7] M. W. Krasny *et al.*, "Gamma Factory for CERN", CERN Yellow Report, in preparation.

[8] E. G. Bessonov and K. J. Kim, "Radiative cooling of ion beams in storage rings by broadband lasers", *Phys. Rev. Lett.* **76** (1996) 431–434.

[9] M. Zolotorev and D. Budker, "Prospects in hydrogenic ions using high-energy accelerators", in *Parity Violation in Atoms and Electron Scattering* (B. Frois and M. A. Bouchiat, eds.), p. 364. World Scientific, 1999.

[10] U. Schramm *et al.*, "Laser cooling of relativistic heavy ion beams", *Conf. Proc.* **C0505161** (2005) 401.

[11] E. G. Bessonov and R. M. Feshchenko, "Stimulated Radiation Cooling", *RuPAC Conf. Proc.* (2008).

[12] I. Lauer *et al.*, "Transverse Laser Cooling of a Fast Stored Ion Beam through Dispersive Coupling", *Phys. Rev. Lett.* **81** (1998) 2052–2055.

[13] M. S. Safronova *et al.*, "Search for New Physics with Atoms and Molecules", *Rev. Mod. Phys.* **90** (2018), no. 2 025008, 1710.01833.

[14] M. W. Krasny, S. Jadach, and W. Placzek, "The Femto-experiment for the LHC: The W-boson beams and their targets", *Eur. Phys. J.* **C44** (2005) 333–350, hep-ph/0503215.

[15] M. W. Krasny, F. Fayette, W. Placzek, and A. Siodmok, "Z-boson as 'the standard candle' for high precision W-boson physics at LHC", *Eur. Phys. J.* **C51** (2007) 607–617, hep-ph/0702251.

[16] F. Fayette, M. W. Krasny, W. Placzek, and A. Siodmok, "Measurement of $MW^+ - MW^-$ at LHC", *Eur. Phys. J.* **C63** (2009) 33–56, 0812.2571.

[17] M. W. Krasny, F. Dydak, F. Fayette, W. Placzek, and A. Siodmok, "$\Delta M_W \leq 10 MeV/c^2$ at the LHC: a forlorn hope?", *Eur. Phys. J.* **C69** (2010) 379–397, 1004.2597.

[18] M. W. Krasny, "Electron beam for LHC", *Nucl. Instrum. Meth.* **A540** (2005) 222–234, hep-ex/0405028.

[19] D. Cooke *et al.*, "Calibration of the AWAKE Electron Spectrometer with Electrons Derived from a Partially Stripped Ion Beam", in *Proceedings, 10th International Particle Accelerator Conference (IPAC2019): Melbourne, Australia, May 19-24, 2019*, p. WEPGW089, 2019.

[20] A. Caldwell *et al.*, "Proton Driven Plasma Wakefield Acceleration", *Nature Phys.* **5** (2009) 363–367, 0807.4599.

[21] T. Suwada *et al.*, "First application of a tungsten single-crystal positron source at the KEK B-factory", *Phys. Rev. ST Accel. Beams* **10** (2007) 073501.

[22] T. Prokscha *et al.*, "The new muE4 beam at PSI: A hybrid-type large acceptance channel for the generation of a high intensity surface-muon beam", *Nucl. Instrum. Meth.* **A595** (2008) 317–331.

[23] M. Antonelli *et al.*, "Novel proposal for a low emittance muon beam using positron beam on target", *Nucl. Instrum. Meth.* **A807** (2016) 101–107, 1509.04454.

[24] F. Zimmermann, "LHC- and FCC-Based Muon Colliders", in *Proc. 9th International Particle Accelerator Conference (IPAC'18), Vancouver, BC, Canada, April 29-May 4, 2018*, no. 9 in International Particle Accelerator Conference, pp. 273–276, JACoW Publishing, Geneva, Switzerland, June, 2018, https://doi.org/10.18429/JACoW-IPAC2018-MOPMF065.

[25] S. Hirlaender *et al.*, "Lifetime and Beam Losses Studies of Partially Strip Ions in the SPS ($^{129}\mathrm{Xe}^{39+}$)", in *Proceedings, 9th International Particle Accelerator Conference (IPAC 2018): Vancouver, BC Canada*, p. THPMF015, 2018.

[26] *Xenon beams light path to gamma factory*, CERN Courier, November 2017, p. 7; `cerncourier.com/xenon-beams-light-path-to-gamma-factory/`.

[27] S. Charley, *LHC accelerates its first "atoms"*, CERN News, 27 July, 2018, `home.cern/news/news/accelerators/lhc-accelerates-its-first-atoms`.

[28] M. Schaumann *et al.*, "First Partially Stripped Ions in the LHC ($^{208}\mathrm{Pb}^{81+}$)", in *Proceedings, 10th International Particle Accelerator Conference (IPAC 2019): Melbourne, Australia*, p. MOPRB055, 2019.

[29] I. Tolstikhina *et al.*, *Basic Atomic Interactions of Accelerated Heavy Ions in Matter: Atomic Interactions of Heavy Ions (Springer Series on Atomic, Optical, and Plasma Physics Book 98)*. Springer, 2018.

[30] P. Indelicato and J. Desclaux, "Multiconfiguration dirac-fock calculations of transition energies with qed corrections in three-electron ions", *Physical Review A* **42** (1990) 5139.

[31] Y.-K. Kim, D. Baik, P. Indelicato, and J. Desclaux, "Resonance transition energies of Li-, Na-, and Cu-like ions", *Physical Review A* **44** (1991) 148.

[32] M. H. Chen *et al.*, "Relativistic configuration-interaction calculations for the n=2 states of lithium-like ions", *Phys. Rev. A* **52** (1995) 266–273.

[33] W. Johnson, Z. Liu, and J. Sapirstein, "Transition rates for lithium-like ions, sodium-like ions, and neutral alkali-metal atoms", *Atomic Data and Nuclear Data Tables* **64** (1996) 279 – 300.

[34] Y. S. Kozhedub *et al.*, "Relativistic recoil, electron-correlation, and qed effects on the $2p_j$-$2s$ transition energies in li-like ions", *Phys. Rev. A* **81** (2010) 042513.

[35] J. Sapirstein and K. T. Cheng, "S-matrix calculations of energy levels of the lithium isoelectronic sequence", *Phys. Rev. A* **83** (Jan, 2011) 012504.

[36] V. A. Yerokhin and A. Surzhykov, "Energy Levels of Core-Excited 1s2l2l' States in Lithium-Like Ions: Argon to Uranium", *Journal of Physical and Chemical Reference Data* **47** (2018) 023105, https://doi.org/10.1063/1.503574.

[37] J. Sapirstein and K. T. Cheng, private communication.

[38] X. Zhang *et al.*, "Measurement of the QED energy shift in the $1s^2 2p_{32} - 1s^2 2s_{12}$ x-ray transition in Li-like $^{208}\mathrm{Pb}^{79+}$", *Phys. Rev. A* **78** (2008) 032504.

[39] S. A. Blundell, "Calculations of the screened self-energy and vacuum polarization in Li-like, Na-like, and Cu-like ions", *Phys. Rev. A* **47** (1993) 1790–1803.

[40] R. Büttner *et al.*, "EUV-spectroscopy of beam-foil excited $14.25\,\mathrm{MeV/u}$ Xe^{52}+ ... Xe^{49}+-ions", *Zeitschrift für Physik D Atoms, Molecules and Clusters* **22** (Dec, 1992) 693–697.

[41] D. Feili *et al.*, "Measurements of $2s^2 S_{1/2} - 2p^2 P_{1/2}$ transition energies in lithiumlike heavy ions. III. Experimental results for Sn^{47+} and Xe^{51+}", *Phys. Rev. A* **62** (2000) 022501.

[42] H. Damerau *et al.*, "RF Synchronization and Distribution for AWAKE at CERN", in *Proc. of International Particle Accelerator Conference (IPAC'16), Busan, Korea, May 8-13, 2016*, no. 7 in International Particle Accelerator Conference, pp. 3743–3746, JACoW, Geneva, Switzerland, June, 2016, doi:10.18429/JACoW-IPAC2016-THPMY039.

[43] X. Altuna *et al.*, "A Momentum calibration of the SPS proton beam", CERN-SL-92-32-EA, 1992.

[44] J. Wenninger *et al.*, "Energy calibration of the SPS with proton and lead ion beams", in *Particle accelerator. Proceedings, Conference, PAC'05, Knoxville, USA, May 16-20, 2005*, vol. C0505161, p. 1470, 2005.

[45] V. Kain, K. Cornelis, and E. Effinger, "New Spill Control for the Slow Extraction in the Multi-Cycling SPS", in *Proceedings, 7th International Particle Accelerator Conference (IPAC 2016): Busan, Korea, May 8-13, 2016*, p. TUPMR051, 2016.

[46] S. Levasseur *et al.*, "Development of a rest gas ionisation profile monitor for the cern proton synchrotron on a timepix3 pixel detector", *Journal of instrumentation* **12** (2017), no. 02 C02050.

[47] E. V. Abakumova *et al.*, "A system of beam energy measurement based on the Compton backscattered laser photons for the VEPP-2000 electronâĂŞpositron collider", *Nucl. Instrum. Meth.* **A744** (2014) 35–40, 1310.7764.

[48] N. Winckler *et al.*, "{BREIT} code: Analytical solution of the balance rate equations for charge-state evolutions of heavy-ion beams in matter", *Nuclear Instruments and Methods in Physics Research Section B: Beam Interactions with Materials and Atoms* **392** (2017) 67 – 73.

[49] H. Bartosik *et al.*, "Injectors beam performance evolution during run 2", in *9th LHC Operations Evian Workshop*, 2019.

[50] J. Coupard *et al.*, "LHC Injectors Upgrade : Technical Design Report V. 2, Ions", CERN-ACC-2016-0041 CERN (2016).

[51] M. Gasior *et al.*, "First Operational Experience with the LHC Diode ORbit and OScillation (DOROS) System", in *Proceedings of the International Beam Instrumentation Conference, Barcelona, Spain, 11 - 15 Sep 2016*, p. 43, 2016.

[52] T. Bohl and J. F. Malo, "The APWL Wideband Wall Current Monitor", preprint CERN-BE-2009-006 CERN, Geneva (Feb, 2009).

[53] T. Bohl, H. Damerau, and S. Hancock, "Longitudinal Tomographic Reconstruction of LHC-type Bunches in the SPS", preprint AB-Note-2007-010. CERN-AB-Note-2007-010 CERN (Feb, 2007).

[54] J. Wenninger, "Orbit Response Measurements at the SPS", preprint CERN-AB-2004-009 CERN, Geneva (Jan, 2004).

[55] F. M. Velotti *et al.*, "SPS stability", *GF SPS PoP Workshop, LAL, Orsay, France* (2019).

[56] C. J. Saraceno *et al.*, "The amazing progress of high-power ultrafast thin-disk lasers", *Journal of the European Optical Society-Rapid Publications* **15** (2019), no. 1 15.

[57] Y. Wang, G. Chen, and J. Li, "Development and prospect of high-power doped fibers", *High Power Laser Science and Engineering* **6** (2018) e40.

[58] J. Hecht, "High-Power Fiber Lasers", *Optics & Photonics News* (2018) 8.

[59] M. N. Zervas, "High power ytterbium-doped fiber lasers — fundamentals and applications", *International Journal of Modern Physics B* **28** (May, 2014) 1442009.

[60] S. P. David *et al.*, "Overview of ytterbium based transparent ceramics for diode pumped high energy solid-state lasers", *High Power Laser Science and Engineering* **6** (2018) e62.

[61] https://www.trumpf-scientific-lasers.com/en_INT/products/dira-series/.

[62] J.-P. Negel *et al.*, "Ultrafast thin-disk multipass laser amplifier delivering 1.4 kW (4.7 mJ, 1030 nm) average power converted to 820 W at 515 nm and 234 W at 343 nm", *Opt. Express* **23** (Aug, 2015) 21064–21077.

[63] https://www.afs-jena.de/index.php/products/#mJkW.

[64] https://amplitude-laser.com/fr/application/micro-usinage/.

[65] https://amplitude-laser.com/fr/produit/tangor/.

[66] J. Pouysegur *et al.*, "Hybrid high-energy high-power pulsewidth-tunable picosecond source", *Opt. Lett.* **40** (Nov, 2015) 5184–5187.

[67] I. Chaikovska *et al.*, "High flux circularly polarized gamma beam factory: coupling a Fabry-Perot optical cavity with an electron storage ring", *Scientific Reports* **6** (2016) 36569 EP.

[68] L. Gallais and M. Commandré, "Laser-induced damage thresholds of bulk and coating optical materials at 1030 nm, 500 fs", *Appl. Opt.* **53** (Feb, 2014) A186–A196.

[69] A. L. Bullington *et al.*, "Modal frequency degeneracy in thermally loaded optical resonators", *Appl. Opt.* **47** (May, 2008) 2840–2851.

[70] H. Carstens *et al.*, "Megawatt-scale average-power ultrashort pulses in an enhancement cavity", *Opt. Lett.* **39** (May, 2014) 2595–2598.

[71] A. Variola, J. Haissinski, A. Loulergue, and F. Zomer (eds.), "ThomX Technical Design Report", preprint LAL/RT 14-21, SOLEIL/SOU-RA3629, http://hal.in2p3.fr/in2p3-00971281 (2014).

[72] http://www.fujicera.co.jp/en/product/.

[73] F. Zomer *et al.*, "Polarization induced instabilities in external four-mirror Fabry-Perot cavities", *Appl. Opt.* **48** (Dec, 2009) 6651–6661.

[74] E. Guillermain, "Study of the SPS radiation environment", preprint SPS-SI-EN-001 CERN, Geneva (July, 2017).

[75] G. Buchs *et al.*, "Radiation hard mode-locked laser suitable as a spaceborne frequency comb", *Opt. Express* **23** (Apr, 2015) 9890–9900.

[76] Y.-S. Jang *et al.*, "Space radiation test of saturable absorber for femtosecond laser", *Opt. Lett.* **39** (May, 2014) 2831–2834.

[77] S. Girard *et al.*, "Radiation hardening techniques for Er/Yb doped optical fibers and amplifiers for space application", *Opt. Express* **20** (Apr, 2012) 8457–8465.

[78] C. Curatolo *et al.*, "New Simulation Programs for Partially Stripped Ions - Laser Light Collisions", in *Proceedings, 9th International Particle Accelerator Conference (IPAC 2018): Vancouver, BC Canada*, p. THPMF076, 2018.

[79] A. Petrenko, Python notebook simulating dependence of ion excitation rate on the laser pulse energy: `https://anaconda.org/petrenko/sps_gf_pop_excitation_vs_laser_power`.

[80] E. Bravin *et al.*, "A new TV beam observation system for CERN",.

[81] "Yttrium Aluminum Garnet Scintillation Material", Saint Gobain, `www.crystals.saint-gobain.com/sites/imdf.crystals.com/files/documents/yag-material-data-sheet_69775.pdf` (2016).

[82] `www.crytur.cz/materials/luagce/`.

[83] `www.hamamatsu.com/eu/en/product/cameras/cmos-cameras/index.html`.

[84] T. Poikela *et al.*, "Timepix3: a 65k channel hybrid pixel readout chip with simultaneous toa/tot and sparse readout", *Journal of instrumentation* **9** (2014), no. 05 C05013.

[85] A. Petrenko, Python notebook simulating ion excitation, photon emission and overall process of longitudinal laser cooling in the SPS: `https://anaconda.org/petrenko/psi_beam_vs_laser`.

[86] A. Petrenko, Python notebook simulating the process of transverse cooling in the SPS: `https://anaconda.org/petrenko/fast_transverse_cooling_of_psi`.

[87] R.-D. Heuer, "Report on new schedule HL-LHC", *CERN Council – Hundred and seventy-sixth session*, 18 June 2015, `indico.cern.ch/event/397373/`.

[88] R. Loudon, *The Quantum Theory of Light*. Oxford University Press, New York, 2000.

[89] H. J. Metcalf and and P. van der Straten, *Laser Cooling and Trapping*. Springer, New York, 1999.

[90] C. Curatolo, *High brilliance photon pulses interacting with relativistic electron and proton beams*. PhD thesis, Milan U., 2016.

[91] W. Płaczek, `GF-CAIN`, code to be obtained from the author: wieslaw.placzek@uj.edu.pl.

[92] K. Yokoya, `CAIN`, https://ilc.kek.jp/∼yokoya/CAIN/Cain242/, 2011.

[93] A. Petrenko, Python notebook producing the distribution of emitted photons: https://anaconda.org/petrenko/sps_gf_pop_photon_distr.

[94] A. Petrenko, Python notebook producing the optical part of the emitted photon distribution: https://anaconda.org/petrenko/sps_gf_pop_optical_photons.